Copper Catalysed Formation of Copper Chelators: A New Approach to the Treatment of Wilson's Disease

by

Dustin James Duncan

B.Sc. Biochemistry, University of Victoria, 2013
B.Sc. Chemistry, University of Victoria, 2013

Thesis Submitted in Partial Fulfillment of the
Requirements for the Degree of
Master of Science

in the
Department of Chemistry
Faculty of Science

SIMON FRASER UNIVERSITY

Spring 2016

Approval

Name: **Dustin James Duncan**

Degree: **Master of Science (Chemistry)**

Title: ***Copper Catalysed Formation of Copper Chelators: A New Approach to the Treatment of Wilson's Disease***

Chair: Roger Linington
Associate Professor

Examining Committee:

Tim Storr
Senior Supervisor
Associate Professor

Charles J. Walsby
Supervisor
Associate Professor

David J. Vocadlo
Supervisor
Professor

Jeffrey J. Warren
Internal Examiner
Assistant Professor

Date Defended/Approved: January 5, 2016

Abstract

Wilson's disease is characterized by an increased concentration of copper in the liver, which damages liver tissue and eventually leads to neurological impairment. This disease affects an estimated 1/30,000 people worldwide. Current treatments for this disease can have severe side-effects, including neurological problems in approximately 20-50 % of the patients. The goal of this thesis is to develop compounds that will strongly bind to copper to remove it from the liver. The mechanism for selectivity in binding copper over other endogenous metals (e.g, zinc and iron) is to utilize copper-activated alkyne-azide cycloaddition to couple two moderate binding moieties to form a ligand with a much greater metal-binding affinity. The HepG2 cell line was used as an *in vitro* model for Wilson's disease. A methodology to evaluate the efficacy of chelators to remove copper from the cell model was developed, and tested with a series of new copper chelating compounds.

Keywords: Click Chemistry; Copper; HepG2; Medicinal Chemistry; Wilson's disease

Dedication

I dedicate this work to those patients in which current treatments of Wilson's disease have failed them. I wish for the continuous progress of research for treatments and cures for those patients that have been left by the way-side for their grievous misfortune of suffering an orphan disease.

Acknowledgements

Thank you to Dr. Tim Storr for accepting me into his research lab to begin this project. I appreciate the continuous and unrelenting confidence in my capabilities despite my wavering confidence when I ran into difficulties. I would also like to thank him for the opportunities he has provided to me, such as my MITACS trip to Brazil. This chance for me to travel and experience different lab environments and the ways that different labs function.

I would also like to thank my lab members for helping me through the various problems that I had trying to perform my experiments with their suggestions. Thank you to Neil Dobson from Cell Services for the space to work at biological safety cabinets and the regular upkeep of the work space. Thank you to Dr. Hamel Tailor for teaching me how to use the AAS and helping with the issues that I may have had. Thank you to Dr. Dirk Kirste in the Earth Sciences Department for allowing for me to use the ICP-AES which proved to be invaluable for me to obtain the results that I did.

Table of Contents

List of Tables

List of Figures

List of Schemes

List of Acronyms

AAS	atomic absorption spectroscopy
ATCC	American Type Culture Collection
ATP	adenosine triphosphate
BAL	British anti-Lewisite
BSA	bovine serum albumin
CuAAC	copper-activated alkyne-azide cycloaddition
Cu-Zn SOD	copper-zinc superoxide dismutase
DCM	dichloromethane
DFT	density function theory
DIPEA	diisopropylethylamine
DMEM	Dulbecco's modified essential media
DMF	dimethylfomamide
DMPA	dimercaptopropanesulfonic acid
DMSA	dimercaptosuccinic acid
DNA	deoxyribonucleic acid
DPA	dipicolylamine
EDTA	ethylenediaminetetraacetic acid
EtOAc	ethyl acetate
ESI (+)-MS	electro-spray ionization mass spectrometry (positive mode)
ESI (-)-MS	electro-spray ionization mass spectrometry (negative mode)
Et_2O	diethyl ether
FACS	fluorescence activated cell sorter
FBS	fetal bovine serum
FDA	food and drug administration
HFE	human haemochromatosis protein gene
HHC	hereditary haemochromatosis
HMG-CoA	3-hydroxy-3-methylglutaryl-coenzyme A
HPLC	high-performance liquid chromatography
ICP-AES	induced coupled plasma atomic emission spectroscopy
IDA	iminodiacetic acid
IDAn	iron-deficiency anaemia
IgG	Immunoglobulin G
i-PrOH	isopropanol
IR	infrared
J	*J*-coupling constant
KF	Kaiser-Fleischer
M:L	metal:ligand
MeCN	acetonitrile
MesCl	mesyl chloride
MT	metallothionein
MTT	3-(4,5-dimethylthiazol-2-yl)-2,5-diphenyltetrazolium bromide
m/z	mass / charge ratio
NAD^+	nicotinamide adenine dinucleotide
$NADP^+$	nicotinamide adenine dinucleotide phosphate
NADPH	nicotinamide adenine dinucleotide phosphate hydride
$N(Et)_3$	triethylamine
NMR	nuclear magnetic resonance
PBS	phosphate-buffered saline

pI	isoelectric point
PMSF	phenylmethanesulfonyl fluoride
ROS	reactive oxygen species
RT	room temperature
TFA	trifluoroacetic acid
THF	Tetrahydrofuran
TPEN	N,N,N',N'-tetrakis(2-pyridylmethyl)ethane-1,2-diamine
TXFS	total reflection X-ray fluorescence spectroscopy

Chapter 1.

Introduction

This Chapter includes excerpts from Chapter 1 of Ligand Design in Medicinal Inorganic Chemistry co-written with Michael Jones and Tim Storr.[1]

1.1. The Role of Metals in the Body

Metals play a number of essential roles in the body depending on the types of organic frameworks attached to these metals (which can tune the reactivity of the metal)[1] and the properties of the metals themselves (Table 1.1). Metals such as sodium and potassium may act as counter-ions or balance osmotic pressures. Other metals such as copper, iron, and zinc are essential components of metalloproteins (Table 1.1). These metal ions are cofactors that confer activity to these proteins by providing structure to the protein site for the substrate to react with the enzyme, or a source of electrons for electron transfer. Metalloproteins perform important processes in the body such as dehydrogenation, oxidation, reduction, and oxygen transport.[1] The coordination number, geometry, and ligand preference also differ between different endogenous metals (Table 1.1).[1] This is important when constructing ligands to simulate biological processes (see Chapter 3). To highlight the role and importance of metals in the body, examples of metalloproteins using zinc, iron, and copper will be described. The homeostases of metal ions is essential, and mismanagement of these ions can lead to severe consequences, which will be described in Section **1.2**.

Table 1.1. Examples of metal ions and their function within the human body.

Metals	Coordination Number, Geometry, Ligand Preference	Function
Na^+	6, octahedral, carboxylate/ether/hydroxyl	Charge balance, osmotic pressure, nerve activity
Mg^{2+}	6, octahedral, carboxylate/phosphate	Structural role in hydrolases, isomerases, phosphate transfer
K^+	6-8, flexible, carboxylate/ether/hydroxyl	Charge balance, osmotic pressure, nerve activity
Ca^{2+}	6-8, flexible, carbonyl/carboxylate/phosphate	Structural, charge balance, reaction initiator, phosphate transfer, signalling
$Fe^{2+/3+}$	4 or 6, tetrahedral/octahedral, carboxylate/oxide/phenolate/thiolate/ imidazole/pyrrole	Electron transfer in oxidases
$Co^{+/2+/3+}$	4 or 6, tetrahedral/octahedral, carboxylate/imidazole/thioether/thiolate	Alkyl transfer group (Vitamin B_{12}), oxidases
$Cu^{+/2+}$	3-5, trigonal planar/tetrahedral/square planar/square pyramid, carboxylate/imidazole/thioether/thiolate	Electron transfer, oxidases, hydroxylases, dioxygen transport
Zn^{2+}	4 or 5, tetrahedral/square planar, carbonyl/carboxylate/imidazole/thiolate	Structure in zinc fingers, anhydrases, dehydrogenases,

1.1.1. Roles of Zinc and Iron in the Body

Zinc is used by the body in two ways. It is used to contribute tertiary structure to proteins, and it can perform a catalytic function.[2] In proteins where zinc is used for tertiary structure of a protein, the absence of zinc can result in a loss of function and/or structure.[2-3] An example of zinc's involvement in tertiary structure is zinc fingers[4] (a group of proteins that interact with DNA).[5] This class of proteins requires zinc to coordinate to amino acids

to form a specific structure that then allows for appropriate geometry of the amino acids to interact with DNA.[4] Two examples for the catalytic function of zinc are carbonic anhydrase and alcohol dehydrogenase.[3] Zinc's catalytic role in carbonic anhydrase is to coordinate to hydroxide, which will increase its nucleophilicity to facilitate a reaction with carbon dioxide.[3] For alcohol dehydrogenase, the role of the catalytic zinc is to coordinate to the substrate alcohol, and allow for NAD^+ to receive hydride from the alcohol, to form the corresponding aldehyde.[3]

Iron is another example of a metal that is essential the body. Aside from binding oxygen in haemoglobin, iron is also used for electron transfer for ferredoxin reductases such as ferredoxin-$NADP^+$ reductase[6] (where it resides in the protein as an iron-sulfur cluster)[6] and as a haem for oxidases, such as cytochrome *c* oxidase.[7] The ferredoxin-$NADP^+$ reductase is responsible for reducing $NADP^+$ to NADPH,[6] which is then used as a reducing agent in cellular respiration.[8] This function of cytochrome *c* oxidase is to oxidize cytochrome *c*,[9] which contributes to the electron transport pathway for oxidative phosphorylation in cellular respiration to synthesize ATP.[8-9] The haem-bound iron is an important part of the cytochrome *c* oxidase active site for reducing oxygen to water.[9] Dysregulation of iron can lead to health defects that will be discussed in Section **1.2.1**.

1.1.2. Role of Copper in the Body

Copper is a vital metal for many processes in the body.[10] It is included in enzymes such as oxidases and reductases, as well as being responsible for the transfer of electrons (Table 1.1). Cytochrome *c* oxidase,[7] Cu-Zn superoxide dismutase (Cu-Zn SOD),[11] and tyrosinase[12] are a few examples of copper-containing proteins. Cytochrome *c* oxidase not only contains iron (as described above), but it also contains copper, which resides in the pathway of electron transfer from cytochrome *c* to oxygen.[7] The role of copper in this protein is to be used as an electron source for electron transport, and contribute to the reduction of dioxygen to water.[13] In the first role, copper accepts electrons from cytochrome *c* and transports them to a haem to transport to the catalytic site where another copper atom and another haem reside.[14] The copper in the catalytic site works with the haem to reduce oxygen to water.[14]

Cu-Zn SOD uses two metals: zinc and copper.[15] Cu-Zn SOD catalyses the disproportionation of superoxide molecules to form hydrogen peroxide and dioxygen.[15-16] It is also capable of peroxidase activity to form water and carbonate in the presence of carbon dioxide.[11] Zinc contributes to the tertiary structure of enzyme and coordinates to a bridging histidine residue (His 61) to copper, where copper serves as the binding site to disproportionate superoxide to peroxide and oxygen.[16] The copper ion bound to Cu-Zn SOD changes between Cu(I) and Cu(II) during turnover.[11, 16] In the Cu(II) state, it can perform two reactions, one of which will oxidize peroxide to form superoxide,[11, 17] and in the other, it will oxidize superoxide to dioxygen.[11] In the Cu(I) state, it will react with another superoxide molecule to reduce it to peroxide, leading to the formation of the Cu(II) species at the beginning of the cycle,[16] or it can react with a peroxide anion to form a Cu(II) hydroxide species, which further reacts with carbon dioxide to form carbonate, release a proton, and the cycle can begin again.[11]

Tyrosinase is an enzyme that is responsible for the synthesis of *ortho*-quinones.[12] *Ortho*-quinones are biologically important for a variety of reasons including synthesis of melanin pigments.[12] This enzyme can perform hydroxylation,[18] oxidation,[12, 18] and reduction reactions.[12] There are two Cu(I) ions in the catalytic site that bind dioxygen side-on.[18] From here, the substrate (e.g, phenol or *ortho*-catechol) enters the catalytic site and coordinates to the copper atoms.[18] In the phenol case, one of the oxygen atoms from dioxygen transfers to phenol to form *o*-catechol, then upon addition of protons, there is a loss of water and an oxidation of *o*-catechol to *ortho*-quinone, whereas in the *ortho*-catechol case, addition of acid releases *ortho*-quinone (like the second step in the phenol case).[18]

The Cu(II) / Cu(I) redox potential (0.16 V)[19] is the basis for many chemical reactions that proteins perform within the cell such as electron transport, oxidase activity, and reductase activity as described above.[1] Although redox activity between these two oxidation states allows for many types of chemical reactions to occur within cells by proteins, tight regulation of redox active metals is absolutely necessary to prevent severe detrimental effects.[10]

1.2. Metal Dysregulation and Disease

1.2.1. Iron Dysregulation

As described above, iron has an important role in dioxygen transport as well as redox chemistry within the cell. To absorb iron, it first passes through the gut, into the blood stream and binds to transferrin.[20] The transferrin-bound iron circulates the body via the blood stream, interacts with a transferrin receptor, then the iron enters the cell via receptor mediated endocytosis.[20] Once transported into the cell, a metallochaperone transports the iron to an iron-protein complex called ferritin.[21] Iron is stored in ferritin as a mixture of iron oxides. The iron oxides supply iron required for the cytosolic proteins.[20]

Limited availability of iron to cellular components reduces their efficacy and hampers function. If the body is incapable of absorbing iron, then disorders such as iron-deficiency anaemia (IDAn) may develop. This is often treated by increasing iron intake by taking iron supplements.[22] While the etiology of IDAn may vary, it is the clinical diagnosis given by a set of differential criteria that include: reduced iron, reduced ferritin, increased transferrin, increased iron-binding capacity, reduced transferrin saturation, increased transferrin receptor expression, increased erythrocyte zinc protoporphyrin, and increased hypochromic erythrocytes.[23] The absence of iron in the body results in a reduced amount of available dioxygen binding sites in the blood, thus reducing the amount of oxygen that can be transported to tissues around the body. This reduces the ability of the body to function properly, and the patient suffers from exhaustion and lethargy.[23]

Iron dysregulation can also result in there being too much iron present and available. Excess iron allows for these cellular components to function, but other effects are observed. Fe(II) that is unbound in the cytosol promotes Fenton chemistry where Fe(II) donates an electron to hydrogen peroxide to produce a hydroxide anion and a hydroxyl radical (Scheme 1.1).[10] The analogous reaction using Cu(I) is also shown in Scheme 1.1.

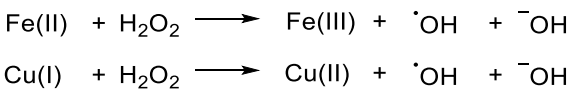

Scheme 1.1. Reactive oxygen species formation with Fe and Cu.

Hydroxyl radicals belong to a class of compounds known as reactive oxygen species (ROS), and react readily with many different types of biomolecules within the cell. This oxidative stress can be severely damaging to the cell and may cause it to undergo apoptosis or necrosis.[24] The Fe(III) ion remaining after this reaction is then reduced within the cell to form the Fe(II) ion which, again, forms another hydroxyl radical.[25]

An example of a disease as a consequence of excess iron is hereditary haemochromatosis (HHC).[20] Where IDAn is the result of a deficiency of iron, HHC is the result of an excess of iron. Patients with HHC have an excessive amount of iron stored, which can be more than 40-fold greater than normal iron stores.[20] The cause of this overloading tends to be from mutations in the human haemochromatosis protein gene (HFE).[20] HFE regulates the iron absorption in the body.[20] Without adequate regulation, iron builds up, which can lead to myriad health problems.[26] The foremost treatment for this disease is therapeutic phlebotomy (using a needle to remove blood), although in certain circumstances, chelation therapy may be considered.[26]

1.2.2. Copper Dysregulation

Copper in the cell is found in the cupric (Cu(I)) and cuprous (Cu(II)) oxidation states. The relatively low potential (0.16 V)[19] between these two states means that there is ample opportunity for free copper to shuttle between each of these two oxidation states since the formal redox level within the cytoplasm is in the range of -160 to -393 mV.[27] As a result, these reduction potentials can lead to the formation of ROS which can then oxidize other biomolecules, leading to cell damage and potentially to cell death.[24, 28] Therefore, cells regulate copper levels with the use of metallothionein as a copper sink,[10] and excretion of excess copper that cannot be handled otherwise. Two diseases that directly relate to copper homeostasis are Menkes disease and Wilson's disease.[29]

Menkes disease arises from copper deficiency in the body due to defects in copper transport.[30] As copper is absorbed into the gut, it passes through intestinal cells, absorbs

into the liver, and is then secreted into the vascular system to be transported to other organs within the body.[10] The liver secretes copper bound to ceruloplasmin for delivery to other organs, whereas, the liver excretes copper into bile to remove it from the body, and this process is dependent upon an ATP-dependent copper transporter called ATP7B.[10] In other organs, the cells (like intestinal cells) utilize a related protein called ATP7A.[31] Since this protein cannot remove copper from the intestinal cells effectively in Menkes disease, copper would then accumulate in the intestinal cells and not reach other organs of the body. Thus, the observation is that these patients experience copper deficiency.[31] The patients who suffer this disease have a high mortality rate and usually die in infancy.[32] Symptoms of this disease include neurodegeneration, arterial changes, hair abnormalities, and connective tissue disorders.[31] There are a variety of different genetic errors that lead to this disease, including about 15-20 % from “gross deletions or rearrangements” (deletion or rearrangement of DNA in the encoding gene).[31] There can be a wide variety of mutations in ATP7A coding region.[33] In a study of multiple patients of Menkes disease, all 41 unrelated patients had different mutations.[33] Current treatment for this disease is to inject intravenously or subcutaneously with copper salts such as copper histidine, copper acetate, and copper ethylenediaminetetraacetic acid (EDTA).[32]

Menkes Disease patients suffer from copper deficiency,[31] whereas Wilson’s disease patients suffer from copper overabundance,[29] despite the etiologies of these diseases arising from the malfunction of analogous proteins (ATP7A and ATP7B, respectively).[10] In Menkes disease, dysfunctional ATP7A does not allow copper to pass through the intestinal walls to be distributed throughout the body, leading to copper deficiency.[34] Conversely in Wilson’s disease, dysfunctional ATP7B does not allow copper to be excreted from the liver into the bile.[29] This build-up of copper in the liver cells leads to oxidative damage and excess copper is released into the blood, which would then be transported to other organs and lead to a build-up of copper in these other organs such as the brain.[29] Despite ATP7A and ATP7B being structurally and functionally similar,[10] the difference in which tissues these proteins are expressed in lead to two clinically very different diseases.[29]

1.2.3. Other Diseases Correlated with Metal Dysregulation

Neurological diseases such as Alzheimer's disease and Parkinson's disease appear to have dysregulated ions such as copper, iron, and zinc within the brain.[35-36] In Alzheimer's disease, there are data that link copper and iron dysregulation to the formation of amyloid-β plaques.[35, 37] This metal dysregulation results in oxidative stress,[35, 38] which leads to cellular damage. Furthermore, these metals are thought to accelerate the formation of amyloid-β plaques.[10, 35] In Parkinson's disease, there is evidence of reduced copper levels in certain regions of the brain and an increase in iron levels.[36, 39] The increased iron levels appears to be associated with the reduced copper levels.[36] There is evidence to suggest the dysregulation of these two metals is related to the oligomerization of α-synuclein and oxidative stress within the brain.[36] The reduced copper affects Cu-Zn SOD and metallothionein proteins, which are suggested to preserve neurological well-being.[36, 40] This appears to be associated with increased iron levels, which promotes oxidative stress.[36]

1.3. Wilson's Disease

1.3.1. Homeostasis of Copper

As previously mentioned, copper is necessary for adequate biological function.[10] This metal can perform chemistry that promotes hazardous oxidative molecule formation (e.g, hydroxyl radicals)[25] within the cells, thus requiring tight regulation. Copper is transported into cells via the copper transporter (CTR1) as Cu(I).[41] The mechanism for which dietary copper (in the Cu(II) state) is reduced to Cu(I) to utilize CTR1 is not yet known,[34] but it is assumed to be through the action of metalloreductases.[42] It is also thought that another copper transporter (CRT2) and divalent metal ion transporter 1 (DMT1) may contribute to copper absorption.[34]

After the transport of copper into the cell, it is thought that the copper ion is delivered to a metallochaperone such as COX7 or CCS to be transported to the mitochondria or to proteins such as Cu-Zn SOD (Figure 1.1).[10, 41] The tripeptide glutathione is also thought to play a role in mediating the uptake into the cell.[43] If the cell receives

signalling that it has been inundated with too much copper, the excess ions are delivered to the distal Golgi complex (the resting site of ATP7B) by the metallochaperone ATOX1.[10, 41, 44] ATP7B is a transmembrane protein which contains 6 copper binding sites and chelates copper through MXCXXC amino acid residue sequences (Figure 1.2) where M is methionine, C is cysteine, and X is any amino acid.[10, 45]

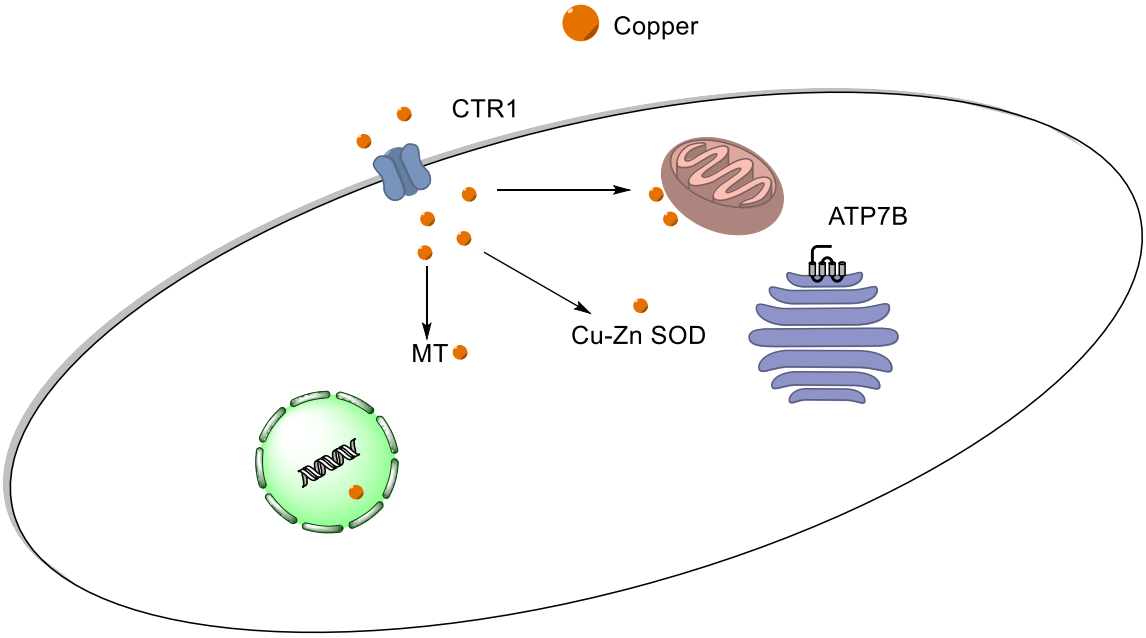

Figure 1.1. Copper uptake by Cu (I) transporter (CTR1) and localization of copper in the cell to metallotheonein (MT), mitochondria, nucleus, and superoxide dismutase (Cu-Zn SOD) with ATP7B residing in the Golgi complex.

Once ATP7B has bound the requisite copper ions, ATP7B is shuttled to the cell membrane, and excretes these excess ions into the biliary system where they are excreted from the body with the solid waste.[10, 41] If this vital function were inhibited or prevented in some way, copper would build up within the liver. Increased copper within the cells affects the expression of various proteins,[46] inhibits nuclear receptor activites,[47] and dysregulates lipid metabolism.[46] It is thought that the impairment of nuclear receptor activity due to high copper levels leads to a decrease in mRNAs for several enzymes such as 3-hydroxy-3-methylglutaryl-coenzyme A (HMG-CoA) reductase and HMG-CoA synthase.[46]

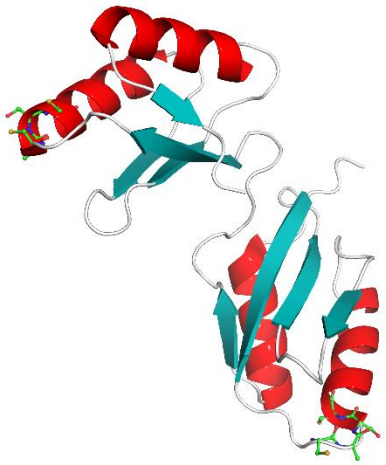

Figure 1.2. NMR solution structure of metal binding domains 3 and 4 of ATP7B. CXXC residue shown as green backbone (PDB: 2ROP).

1.3.2. History and First Treatments

Wilson's disease was first characterized by Dr. Samuel Alexander Kinnier Wilson in 1912,[48] described as "progressive lenticular degeneration". He had found that common symptoms for those suffering this disease included: involuntary movements (i.e. tremors), spasticity, contractures, speech impairment, difficulty in swallowing, muscular weakness/emaciation, pain, varied reflexes (normal tendon reflexes, reduced abdominal reflexes), reduced mental capacity, and advanced hepatic cirrhosis.[48] At the time, no treatment could be prescribed, and "[t]he outlook, once a diagnosis is made, is always serious and may at any time become grave."[48] Once this disease was further researched, it was determined that copper overloading in the liver played a crucial role in this disease,[49] and advanced forms of the disease began to affect muscles and other organs such as the brain.

The first treatment for Wilson's disease, in 1951,[49-50] was dimercaprol (Figure 1.3), also known as British anti-Lewisite (BAL).[49-50] Although BAL treatments reduced hepatic copper and allowed Wilson's disease patients to live full lives, it has low bioavailability and BAL must be injected intramuscularly.[50] D-penicillamine (Figure 1.3) was introduced in 1956 as an orally administered alternative to BAL.[51] Despite functioning well to reduce

hepatic copper levels and having appreciable oral bioavailability, it is poorly tolerated by many patients.[51] With FDA approval of trientine (Figure 1.3) in 1969,[50] trientine joined D-penicillamine to be one of the drugs used for primary treatment in Wilson's disease to reduce copper levels in the body.[34] Once the copper levels in the body were reduced, Zn salts (first approved in 1997)[51] would be prescribed to prevent further copper uptake. Zn salt treatment is also prescribed to patients who are pre-symptomatic.[34]

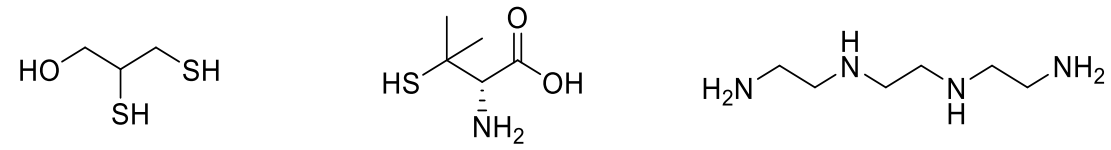

British Anti-Lewisite D-Penicillamine Trientine

Figure 1.3. Structures of British anti-Lewisite, D-penicillamine, and trientine.

1.3.3. Diagnosis of Wilson's Disease

Wilson's disease is a rare disease that affects an estimated 1/30,000 people.[29] Due to its rarity, it may be difficult to diagnose immediately. Using a series of clinical tests that include the measure of copper-serum levels, copper levels in liver tissue (from liver biopsy), and genotyping,[50] it can be determined that a patient suffers from Wilson's disease. This series of tests provides a score, and how the patients score on this test describes the likelihood or severity of Wilson's disease.[52-53] Since Wilson's disease is a clinical diagnosis, rather than a diagnosis based upon a single particular event (such as ATP7B mutation), there are a variety of different biochemical features that may be present within a person suffering from Wilson's disease, and no definition covers all patients aside from the scoring system.

Within this scoring system to determine whether or not a patient has Wilson's disease,[52-53] it becomes clear that copper is present in higher concentrations than normal levels and intervention must occur to ensure the health of the patient does not deteriorate since the disease is progressive and fatal if left untreated.[50] If left unchecked, the copper levels in the liver will continue to increase, which promotes the formation of ROS that will irreparably damage the cells.[24] Oxidative stress leads to apoptosis,[54] and there has been evidence that apoptosis is linked to Wilson's disease.[54] In this type of cell death, the cell

contents (which contain the excess copper) is consumed by macrophages,[55] which does little to ameliorate the issue that there is too much copper present within the system. Necrotic cell death is also thought to contribute to complications observed in some Wilson's disease patients.[50] This is another mode of cell death stimulated by factors including metabolic stress, resulting in lysis of the cell and leading to the cell contents leaking into the extracellular space and affecting neighbouring cells.[56] Clinically, it may be difficult to observe hepatitis or cirrhosis, and some patients never appear to experience these symptoms at all.[51] Although, the recirculation of copper leads to deposits in other organs. One of the organs affected is the eye. As a consequence of this, patients with Wilson's disease tend to exhibit Kaiser-Fleischer (KF) rings,[50, 52] which are copper-coloured rings in the iris within Descemet's membrane.[29] This is one of the best indicators available to the clinician[29] to begin testing for this disease that would unlikely be otherwise tested for, given the scarcity of Wilson's disease in the general population. Although there is not conclusive evidence to suggest that vision is impaired in KF rings, the brain can be severely impaired from Wilson's disease.[50] Magnetic resonance imaging (MRI) of patients with this disease has shown lesions in many regions of the brain.[50] Clinically, it has been observed that late-stage Wilson's disease tends to have a severe neurological impact on the patient.[50, 57] The regions of the brain that are affected the most are called the extrapyramidal regions,[29] which are responsible for gross-motor movement. Those who have suffered deposition of copper into these regions have difficulties controlling their gait, writing, and speech.[48, 57-58] This damage is thought to be irreversible. If Wilson's disease is left untreated, the patient will die.[48]

1.3.4. Current Treatments

D-penicillamine (Figure 1.3) is the first prescribed drug for Wilson's disease.[52] If D-penicillamine is poorly tolerated by the patient, trientine (Figure 1.3) is the next drug prescribed.[59] These are currently the only two approved treatments upon diagnosis of Wilson's disease. Although these drugs do tend to effectively reduce copper levels, there can be serious side-effects.[29, 60] D-penicillamine is typically prescribed first for the treatment of Wilson's disease, in which it removes copper and promotes metallothionein synthesis.[29, 50] However, D-penicillamine treatment is linked to an "exacerbation of the neurological symptoms" in 20-30 % of patients[29] or neurological deterioration in 20-50 %

of the patients[50] depending on the studies performed. Switching to another chelator, such as trientine, or zinc (elemental[61] or salts such as acetate[62] or sulfate[63]) is suggested to prevent worsening of these symptoms.[29] Trientine is typically thought to be more tolerable.[29, 51] It has been observed that in certain cases trientine can also lead to severe neurological problems[60] and ultimately lead to death. There have been reports of the use of ammonium tetrathiomolybdate[29, 50, 64] in lieu of D-penicillamine or trientine, but it has yet to complete clinical trials. Ammonium tetrathiomolybdate forms complexes with copper and protein, and inhibits copper absorption.[29, 65] Other works on novel approaches to Wilson's disease and copper chelation have been explored by modifying D-penicillamine to make a tripodal derivative[66] and a bioconjugated tripodal derivative activated by cytosolic glutathione (Figure 1.4).[67-68] The glycosylated tripodal ligand is cell permeable, and complexes with intracellular copper with an affinity for Cu(I) that is comparable to metallothionein (K_d: ~10^{-19}).[68] This is significant because metallothionein is used as a storage site of copper in the cell,[69] and must have very strong binding to prevent release of free copper.[25]

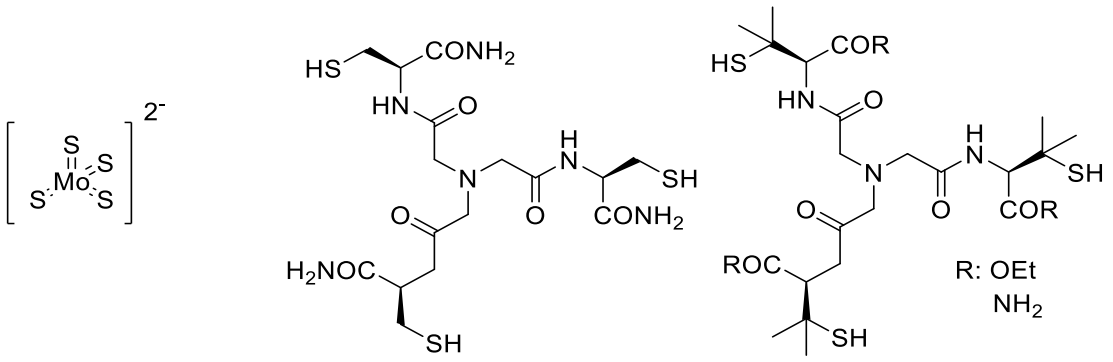

Tetrathiomolybdate High affinity Cu(I)-chelator D-Penicillamine tripodal derivative

Figure 1.4. Recent developments in other treatments for Wilson's disease include tetrathiomolybdate, a high affinity Cu(I) chelator, and a D-penicillamine tripodal derivative.

It is imperative to note that the worsening of side-effects associated with D-penicillamine or trientine tends to present in patients that already present neurological symptoms.[29, 50, 60, 64] Those patients who do not present neurological symptoms, and who are treated with D-penicillamine may still experience side-effects that include fever, rash, inflamed lymph nodes, low neutrophil count, low thrombocyte count, and excess serum

protein levels in urine, whereas those treated with trientine tend to experience fewer side-effects.[50] Pre-symptomatic patients are expected to have good response to zinc treatment[29, 58] or copper chelators.[29] After primary treatment with any of the aforementioned chelators to reduce copper levels, zinc salts are prescribed to prevent further copper uptake[29] into the intestines.[51] Zinc salts increase the metallothionein concentrations in the small intestine by 1500 %,[70] which then limits the amount of copper that can pass through the intestinal walls and into the blood stream to pass into the liver. It has been suggested that neurologically presenting patients (i.e. patients who are presenting neurological symptoms of Wilson's disease) be prescribed zinc salts rather than copper chelators in light of the tendency for these patients to worsen after treatment with chelators begins.[51] If the patient does not respond well to any of the approved treatments, the last resort is a liver transplant.[58]

1.4. **Thesis Outline**

Wilson's disease is diagnosed based upon high copper levels from the incapacity of the liver to excrete copper. Therefore, the removal of copper is necessary to treat this disease. Current treatments include D-penicillamine (a Cu(I) chelator) and trientine (a Cu(II) chelator). Since the goal is to chelate copper, the designed drug should preferentially bind copper over other endogenous metals. By limiting the ability of the drug to chelate these other metals, potential side-effects associated with disturbing the homeostasis of these other metals can be avoided. The proposed method of doing so is to activate the drug at the site of the disease. Huisgen 1,3-dipolar cycloaddition of azides and alkynes is synthetically very useful, because it is reliable, stable toward dimerization and/or hydrolysis, and orthogonal to many types of reactions used in organic synthesis.[71-72] It is synthetically straightforward to introduce an azide or an alkyne to chelating moieties, and considering Huisgen 1,3-dipolar cycloaddition can be catalysed by the presence of Cu(I)[73-74] (Scheme 1.2) (the oxidation state of copper typically found in the cell), this is an attractive route to couple two moderate copper chelators together to form a product with a stronger metal-binding affinity. Since Wilson's disease is characterised by high copper concentrations within the liver, developing a copper chelating drug *in situ* utilizing the endogenous copper makes for an attractive approach to treat this disease.

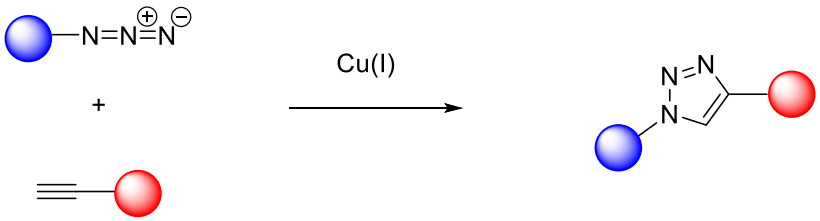

Scheme 1.2. Formation of triazole from alkyne and azide with copper.

This approach allows for two weak to moderate chelating pro-drugs to come together in a copper-rich environment to "click" together to form a much stronger chelator directly in the presence of copper. Since the local concentration of copper during the *in situ* synthesis of the active compound is elevated in Wilson's disease, this compound should complex the copper ion. In essence, the disease itself promotes the drug formation. Once the copper levels have been reduced sufficiently, the rate of drug formation will slow, and the disease will have been treated.

The concept of using copper-activated alkyne-azide cycloaddition (CuAAC) chemistry to synthesize chelators has also been recently explored, but with greater emphasis on developing ^{99m}Tc(I) complexes.[75-76] The concept of "click-to-chelate" appears to work well for synthesizing ^{99m}Tc(I) complexes, but it should be able to translate into synthesizing copper complexes as well. By using the endogenous copper of the liver, the pre-click pro-drugs should click together to form a stronger binding ligand for copper than either of the pre-click components alone.

In addition to "click-to-chelate," the pre-clicked compounds are proposed to be weak to moderate chelators, which can also accelerate the rate of CuAAC.[77-78] Chelators with pendent azides have been explored in biological systems to utilize the CuAAC reaction.[78-80] The click reaction is bioorthogonal[79] which allows for an azide and alkyne to persist in cells without reactivity. For example, this reaction is useful for labelling of modified proteins with a fluorophore to track protein movement or protein interactions.[80] CuAAC uses Cu(I) as the catalytic species, which is toxic to cells through formation of ROS, but if the copper species has been chelated, then ROS formation is limited. Thus, with copper-chelating pre-click compounds, the local copper concentration is high (due to chelation of copper), and the reaction is accelerated.[77, 80] This chelation assisted CuAAC has been observed using both, Cu(I) and Cu(II) species.[77, 81] The chelating compounds

are thought to help reduce Cu(II) to Cu(I), which would then initiate the Cu(I) catalysed cycloaddition.[77]

This thesis will discuss two approaches to synthesize a potential drug for Wilson's disease. The first of which is based upon a known water-soluble, cell-permeable copper and zinc chelator called N,N,N',N'-tetrakis(2-pyridylmethyl)ethane-1,2-diamine (TPEN) (Figure 1.5).[82] Chapter 2 will discuss the synthesis of an analogue of TPEN and an EDTA/TPEN analogue hybrid. Chapter 3 will discuss a biomimetic model of the active site of a bacterial copper-transporting protein known as CusF. Chapter 4 will discuss the testing of a cellular model of the disease for *in vitro* testing of the drugs synthesised and their efficacies. Chapter 5 will present ideas on further steps that can be performed for this research.

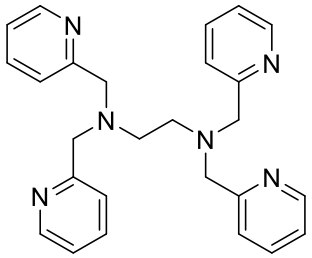

Figure 1.5. Structure of TPEN.

Chapter 2.

Synthesis of a TPEN Analogue and a DPA/IDA Mixed Ligand for Cu-Chelation

Structures calculated using Density Functional Theory[83] (DFT) completed by Ryan Clarke.

2.1. Introduction

Chelation therapy has been used as a strategy for treating various ailments.[22, 50] This approach (e.g. EDTA) has not always been effective in some cases, such as heart attacks[84] or coronary artery disease.[85] Despite the lack of evidence of efficacy,[86] many patients still seek chelation therapy as an alternative medicine.[84-86] In some other circumstances, it is a legitimate approach for heavy metal detoxification (e.g, mercury poisoning[87] or uranium exposure[88]) and particular diseases associated with metal homeostasis.[22] For mercury poisoning, compounds such as dimercaptosuccinic acid (DMSA),[87] and dimercaptopropanesulfonic acid (DMPA)[87] are used (Figure 2.1), whereas in the case of hyperaccumulation of iron in thalassaemia major (a type of blood disorder due to haemoglobin chains that are not effectively synthesized,[89] and characterized by low haemoglobin and fewer red blood cells[90]), desferrioxamine is particularly useful to treat the increased iron levels (Figure 2.1).[91] Other diseases in which using metal chelators as potential therapeutic agents is an attractive strategy are neurodegenerative disorders such as Alzheimer's disease or Parkinson's disease.[35, 92] Chelation therapy has been an approach to remove metal ions that appear to be associated with amyloid-β extracellular protein deposits that are hallmarks of Alzheimer's disease.[35] Chelation therapy for Alzheimer's disease used drugs such as clioquinol,[93] and later generations, such as PBT-2 (Figure 2.1),[94] although there has not yet been any compelling evidence that these particular chelators are effective in treating Alzheimer's disease.[95] Parkinson's disease has also received attention from the inorganic medicinal chemistry community for chelation as a therapeutic approach[92] since metal ions (iron and copper) appear to be implicated in α-synuclein oligomerization.[36]

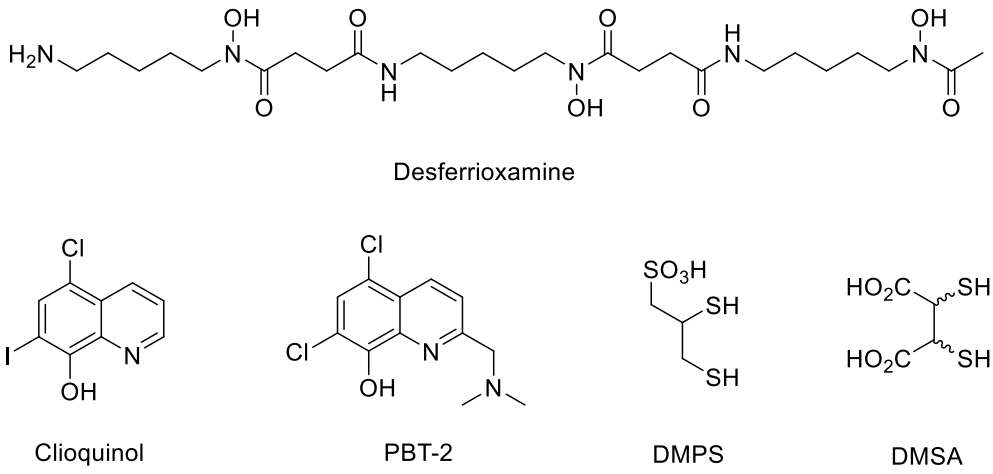

Figure 2.1. Structures of Desferrioxamine, Clioquinol, PBT-2, DMPS, and DMSA.

There are currently two FDA approved drugs for Wilson's disease: D-penicillamine, and trientine (Figure 1.1).[29] D-penicillamine can form different kinds of complexes with copper, which includes a cluster with multiple copper species (both Cu(I) and Cu(II)),[96] and different stoichiometries with Cu(I),[97-98] whereas trientine binds in a 1:1 stoichiometry with Cu(II).[99] The stability constants (Equations 2.1 and 2.2 where [L] is ligand concentration, [M] is metal concentration, [LM] is the concentration of a complex with one ligand and one metal, and [L_2M] is the concentration of a complex with two ligands and one metal) of D-penicillamine vary depending on the state of the ligand. As the reduced form, D-penicillamine has a Log K (Cu(I)) = 19.5;[97] but as the disulfide (protonated), it has a Log K (Cu(I)) = 15.82;[98] and as a dimerized disulfide, it has a Log β_{12}(Cu(I)) = 27.97,[98] (where β_{12} is the product of K_1 and K_2 where K_1 and K_2 are the stability constants for the first ligand binding and second ligand binding to the metal, respectively). The stability constant for trientine copper complex is 21.74 for Cu(II).[100]

$$Log\ K = \log\frac{[LM]}{[L][M]} \qquad \textbf{Equation 2.1}$$

$$Log\ \beta_{12} = \log\frac{[L_2M]}{[L]^2[M]} \qquad \textbf{Equation 2.2}$$

A new chelator for the treatment of Wilson's disease should effectively bind copper (hopefully as strongly or with greater strength in comparison D-penicillamine or trientine), and lead to the excretion of the complex without trafficking the copper to other organs.

Each leading drug targets a different oxidation state of copper (Cu(I) for D-penicillamine and Cu(II) for trientine). As described in Chapter 1, the ideal drug will be activated to bind copper upon reaching the site of the disease (i.e. the copper-loaded liver), and will not interfere with the homeostasis of other ions within the body (e.g, Fe and Zn). These ligands designed for Wilson's disease treatment should also be water-soluble and cell-permeable if they are to be useful as a drug to target copper in the liver. An example of a well-established water-soluble, cell-permeable chelator is TPEN (Figure 1.5).[82] This compound strongly binds copper (Cu(II) = Log K: 20.6).[101]

A desired trait of the drug, is that it is activated upon reaching a high copper concentration. This could be achieved by CuAAC from the conceptual bisection of TPEN into two dipicolylamine (DPA) moieties with a pendent azide or alkyne. The stability constant for DPA is less than that for TPEN (DPA: Log K = 14.4, Log β_{12} = 19.0),[101] and thus triazole formation is expected to afford a chelator with increased affinity for copper in comparison to the DPA-alkyne and DPA-azide components (Scheme 2.1).

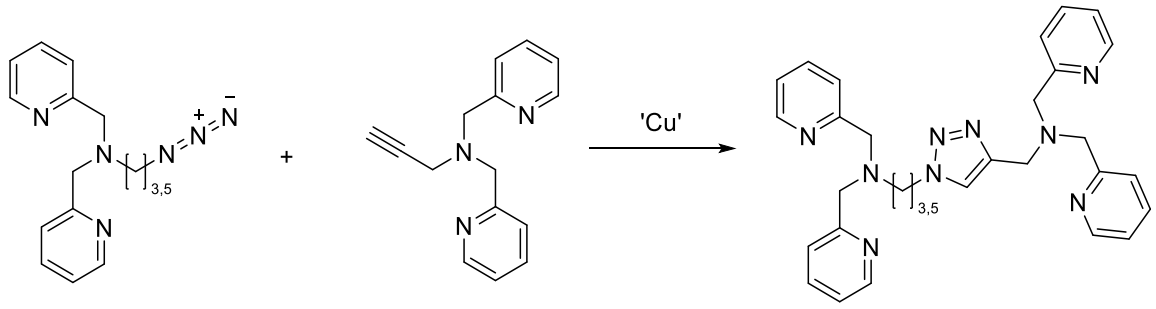

Scheme 2.1. Proposed synthetic scheme for the TPEN analogue in this work.

DFT-optimized structures of the Zn-bound TPEN analogues containing a triazole show these analogues to be hexadentate (Figure 2.2). The primary purpose for these calculations were to determine the length of alkyl chain necessary between the triazole and DPA moiety to allow for the ligand to form a hexadentate complex. Zn(II) was used as an ion that will form a 6-coordinate structure. The ligand should bind in the same manner as TPEN considering there are still four pyridyl-metal and two amine-metal interactions, but with a linking chain that is flexible enough to allow for both DPA units to efficiently bind to the metal ion. Based upon these calculated structures, it is likely that the 5-carbon chain would bind more tightly in comparison to the 3-carbon chain due to the increased flexibility in the alkyl chain between the triazole and the DPA moiety. The

suggestion that the 5-carbon chain would bind more strongly is based on a comparison the bond angle between the triazole ring and the carbon chain, where the smallest angle is the most planar structure, which would be the most preferable for triazole (Figures S.1, S.2). The triazole is aromatic which means that all atoms bound to this unit should be in the same plane to minimize distortion. Therefore, the smaller angle between the triazole and the triazole-bound carbon of the alkyl chain, the less distorted the triazole is.

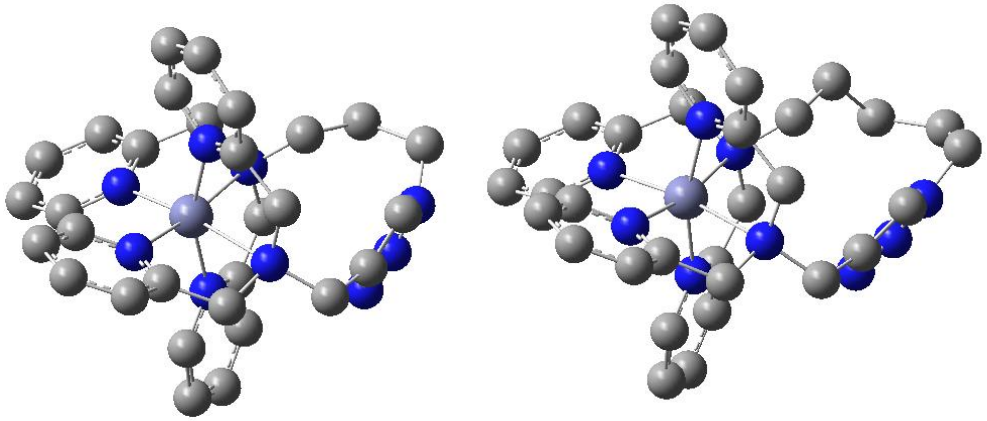

Figure 2.2. DFT calculated structures of TPEN analogues with 3-carbon (left) and 5-carbon (right) linkers between the DPA moiety and the triazole binding with Zn^{2+} to establish expected hexadentate structure (calculated with the uB3LYP functional of the 6-31g(d) basis set). Grey: carbon, blue: nitrogen, blue-grey: zinc.

2.2. **Experimental**

Caution: The synthesis of compounds with pendent azides can be hazardous. Azides are known to be sensitive to friction and temperature, and are potentially explosive. Handle with care, and keep in solution whenever possible. All ^{1}H and ^{13}C NMR are compiled in the Appendix (Figures S.3 – S.14).

2.2.1. Synthesis

1.5-diazidopentane (1)

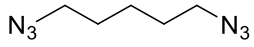

This compound was made as described in the literature.[102] The reagent 1,5-dibromopentane (1.078 g, 4.69 mmol) was dissolved in 6 mL DMF, then sodium azide (0.632 g, 9.72 mmol) was added. The solution was stirred for five hours at 80 ^{o}C, then quenched with H_2O (3 mL), extracted with ether (2 x 10 mL), and dried with $MgSO_4$, filtered, and concentrated *in vacuo*. Yield: 0.644 g (89 %). ^{1}H NMR($CDCl_3$): 3.28 (t, 4H, *J* = 6.8 Hz),1.67-1.55 (m, 4H), 1.51-1.39 (m, 2H). ^{13}C NMR ($CDCl_3$): 51.33, 28.55, 24.06. IR (neat): 2101 cm^{-1} (s, N_3).

1-amino-5-azidopentane (2)

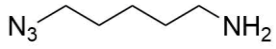

This compound was made as described in the literature.[103] The reagent 1,5-diazidopentane (**1**) (1.151 g, 7.66 mmol) was dissolved into EtOAc (5 mL), Et_2O (5 mL), and then 5 % HCl (10 mL) was added to form a biphasic system. After cooling to 0 ^{o}C in an ice bath, triphenylphosphine (2.018 g, 7.69 mmol) was slowly added over one hour, then the reaction was stirred vigorously for 25 hours. A 1 M HCl solution (10 mL) was added to separate the phases. The organic layer was discarded, then the aqueous layer was washed with dichloromethane (DCM) (2 x 20 mL). After adjusting the pH of the aqueous layer with a 1MNaOH solution to ~12, the product was extracted with 4 x 20 mL of DCM, then dried with $MgSO_4$, filtered and concentrated to afford **2**. Yield: 0.646 g (66 %). ^{1}H NMR ($CDCl_3$): 3.26 (t, 2H, *J* = 6.9 Hz), 2.69 (t, 2H, *J* = 6.9 Hz), 1.60 (p, 4H, *J* = 7.0 Hz (CH_2 + NH_2), 1.51-1.43 (m, 2H), 1.43-1.34 (m, 2H). ^{13}C NMR ($CDCl_3$): 51.49, 41.99, 33.13, 28.82, 24.15. IR (neat): 2091 cm^{-1} (s, N_3).

5-azido-*N*,*N*-bis(pyridin-2-ylmethyl)pentan-1-amine (3)

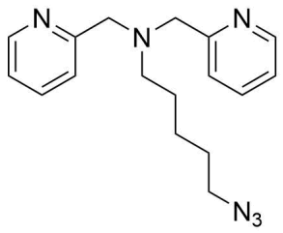

The reagent 1-amino-5-azidopentane (**2**) (0.186 g, 1.45 mmol) was dissolved in MeCN (5 mL) and then 2-picolyl chloride hydrochloride (0.484 g, 2.95 mmol) and potassium carbonate (0.959 g, 6.94 mmol) were added to the solution. The reaction was heated for two days at 80 ^{o}C. The reaction mixture was filtered, and the filtered solid was washed with DCM to extract the remaining product. The DCM solution was concentrated *in vacuo*. Yield: 0.417 g (93 %). ^{1}H NMR ($CDCl_3$): 8.51 (ddd,2H, *J* = 4.9, 1.7, 0.9 Hz), 7.65 (td, 2H, *J* = 7.7, 1.8), 7.52 (d, 2H, *J* = 7.8 Hz), 7.14 (ddd, 2H, *J* = 7.4, 4.9, 1.1 Hz), 3.80 (s, 4H) 3.20 (t, 2H, *J* = 6.9 Hz), 2.54 (t, 2H, *J* = 7.2 Hz), 1.44-1.60 (m, 4H), 1.29-1.39 (m, 2H). ^{13}C NMR ($CDCl_3$): 160.11, 149.12, 136.47, 122.98, 122.02, 60.69, 54.22, 51.53, 28.81, 26.77, 24.55. IR (neat): 2092 cm^{-1} (s, N_3), ESI (+)-MS m/z (M+1): 311.20.

1-amino-3-azidopropane (4)

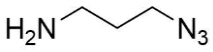

This compound was made as described in the literature.[104] The reagent 1-amino-3-bromopropane hydrobromide (2.253 g, 10.3 mmol) was dissolved into H_2O (5 mL) then sodium azide (1.85 g, 28.5 mmol) was added and the reaction was stirred for 22 hours at 100 ^{o}C. The solution was cooled, and NaOH pellets were added to increase the pH to 10, then the product was extracted with DCM and dried with $MgSO_4$. The product was concentrated on the rotary-evaporator using no heat, and then left open in a fumehood to allow for the remainder of the DCM to evaporate. Yield: 0.876 g, (84 %). ^{1}H NMR ($CDCl_3$): 3.35 (t, 2H, *J* = 6.7 Hz), 2.78 (t, 2H, *J* = 6.8 Hz), 1.70 (p, 2H, *J* = 6.8 Hz), 1.26 (s, 2H). ^{13}C NMR ($CDCl_3$): 49.24, 39.41, 32.50. IR (in $CDCl_3$): 2100 cm^{-1} (s, N_3).

3-azido-*N*,*N*-bis(pyridin-2-ylmethyl)propan-1-amine (5)

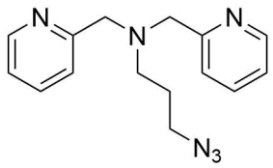

The reagent 1-amino-3-azidopropane (**4**) (0.518 g, 5.17 mmol) was dissolved in MeCN (5 mL) then 2-picolyl chloride hydrochloride (1.702 g, 10.38 mmol) and potassium carbonate (2.920 g, 21.13 mmol) were added and stirred for two days at 80 ^{o}C. The reaction mixture was filtered, and the filtered solid was washed with MeCN to collect the remaining product. The MeCN solution was concentrated *in vacuo*. Yield: 1.200 g, (82 %). ^{1}H NMR ($CDCl_3$): 8.525 (dq, 2H), 7.655 (dt, 2H), 7.48 (dd, 2H), 7.15 (dt, 2H), 3.81 (s, 4H), 3.30 (t, 2H), 2.63 (t, 2H), 1.78 (q, 2H). ^{13}C NMR ($CDCl_3$): 159.61, 149.20, 136.53, 123.04, 122.16, 60.04, 51.37, 49.57, 26.71. IR (neat): 2095 cm^{-1} (s, N_3), ESI (+)-MS m/z (M+1): 283.17.

***N,N*-bis(pyridin-2-ylmethyl)prop-2-yn-1-amine (6)**

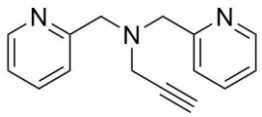

This compound was made as described in the literature.[105] The reagent 2-picolyl chloride hydrochloride (0.634 g, 3.86 mmol) was dissolved in MeCN (10 mL) then propargylamine (125 µL, 0.107 g, 1.95 mmol) and potassium carbonate (1.1 g, 8.0 mmol) were added and the reaction stirred for two days at 80 ^{o}C. The reaction mixture was filtered, and the filtered solid was washed with MeCN to collect the remaining product. The MeCN solution was concentrated *in vacuo*. Yield: 0.442 g, (96 %). ^{1}H NMR ($CDCl_3$): 8.54-8.52 (m, 2H), 7.63 (dt, 2H, *J* = 7.7, 1.8 Hz), 7.49 (d, 2H, *J* = 7.8 Hz), 7.13 (ddd, 2H, *J* = 7.4, 4.9, 1.0 Hz), 3.89 (s, 4H), 3.40 (d, 2H, *J* = 2.4 Hz), 2.27 (t, 1H, *J* = 2.4 Hz). ^{13}C NMR ($CDCl_3$): 158.89, 149.35, 136.56, 123.23, 122.20, 78.46, 73.72, 59.57, 42.69. IR (neat): 2104 cm^{-1} (w, -CCH), ESI (+)-MS m/z (M+1): 138.14.

di- *tert*-butyl 2,2'-(prop-2-yn-1-ylazanediyl) diacetate (7)

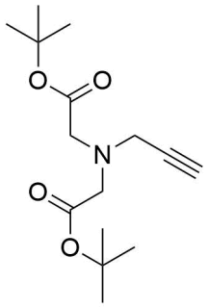

This compound was made as described in the literature.[106] The reagents propargylamine (~640 µL, 0.547 g, 9.93 mmol) and bromoacetic acid *tert*-butyl ester (2.913mL, 3.87 g, 19.8 mmol) were dissolved in MeCN (15 mL) and then potassium carbonate (4.917 g, 35.6 mmol) was added and the reaction was stirred for two days at 80 ^{o}C. The reaction mixture was filtered, and the filtered solid was washed with MeCN. The MeCN solution was concentrated *in vacuo*. Yield: 2.325 g, (83 %). ^{1}H NMR ($CDCl_3$): 3.65 (d, 2H, *J* = 2.4 Hz), 3.43 (s, 4H), 2.23 (t, 1H, *J* = 2.4 Hz), 1.46 (s, 18H). ^{13}C NMR ($CDCl_3$): 169.87, 81.33, 78.94, 73.48, 55.10, 43.17, 28.27. IR (neat): 2037 cm^{-1} (w, -CCH), ESI (+)-MS m/z (M+1 (10 %)): 284.1861, (M-2(*t*-bu)+2H (100 %)): 172.06.

2,2'-(prop-2-yn-1-ylazanediyl) diacetate (8)

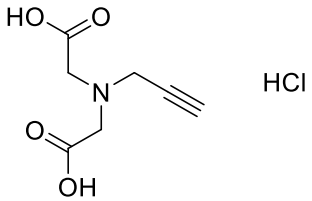

This compound was made as described in the literature.[106] The reagent di-*tert*-butyl 2,2'-(prop-2-yn-1-ylazanediyl) diacetate (**7**) (0.112 g, 0.395 mmol) was dissolved in ~10 % HCl solution. This mixture was stirred for 12 hours and then concentrated *in vacuo*. Quantitative transformation. ^{1}H NMR (MeOD): 4.31 (d, 2H, *J* = 2.2 Hz), 4.23 (s, 4H), 3.35 (s, 1H). ^{13}C NMR (MeOD): 168.71, 81.46, 73.06, 54.50, 45.81. IR (neat): 2125 cm^{-1} (w, -CCH).

di-*tert*-butyl 2,2'-(((1-(3-(bis(pyridin-2-ylmethyl)amino)propyl)-1*H*-1,2,3-triazol-4-yl)methyl)azanediyl)diacetate (9)

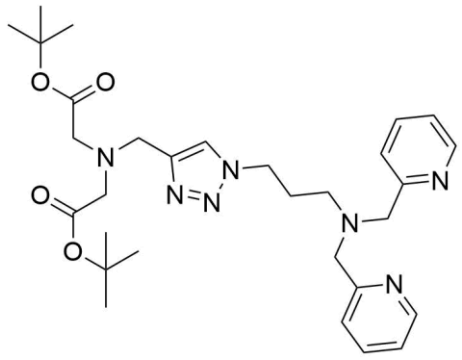

The reagent di-*tert*-butyl 2,2'-(prop-2-yn-1-ylazanediyl)diacetate (**7**) (0.179 g, 0.630 mmol) and 3-azido-*N*,*N*-bis(pyridin-2-ylmethyl)propan-1-amine (**5**) (0.178 g, 0.630 mmol) were dissolved in MeCN (~1 mL), then copper iodide (0.179 g, 0.939 mmol) and DIPEA (549 μL, 0.407 g, 0.315 mmol) were added. The reaction mixture was then stirred for 19 h. A saturated solution of EDTA (pH 10) was then added to chelate all copper before extracting the product with EtOAc (2 x 5 mL). The organic layer was washed several times with a saturated pH 10 EDTA solution, and re-extracted with EtOAc (2 x 5 mL). The crude product was purified using silica gel chromatography. Eluent: 7.5 % MeOH, 1 % NH_4OH in DCM. Yield: 0.126 g, (35 %). ^{1}H NMR ($CDCl_3$): 8.52 (dd, 2H, *J* = 4.8, 0.7 Hz), 7.65 (td, 2H, 7.7, 1.7 Hz), 7.49 (s, 1H), 7.45 (d, 2H, *J* = 7.8 Hz), 7.15 (dd, 2H, *J* = 6.9, 5.4 Hz), 4.32 (t, 2H, *J* = 7.3 Hz), 3.95 (s, 2H), 3.81 (s, 4H), 3.41 (s, 4H), 2.62 (t, 2H, *J* = 6.7 Hz), 2.15-2.07 (m, 2H), 1.44 (s, 18H). ^{13}C NMR (MeOD): 170.53, 159.23, 149.21, 145.59, 136.66, 123.27, 123.04, 122.28, 81.20, 60.51, 55.44, 53.55, 51.03, 49.11, 48.30, 28.29. ESI (+)-MS m/z (M+1): 566.34.

2,2'-(((1-(3-(bis(pyridin-2-ylmethyl)amino)propyl)-1*H*-1,2,3-triazol-4-yl)methyl)azanediyl)diacetic acid (10)

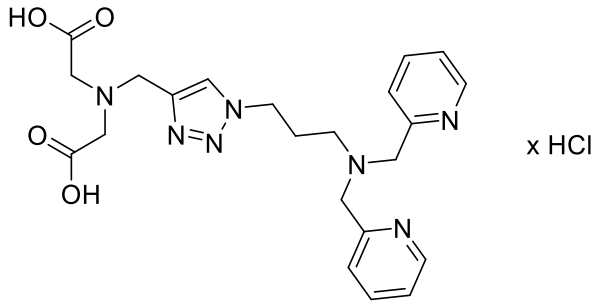

The reagent di-*tert*-butyl 2,2'-(((1-(3-(bis(pyridin-2-ylmethyl)amino)propyl)-1H-1,2,3-triazol-4-yl)methyl)azanediyl)diacetate (**10**) (0.055 g, 0.097 mmol) was dissolved into 10 % HCl (1-2 mL) and stirred for 16 hours. The solvent was concentrated *in vacuo* to afford a brown, hygroscopic solid. Quantitative transformation. ^{1}H NMR (MeOD): 8.88 (d, 2H, *J* = 5.5 Hz), 8.59 (t, 2H, *J* = 7.6 Hz), 8.32 (s, 1H), 8.16 (d, 2H, *J* = 8.0 Hz), 8.03 (t, 2H, *J* = 6.6 Hz), 4.71 (s, 2H), 4.53 (t, 2H, *J* = 6.6 Hz), 4.38 (s, 4H), 4.25 (s, 4H), 2.80-2.72 (m, 2H), 2.31-2.22 (m, 2H). ^{13}C NMR (MeOD): 168.17, 154.26, 147.99, 143.28, 136.93, 128.92, 128.47, 127.46, 56.94, 54.65, 52.80, 50.69, 27.75. ESI (-)-MS m/z (M-1): 452.21.

di- *tert*-butyl 2,2'-(((1-5-(bis(pyridin-2-ylmethyl)amino)pentyl)-1*H*-1,2,3-triazol-4-yl)methyl)azanediyl diacetate (11)

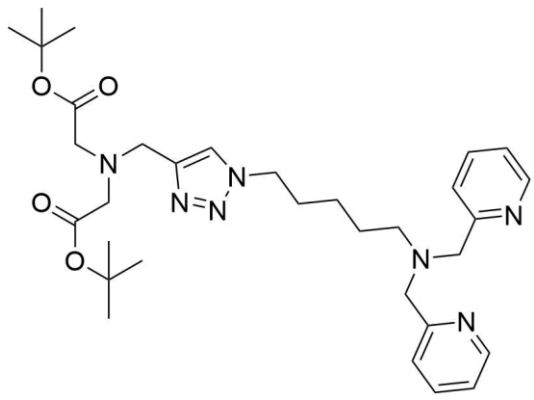

The reagents di-*tert*-butyl 2,2'-(pent-2-yn-1-ylazanediyl)diacetate (**7**) (0.148 g, 0.521 mmol) and 5-azido-N,N-bis(pyridin-2-ylmethyl)pentan-1-amine (**3**) (0.151 g, 0.486

mmol) were dissolved in THF under N_2 atmosphere (1 mL), diisopropylethylamine (423 µL, 0.314 g, 2.43 mmol) and copper iodide (0.135 g, 0.710 mmol) were subsequently added. After 3.5 hours of stirring, a saturated solution of EDTA (pH 10) was added, and then the product was extracted into DCM (2 x 10 mL). The product was purified on silica gel. Eluent: 5 % MeOH in DCM, then 10 % MeOH and 1 % NH_4OH in DCM. Yield: 0.093 g (30 %). ^{1}H NMR (MeOD): 8.43 (d, 2H, *J* = 4.5 Hz), 7.89 (s, 1H), 7.82 (td, 2H, *J* = 7.7, 1.4 Hz), 7.61 (d, 2H, *J* = 7.8 Hz), 7.29 (dd, 2H, *J* = 6.8, 5.6 Hz), 4.35 (t, 2H, *J* = 6.9 Hz), 3.98 (s, 2H), 3.76 (s, 4H), 3.42 (s, 4H), 2.49 (t, 2H, *J* = 7.0 Hz), 1.85-1.72 (m, 2H), 1.63-1.51 (m, 2H), 1.45 (s, 18H), 1.32-1.21 (m, 2H). ^{13}C NMR (MeOD): 171.79, 160.72, 149.32, 145.75, 138.77, 125.34, 124.84, 123.81, 82.69, 61.07, 56.01, 55.09, 51.24, 49.81, 30.99, 28.37, 27.34, 25.06. ESI (+)-MS m/z (M+1 (90 %)): 594.37.

2,2'-(((1-(5-(bis(pyridin-2ylmethyl)amino)pentyl)-1*H*-1,2,3-triazol-4-yl)methyl)azanediyl)diacetic acid (12)

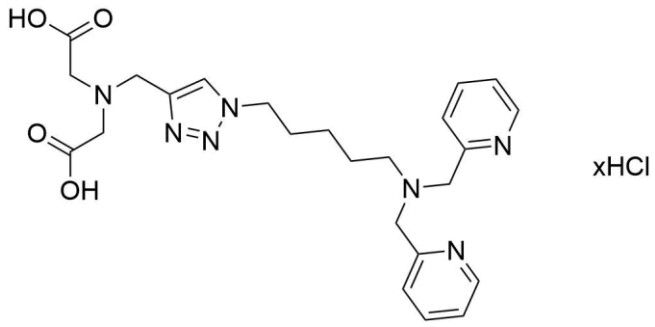

The reagent di-*tert*-butyl 2,2'-(((1-(3-(bis(pyridin-2-ylmethyl)amino)pentyl)-1H-1,2,3-triazol-4-yl)methyl)azanediyl)diacetate (**11**) (0.044 g, 0.074 mmol) was dissolved in DCM (1 mL) and TFA (1mL). The reaction mixture was stirred for 16 hours while the solvent slowly evaporated in the fumehood. The TFA was exchanged with HCl by dissolving the deprotected product in ~10 % HCl. The solvent was concentrated *in vacuo* to afford a brown, hygroscopic solid. Quantitative transformation. ^{1}H NMR (MeOD): 8.91 (d, 2H, *J* = 5.8 Hz), 8.62 (td, 2H, *J* = 7.9, 1.3 Hz), 8.33 (s, 1H), 8.20 (d, 2H, *J* = 4.0 Hz), 8.07-8.03 (m, 2H), 4.75 (s, 2H), 4.44 (t, 2H, *J* = 6.8 Hz), 4.39 (s, 4H), 4.30 (s, 4H), 2.69-2.65 (m, 2H), 1.90-1.82 (m, 2H), 1.68-1.59 (m, 2H), 1.29-1.21 (m, 2H). ^{13}C NMR (MeOD): 168.11, 154.42, 148.29, 142.96, 136.86, 128.86, 128.51, 127.52, 56.91, 56.04, 54.74, 51.18, 50.89, 30.70, 26.30, 24.77. ESI (-)-MS m/z (M-1): 480.25.

3-(4-((bis(pyridin-2-ylmethyl)amino)methyl-1*H*-1,2,3-triazol-1-yl)-*N*,*N*-bis(pyridin-2-ylmethyl)propan-1-amine (13)

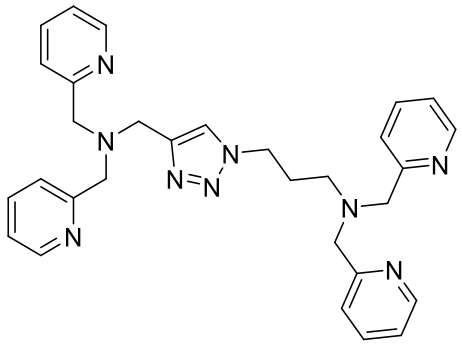

The reagents 3-azido-*N*,*N*-bis(pyridin-2-ylmethyl)propan-1-amine (**5**) (0.074 g, 0.262 mmol) and *N*,*N*-bis(pyridin-2-ylmethyl)prop-2-yn-1-amine (**6**) (0.063 g, 0.262 mmol) were dissolved in *i*-PrOH (1 mL). The reagents $CuSO_4 \cdot 5H_2O$ (0.146 g, 0.585 mmol) and ascorbic acid (0.206 g, 1.17 mmol) were dissolved in H_2O (1 mL). These solutions were then mixed, and stirred for 3 days. Compound not isolated. ESI (+)-MS m/z (M+Cu (60 %)): 582.22.

2.2.2. Job's Plot Analysis of Compounds 10 and 12

The stoichiometry of the ligand:metal (L:M) interaction was determined using a Job's plot analysis.[107] A total L+M concentration was set at 1.33 mM. The mixtures analyzed varied from 100 mol % ligand to 100 mol % copper at 10 mol % intervals. The wavelengths chosen were based upon those with the greatest change in absorbance throughout the experiment. The pH was held constant at 7.4 using phosphate buffered saline (PBS). The Job's plots (Figures 2.5B-2.8B) show absorbance as a function of mole fraction copper. The spectra were measured using a Cary UV/Vis/NIR instrument. The absorbances measured were within the linear range of the instrument. When plotting the Job's plots (Figures 2.5B-2.8B), the absorbances of 1:0 M:L and 0:1 M:L were adjusted to 0 to accommodate for the molar absorptivities of the ligand and metal ion when performing the experiment.

2.2.3. pK_a Determination of Compounds 10 and 12

The pK_a values of the click products were determined using NMR spectroscopy.[108] These values were determined by dissolving ~35-85 mg of the sample (**10** or **12**) in 4-8 mL of D_2O. The pH meter was calibrated using a two-point method of pH 4.01 and pH 10.01. The pD of the sample was measured, and adjusted to varying pD values by adding NaOD and DCl solutions. NMR samples were taken at varying pD values. The pH was found from the pD measured by applying Equation 2.2.[109]

$$pK_a(H_2O) = (pK_a(D_2O - 0.45))/1.015 \qquad \textbf{Equation 2.2}$$

2.2.4. HPLC Analyses

The analyses were performed on an Aligent 1100 Series High Pressure Liquid Chromatograph using a C8-nitrile column (Aligent Technologies, Zorbax RX-C8, 5 µm, 2.1 x 150 mm) with the following conditions: H_2O (0.1 % formic acid) and MeCN (0.1 % formic acid) eluents; injection volume: 5 µL; flow rate: 0.5 mL/min; 0.00-0.50 min: 5 % MeCN, 0.50-3.00 min 5→90 % MeCN, 3.00-5.00 min 90 % MeCN, 5.00-5.10 min 90→5 % MeCN, 5.10-6.00 min 5 % MeCN.

2.3. Results and Discussion

2.3.1. Design and Synthesis of Ligand Precursors

Two target compounds with varying lengths of alkyl chain were chosen that could form these complexes based on the calculated structures (Figure 2.2). Synthetically, it was more sensible to allow for the DPA-azide target to have the variable chain length. Propyl and pentyl chains were synthesized as described in Section **2.2.1**. The method for synthesizing these chains differed due to the initial starting materials available.

Two synthetic routes to the Compound **3** were designed. The first of which (outlined in Section **2.2.1**) started with reaction of 1,5-dibromopentane and sodium azide to afford 1,5-diazidopentane (Scheme 2.2). Next, a Staudinger reduction[110] in a two-phase

solution of ethyl acetate and 5 % HCl was completed (Scheme 2.2). The di-azide is soluble in the organic layer along with triphenylphosphine, which then reduces one of the two azides into an amine. The vigorous stirring of the solution allowed for the product (**2**) to become protonated and transfer into the acidic aqueous layer. Washing the aqueous layer with ethyl acetate helped remove triphenylphosphine and/or triphenylphosphine oxide. The aqueous layer of the reaction mixture was neutralized and the product was extracted into DCM. The organic layer was then washed with water to help remove further impurities. Compound **2** was then reacted with 2-(chloromethyl)pyridine·HCl to afford product **3** (Scheme 2.3).

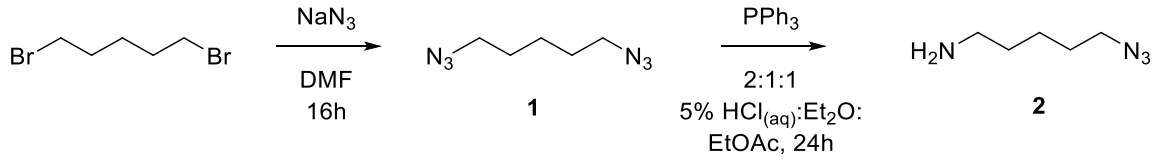

Scheme 2.2. Synthesis of Compound 2 employing a Staudinger reduction.

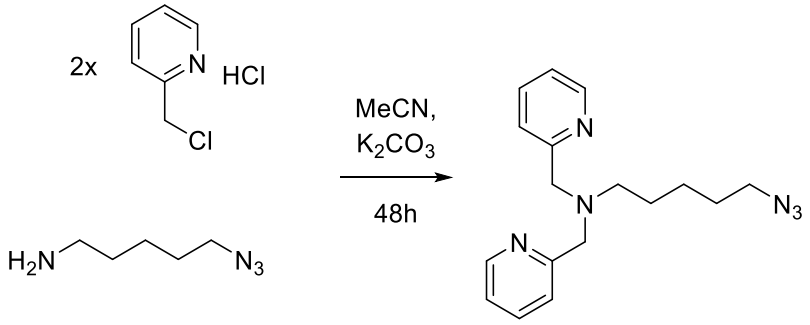

Scheme 2.3. Synthesis of Compound 3.

The second synthetic route shown in Scheme 2.4 does not require the use of the Staudinger reduction, and also does not require the isolation of the di-azide (**1**). This one-pot reaction started with 1,5-dibromopentane and one equivalent of sodium azide dissolved in DMF. After this reaction mixture was heated for 16 hours at 80 ^{o}C, one equivalent of DPA was added, and this mixture was kept at 80 ^{o}C with stirring for a further two days.

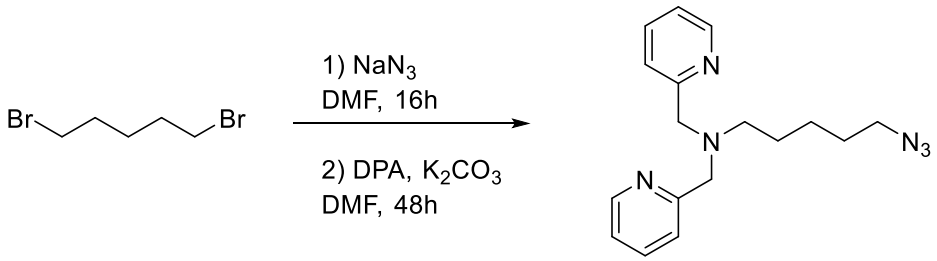

3

Scheme 2.4. Alternative synthesis for Compound 3.

In this synthetic route, DPA should either react with the 1-azido-5-bromopentane to afford the desired product, or with unreacted 1,5-dibromopentane. The latter reaction forms a cyclized product with a quaternary amine (Scheme 2.5). The formation of this cyclized product is known by previously attempted chemistry in the laboratory to target **3**. The reaction mixture was concentrated and the reaction mixture was redissolved into DCM. This reaction mixture was then concentrated *in vacuo*, and redissolved into MeOH before washing with n-pentane.

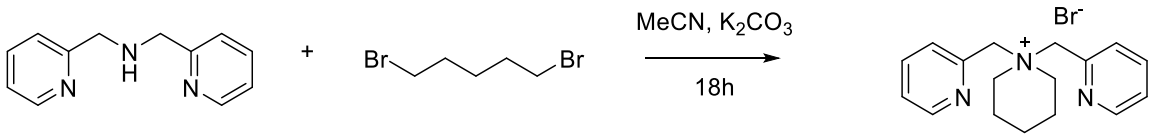

Scheme 2.5. Synthesis of ammonium bromide salt using DPA and 1,5-dibromopentane.

This alternative synthesis does reduce the number of steps to synthesize **3**, although this may come at the cost of reducing the maximum potential yield (24 % in this case). The first step should have a statistical mixture of the di-azide, mono-azide, and unreacted starting material. This statistical mixture limits the amount of reagent alkyl azide-bromide available to synthesize the target. The first preparation had twice the yield of the second preparation. It will take further efforts to optimize this synthesis, and determine if there is any appreciable benefit to this alternative synthetic approach to form **3**.

The propyl chain required for the synthesis of Compound **5** (Scheme 2.6) was synthesized from 1-amino-3-bromopropane·HBr. The first reaction towards the propyl chain was to replace the bromine atom with an azide by reaction of 1-amino-3-

bromopropane·HBr with sodium azide. This product was then reacted with 2-(chloromethyl)pyridine·HCl (Scheme 2.6). This reaction is clean enough that filtration of the solid base provides the target compound (estimated 95 % purity based upon ^{1}H NMR).

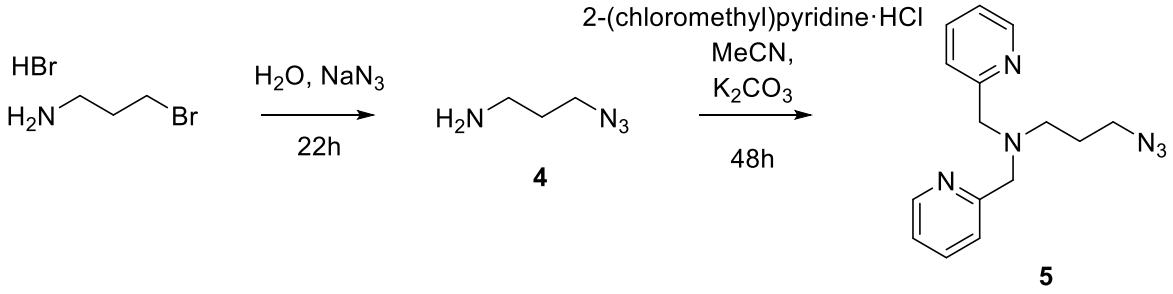

Scheme 2.6. Synthesis of Compound 5.

This synthesis of **5** differs from another recent preparation in the literature (Scheme 2.7)[78] in which the DPA scaffold of this compound was made using pyridine carboxaldehyde, and an amine with sodium triacetyoxyborohyride as the reducing agent.

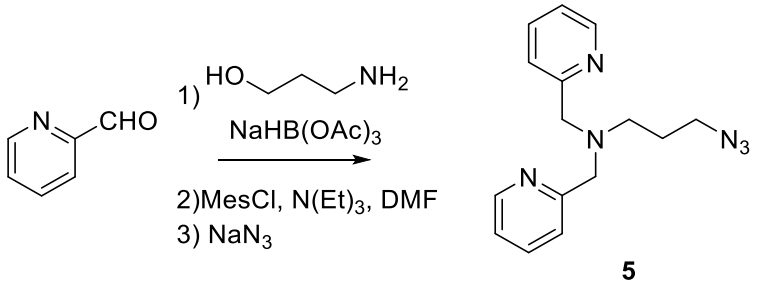

Scheme 2.7. Reported literature synthesis of Compound 5.

The synthesis of DPA-alkyne **(6)** (Scheme 2.8) was performed as described in the literature.[105] The work-up was straightforward, including filtration of the solid base and washing with acetonitrile to collect the product. Compound **6** was used without further purification for the click reaction to form the triazole target **13** (Scheme 2.9).

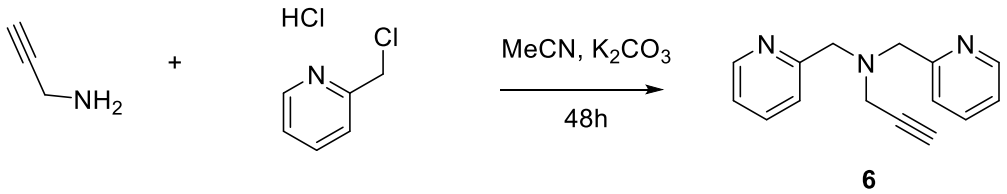

Scheme 2.8. Synthesis of Compound 6

2.3.2. TPEN Analogue Synthesis

The synthetic procedure for **13** (Scheme 2.9) involved dissolution of **5** and **6** in a 1:1 isopropanol:water solution with 2.2 equivalents of copper sulfate and 4.4 equivalents of ascorbic acid for three days. The product, as a Cu-complex, was observed by mass spectrometry (Figure S.15). This reaction was following by IR spectroscopy by monitoring the loss of azide stretch of **5**. The loss of azide occurred over the course of approximately 2 hours before the concentration of **5** was below detectable limits. In previous attempts of this reaction, the initial starting concentrations of the starting materials (i.e. compounds **5** and **6**) were below the detection limit of the IR spectrometer. Therefore, the use of IR spectroscopy was only used to determine that the reaction was proceeding (provided the starting materials were concentrated enough) rather than to determine the completion of the reaction. The reaction was left to allow an abundance of time for the reaction to go to completion. Unfortunately, after using Chelex® to remove the copper from the reaction mixture, a brown solution was obtained in which the product was not observed to move by TLC on silica or alumina using 100 % DCM, and increasing polarity by adding methanol and ammonium hydroxide solution (28 % in H_2O). An alternative reaction using acetonitrile (to stabilize Cu(I)), CuI, and DIPEA was also investigated, but there was no improvement in product formation by using this method. Compound **13** was very difficult to isolate by column chromatography or by extraction. In the future, further attempts to determine eluent conditions for column chromatography using reverse-phase silica can be performed.

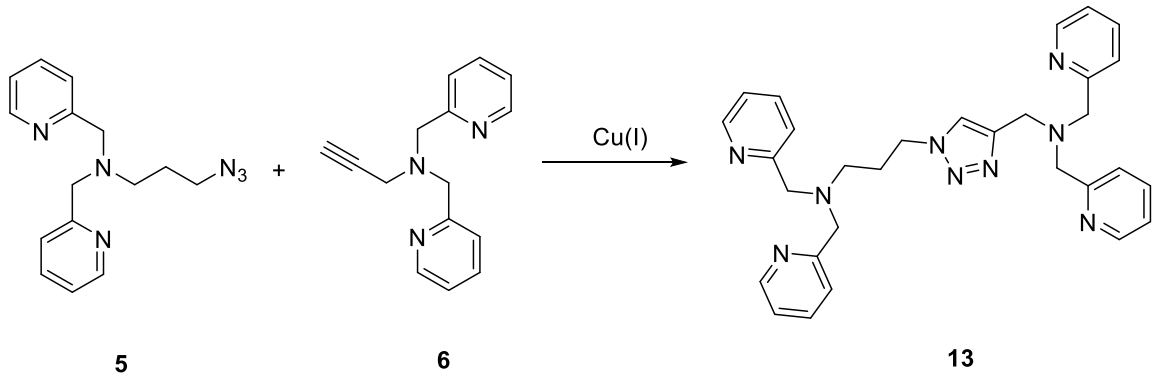

5 **6** **13**

Scheme 2.9. Synthesis of Compound 13.

Further attempts to isolate this compound by high pressure liquid chromatography (HPLC) were performed. The HPLC chromatogram of **13** was compared to compounds **5**, and **6** (Figure 2.3). The target TPEN analogue (**13**) exhibited two peaks that did not appear in compounds **5**, or **6**. Using the procedure described in **2.2.4**, the retention time for these peaks were 0.57 minutes whereas the retention times for **5** and **6** were 2.72 minutes and 1.43 minutes respectively. Further experimentation is required to determine that one of the new peaks is Compound **13**, and if confirmed, these results suggest that this HPLC method may be a useful protocol for purifying the TPEN analogue **13**.

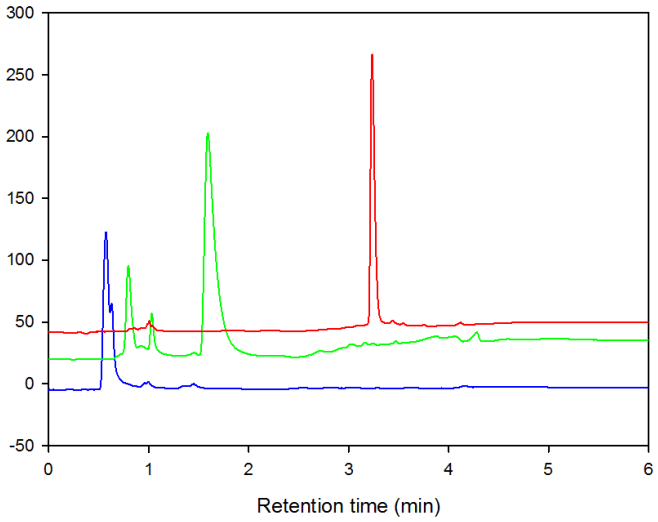

Figure 2.3. HPLC Chromatograms of Compounds 5 (red), 6 (green), and 13 (blue). See Section 2.2.4 for conditions.

2.3.3. Synthesis of a Mixed Acid / Pyridine Ligand

The synthesis of an alternative chelator where it would be easier to isolate the triazole product was undertaken. Exchanging two pyridyl moieties for t-butyl esters would make the new triazole product less polar, allowing for the triazole to be more easily purified before final deprotection to form a bis-carboxylic acid. The synthetic schemes for the components made it more reasonable to amend the synthesis of the alkyne to adopt a less polar character. Propargyl amine was reacted with 2 equivalents of bromoacetic acid *tert*-butyl ester to afford **7** (Scheme 2.10).

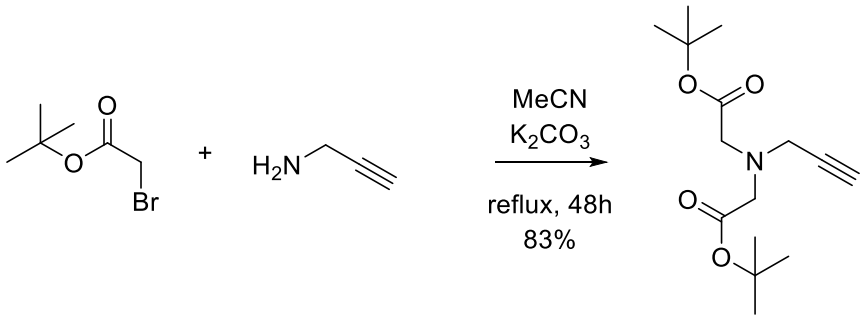

7

Scheme 2.10. Synthesis of Compound 7.

The decreased polarity of **7** required a less polar solvent mixture for the subsequent click reaction. Therefore, the reaction conditions were augmented to accommodate solubility of **7** and to allow for a different Cu(I) source to be used. Acetonitrile was chosen to promote Cu(I) stability, since Cu(I) is the active catalyst for CuAAC.[74] The product of this reaction is a copper chelator, therefore an excess concentration of CuI was used. Work-up of this reaction did not require Chelex® since a pH 10 EDTA solution could be used to chelate all of the copper in solution. This liberated the ligand (**9** or **11**), which was then be extracted with ethyl acetate, and purified via column chromatography.

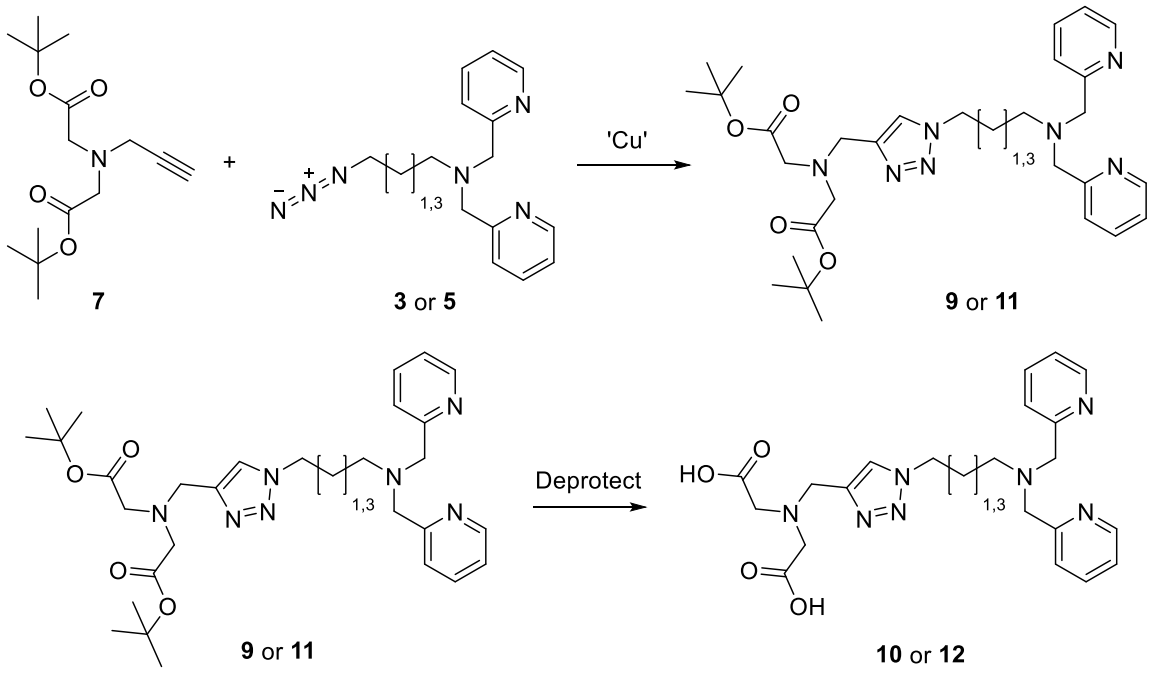

Scheme 2.11. Synthetic scheme for alternative hexadentate ligands using Compound 7 and Compounds 3 or 5 to afford Compounds 9 or 11, and then 10 or 12 following deprotection.

The isolated t-butyl ester product (**9** or **11**) was deprotected in two ways to afford final target **10** or **12**. The first of which involved dissolving the product in a 1:1 solution of trifluoroacetic acid (TFA) and DCM. This was then stirred for ~16 hours, and concentrated *in vacuo*. It was found via NMR that DCM was difficult to remove. An acid salt exchange of the compound was then performed. The TFA salt of this compound was dissolved in approximately 10 % HCl solution (~1 mL), then the product was concentrated *in vacuo*. This removed TFA by replacing the trifluoroacetate counterion with chloride, which allowed for TFA to be removed *in vacuo*.[19]F NMR could no longer detect any TFA in the sample.

The second method was to dissolve **9** in a 10 % HCl solution. This was also allowed to stir for ~16 hours, and was then concentrated *in vacuo*. The method was equally as effective, and circumvented the issue of removing TFA or DCM. This product is likely a mixture of HCl salts (i.e. ammonium chloride and pyridinium chloride). This suggestion is based upon the isolated mass of the material. The deprotection of **11** to afford **12** (Scheme 2.11) was performed by dissolving the protected t-butyl ester **11** in ~1 mL of a 10 % HCl solution and the solution was stirred for ~16 hours. The solvent was then

concentrated *in vacuo* affording **12** as a mixed HCl salt. The products (**10** and **12**) are hygroscopic, pale yellow/brown solids.

2.3.4. Metal Binding Stoichiometry

The Cu(II) binding stoichiometry of ligands **10** and **12** were investigated using a Job's plot analysis.[107] Varying the ligand to metal ratios while keeping the sum of the ligand and metal concentrations constant showed that the complexes prefer a 2:1 ligand to metal ratio under the conditions studied (Figure 2.4). The decision to perform the Job's plot analysis using Cu(II) rather than Cu(I) (the oxidation state of copper in the cell) is based upon the fact that trientine is a Cu(II) chelator[100] that is effective at treating Wilson's disease, and the solubility of Cu(II) species in aqueous solutions, whereas Cu(I) species tend to be insoluble.

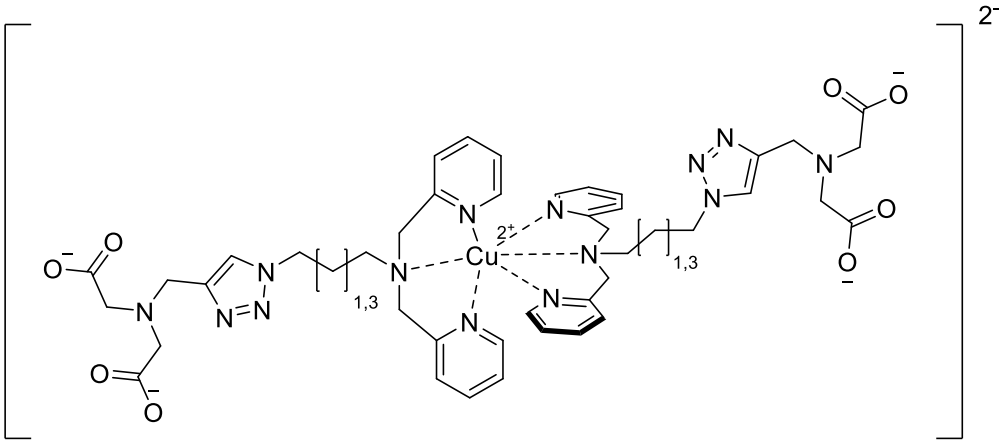

Figure 2.4. Proposed structure of the Cu-complex of compounds 10 or 12 as determined by the Job's plot analysis.

The analysis was performed in 12 mM pH 7.4 PBS, holding the sum of the ligand and metal concentrations at 1.33 mM. This relatively high concentration allows for the observation of a d-d band transition in the visible region. EDTA and DPA were chosen as the analogues for the two binding moieties of the ligands **10** and **12**. The spectrum for Cu-EDTA (Figure 2.5A) exhibits a peak increase at 755 nm, which is one of the known absorbances for Cu-EDTA.[111] It is important to recognize that the y-axis of the Job's plots are adjusted absorbances. This is to take into consideration the molar absorptivities of the

ligand and the metal in the metal-binding analysis (Equation 2.3). The molar absorptivities for the ligand and metal are calculated using the absorbance at a given wavelength during the 0:1 L:M and 1:0 L:M measurements. The plot shape of the Job's plot (Figure 2.5B) suggests that a strongly bound copper-complex was formed (Log K = 18.70)[97] due to its sharp maximum.[107] The Cu-EDTA complex exhibits a 1:1 L:M ratio (Figure 2.5B), which is expected.[111] The UV-Vis spectrum for Cu-DPA (Figure 2.6A) was found to exhibit an absorbance at 666 nm, but the apex of the Job's plot (Figure 2.6B) was not as well-defined in comparison to Cu-EDTA. This broader apex suggests weaker binding;[107] it is known that DPA binds more weakly than EDTA to Cu(II) (EDTA Log K = 18.70 vs. DPA Log K = 14.4)[97, 101]. Another potential source for error may include competing equilibria with copper and the phosphate of the buffer.

$$Adjusted\ absorbance = Measured\ absorbance - (\varepsilon_M[M] + \varepsilon_L[L]) \quad \textbf{Equation 2.3}$$

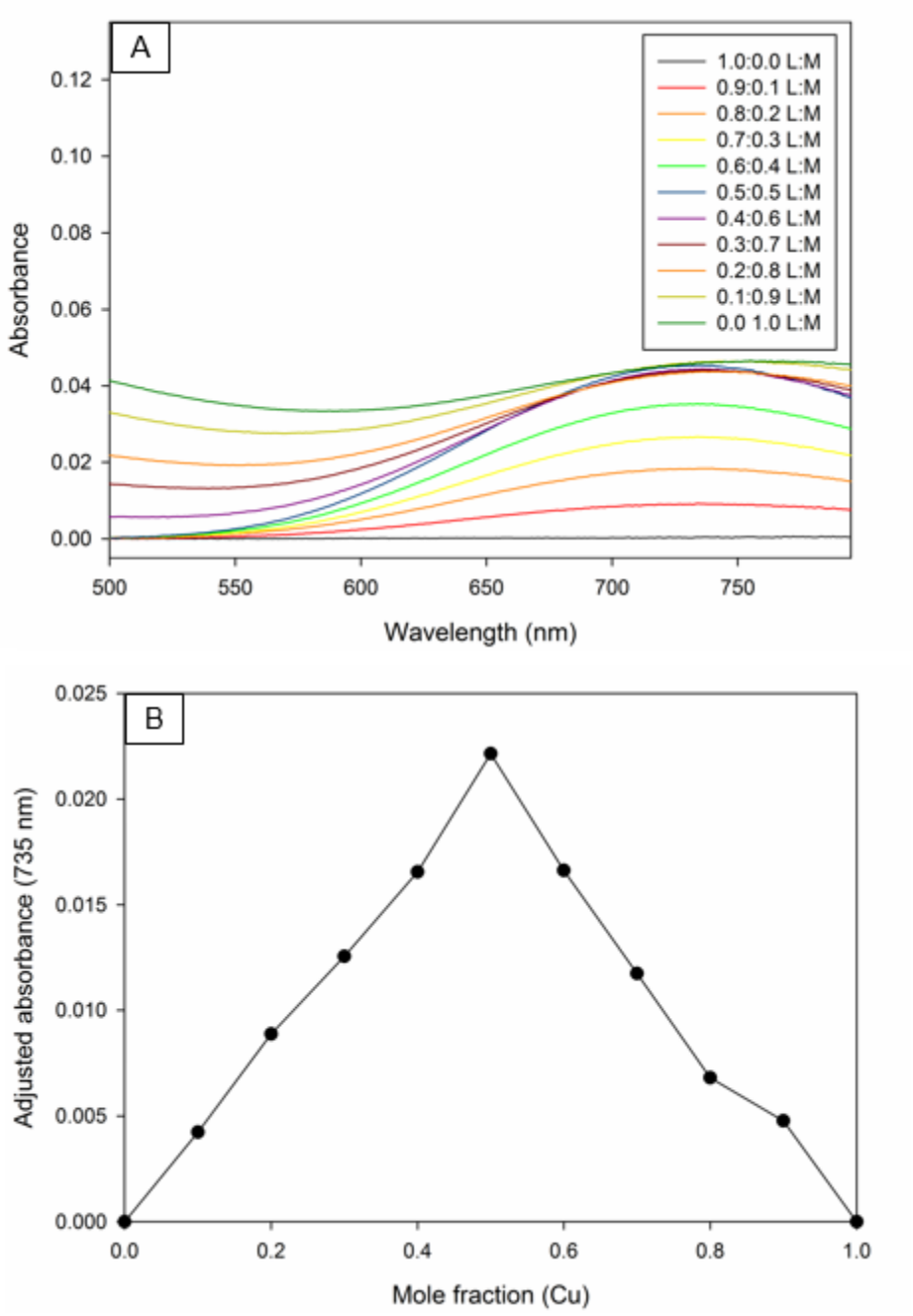

Figure 2.5. **UV-Vis spectrum (A) and Job's plot (B) of EDTA in 12 mM PBS at pH 7.4 at 1.33 mM total ligand and copper concentrations.**

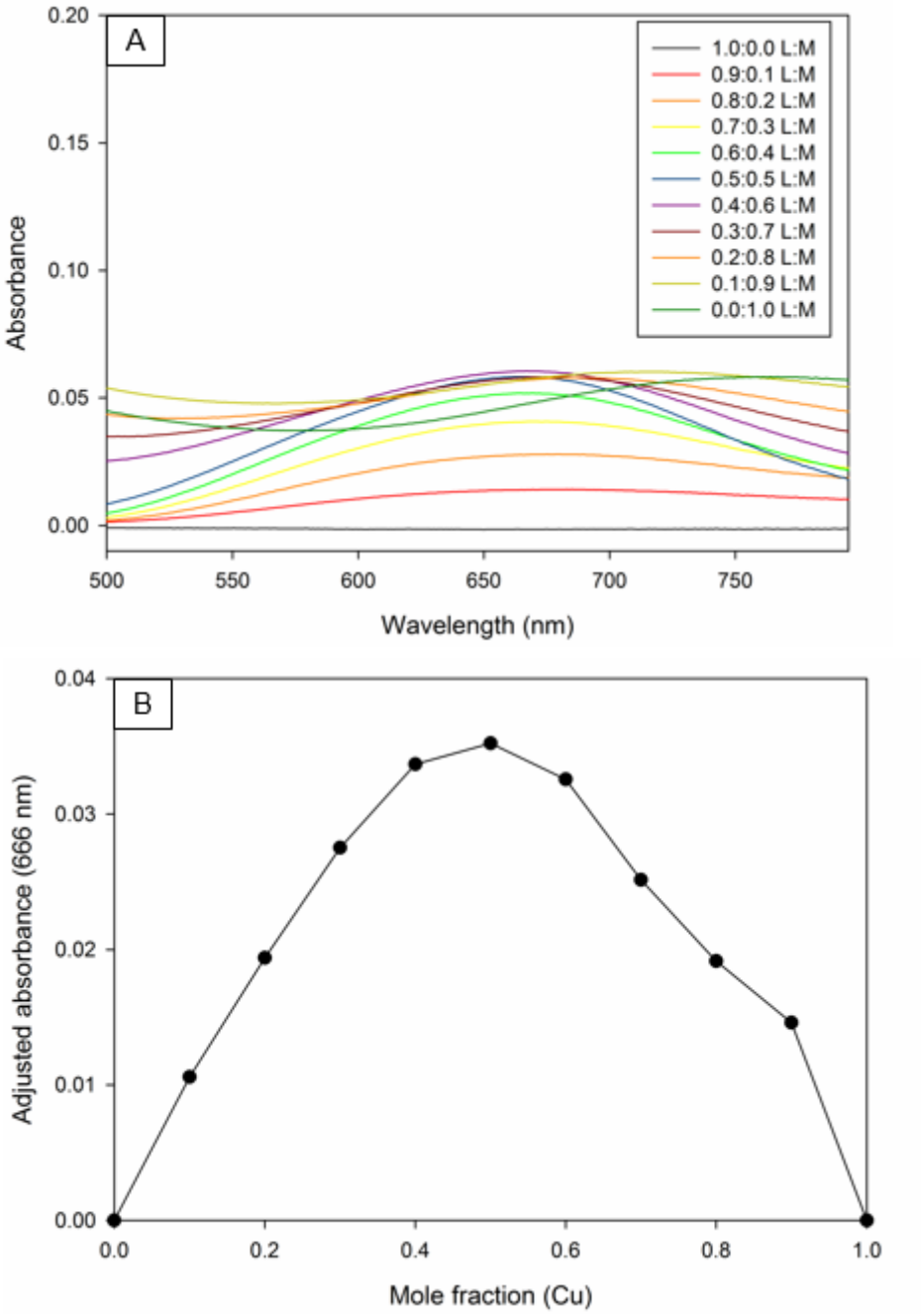

Figure 2.6. UV-Vis spectrum (A) and Job's plot (B) of DPA in 12 mM PBSat pH 7.4 at 1.33 mM total ligand and copper concentrations.

In performing the Job's plots for ligands **10** and **12**, it was found that the wavelengths of 645 and 655 nm (typical electronic transitions of a Cu(II) complex),[111-112] were the most useful to investigate the stoichiometry of the ligand to metal ratio of the complex formed. Comparison of these plots (Figures 2.7A, 2.8A) to those of EDTA and DPA (Figures 2.5A, 2.6A) suggests that it is likely the DPA components of **10** and **12** are responsible for binding to copper rather than the iminodiacetic acid (IDA) components. The wavelengths observed in the plots were most similar to DPA (645 nm for DPA[113], 755 nm for EDTA[111]), which suggests ligand binding that is more similar to that of DPA than EDTA. Furthermore, it is known that the binding constant for Cu-DPA is greater than that of Cu-IDA ($Log\beta_{12}$ Cu-DPA = 19.0, $Log\beta_{12}$ Cu-IDA = 16.7).[97, 101] Therefore, it is reasonable to suggest that the DPA component is binding under the conditions studied.

The Job's plots (Figures 2.7B, 2.8B) show maxima between 0.3 and 0.4 mole fractions of copper. These plots do not exhibit sharp maxima, so it can be inferred the ligand either weakly bind copper or a mixture of binding stoichiometries occurs.[107] From these experiments, it is not possible to tell with certainty about the stoichiometry of the complexes formed. Calculated best fits through the data on each side of the Job's plot (Figures S16, S17) suggest a 2:1 L:M ratio with intersections at approximately 0.33. At this point, crystalizing the complexes may be the best way to determine stoichiometry, albeit with the caveat that the crystal structure is not necessarily a perfect model for ligand-metal binding in solution.

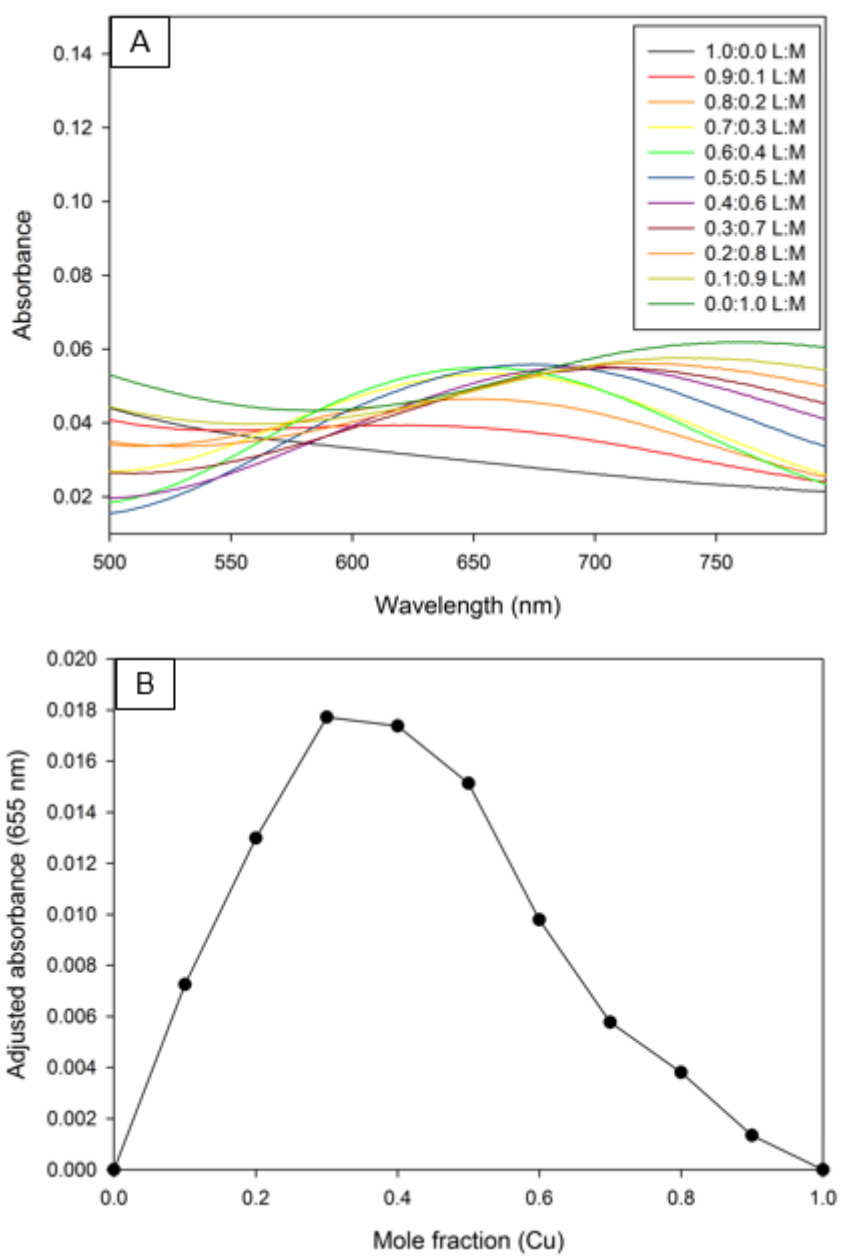

Figure 2.7. **UV-Vis spectrum (A) and Job's plot (B) of Compound 10 in 12 mM PBS at pH 7.4 at 1.33 mM total ligand and copper concentrations.**

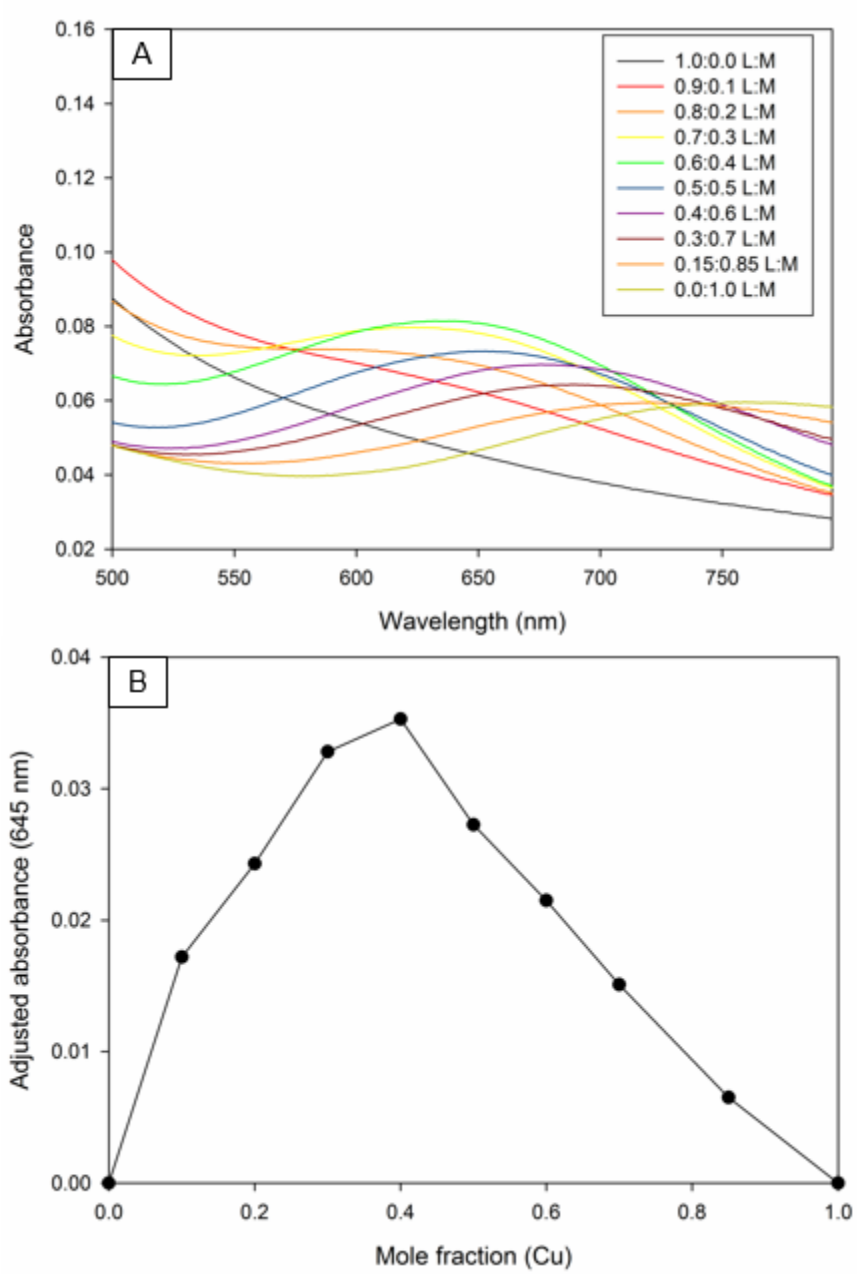

Figure 2.8. **UV-Vis spectrum (A) and Job's plot (B) of Compound 12 in 12 mM PBS at pH 7.4 at 1.33 mM total ligand and copper concentrations.**

2.3.5. pK_a Determination of Compounds 10 and 12

The pK_a values of compounds **10** and **12** were determined via titration and ^{1}H NMR analysis. The compounds were initially dissolved in D_2O, and NMR spectra were collected. Using NaOD and DCl to increase and decrease the pH, NMR samples were collected at approximately 0.5 pH unit intervals between pH 1.2 and 11.6. The chemical shifts of each of the proton resonances in the spectra collected of **10** and **12** were plotted as a function of pH, and sigmoidal curves were further evaluated. The designation of the proton resonances in **10** and **12** was based upon chemical shifts of the starting materials, the multiplicity, the coupling constants, and predicted shifts (Figure 2.9).

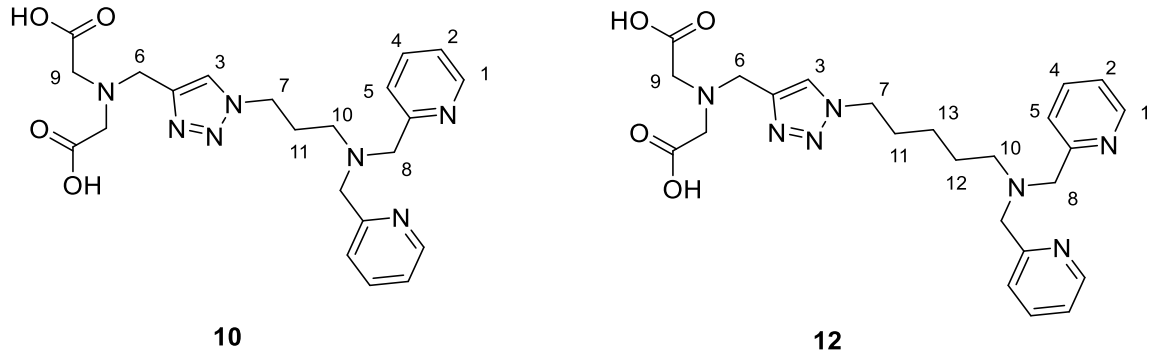

10 **12**

Figure 2.9. Structures of Compounds 10 and 12 with proton resonance assignments ordered based upon chemical shifts from most upfield to least upfield.

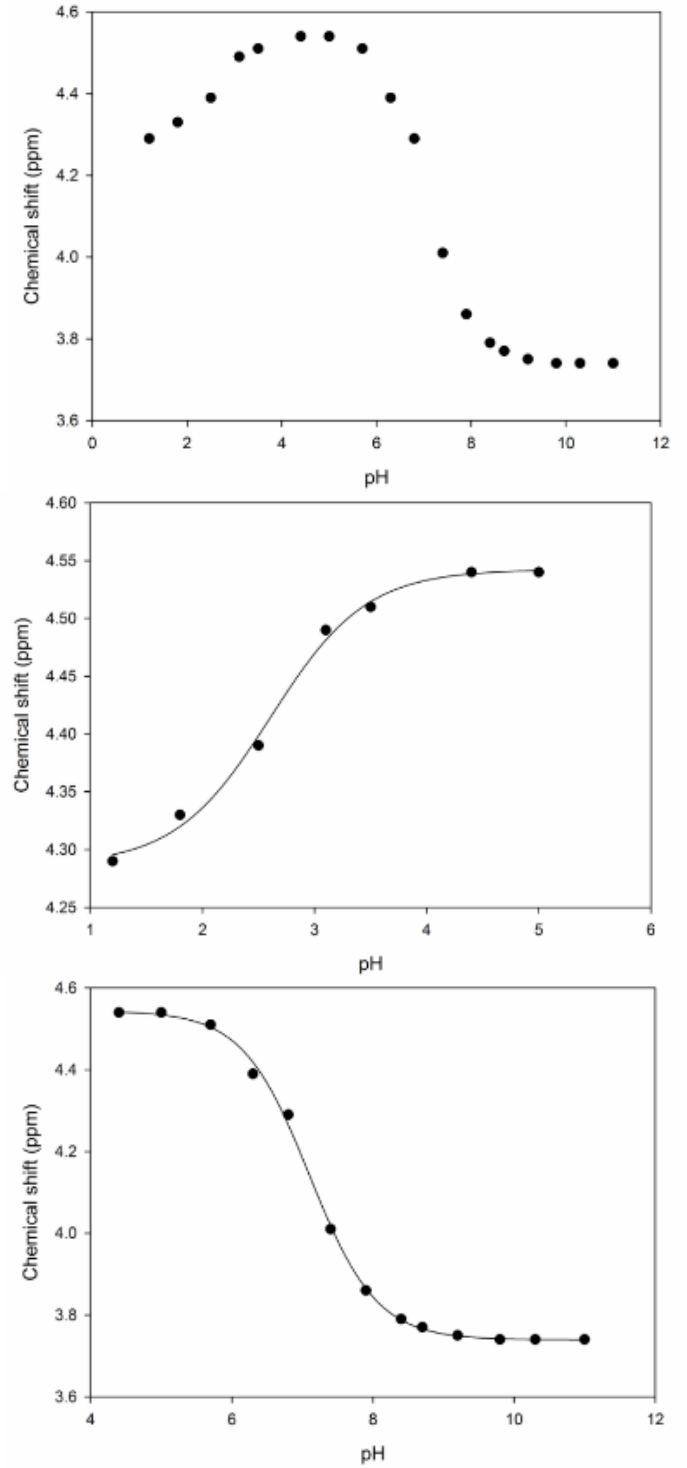

Figure 2.10. NMR titrations of the H_8 of Compound 12 without any fit, and then sigmoidal fitting for the two inflection points.

By plotting the chemical shifts against pH (example in Figure 2.10 and remainder in Figures S.19-S.29, S.31-S.43), the pK_a values of these compounds were elucidated by using Equation 2.4 to best fit the data with calculated R^2 values (Figures S.18, S.30).

$$f = y0 + \frac{a}{1+\exp\left(-\frac{x-x0}{b}\right)} \qquad \textbf{Equation 2.4}$$

This 4-parameter sigmoidal fit has $y0$, a, $x0$, and b as the parameters that are optimized to form the equations to determine the pK_a values of compounds **10** and **12**. The variable $y0$ is a vertical translation of the graph, a is the compression/expansion coefficient that will describe the "height" of the graph, $x0$ is the lateral translation of the graph, and b is the slope of the graph around the inflection point. Since the origin of a sigmoidal graph is at 0,0 on an x,y-plane and the x-axis is the pH, the optimized value for $x0$ is the inflection point (i.e. the pK_a). These values have to be changed from pD (since the experiment was performed using deuterated solvents) into pH using Equation 2.2.

Table 2.1. pK_a values for Compounds 10 and 12 as determined by NMR titration.

pK_a	Compound **10**	Compound **12**
1	3.21 ± 0.09	2.12 ± 0.07
2	5.51 ± 0.03	6.55 ± 0.03
3	7.42 ± 0.05	7.45 ± 0.02

The pK_a values in Table 2.1 were determined using ^{1}H resonances of compounds **10** and **12**. These resonances were chosen based upon their proximity to the protonation site.

These experiments showed three pK_a values for both **10** and **12**. The proposed structures are shown in Figures 2.11 and 2.12. The most acidic proton is likely associated with one of the pyridines of the DPA moieties. Evidence to support this suggestion is that

the pyridine ^{1}H NMR shifts changed with pH to afford an inflection point at approximately pH 3 and 2 for **10** and **12** respectively (Table 2.1). To rationalize this observation, first consider the first protonation of DPA (pK_a = 7.29).[101] This protonation is associated with the secondary amine (analogous to the tertiary amine of **10** and **12**). The second pK_a (pK_a = 2.60)[101] would be the protonation at one of the pyridine moieties. This second protonation requires a relatively low pH in order to disrupt one of the N-H hydrogen bonds. The final protonation of DPA (pK_a = 1.12)[101] requires an even lower pH to disrupt another N-H hydrogen bond to protonate the second pyridine moiety. Refer to Figures 2.11 and 2.12 for the proposed protonations of **10** and **12** respectively. The protonation (at the tertiary amine) is proposed to exhibit a pK_a value of 5.50 for **10** and 6.55 for **12**. Compound **12** has a longer alkyl chain, which could reduce steric effects associated with the triazole, resulting in a higher pH necessary to protonate the tertiary amine of the DPA moiety of **12** (Figure 2.12). Both of these values are less than that of DPA since there is steric crowding that reduces the ability for a proton to effectively bind to the tertiary amine of **10** and **12**. The next protonation that was measured (at one of the pyridines) was found to exhibit pK_a values of 3.21 and 2.22 for compounds **10** and **12** respectively. A possible reason that **12** has a lower pK_a value in comparison to **10** (2.22 vs. 3.21) is that it is more difficult to disrupt the binding of one of the N-H hydrogen bonds. With a sufficient alkyl chain length from the DPA-moiety, steric crowding interferes less with the binding and strength of binding to the proton, hence the pyridine protonation of **12** is of the same order as DPA (2.22 vs. 2.60).

To calculate these pK_a values for compounds **10** and **12** in Table 2.1, the proton resonances shown in Figure 2.9 with their corresponding label were used. Resonances H_2, H_4, and H_5 of **10** (Figures S.20, S.22, S.23) were compiled to approximate the pK_a of the pyridyl moiety, whereas resonances H_1, H_2, H_4, H_5, and H_8 of **12** (Figures S.31, S.32, S.34, S.35, S.38) were averaged to determine the pyridyl pK_a. It is unknown why resonances H_1 and H_8 (Figures S.19, S.26) of **10** did not fit this pK_a well, but resonances H_1 and H_5 (Figures S.31, S.35) of **12** did. The resonances used to determine the pK_a values of 5.59 and 6.55 (for **10** and **12** respectively) are H_8 and H_{10} since these resonances flank the amine in question, and should have the largest dependence on pH for the change of chemical shifts. Despite this proposed protonation site being at a tertiary amine (Figures 2.11, 2.12), the pK_a value differs from the protonation of other tertiary amines which tend to exhibit pK_a values in the range of 10-11 (e.g. pK_a of trimethylamine: 10.75).[97] It is

important to consider the whole molecule and the environment of the protonation site. Where there are multiple protonatable sites in the same region (e.g. DPA moieties of **10** and **12**), all electron donors contribute to proton binding (i.e. tertiary amine and pyridines). This pK_a value is still in the range that would be expected for DPA (pK_as of DPA: 1.12, 2.60, 7.29),[101] so the experimental value for the second pK_a in this thesis is reasonable based on the discussion above. Furthermore, with increased flexibility of the molecule with the pentyl-chain versus the propyl chain (Figure 2.12 vs. Figure 2.11), the pK_a values of **12** begin to approach those of DPA.

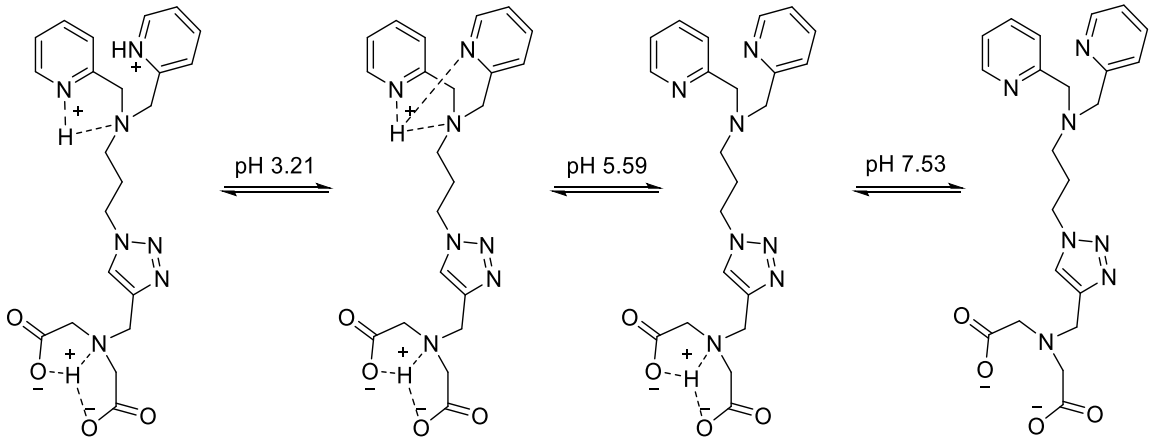

Figure 2.11. Proposed structures of protonation states of Compound 10.

The third pK_a of **10** at 7.53 and of **12** at 7.45 are expected to be associated with the IDA moiety of these compounds. The evidence for this is based upon the inflection point of the pH versus chemical shift plots associating with resonances H_6 and H_9 of **10** and **12** (Figures S.24, S.27, S.36, S.39). This pK_a is similar to the third pK_a of IDA (pK_a values of IDA: 1.82, 2.61, 9.34),[97] but it is slightly lower, perhaps due to the steric crowding of the triazole which reduces the "proton chelating" capacity of the IDA moiety of **12**. There was evidence of a second exchangeable proton using H_9 (Figure S.27, S.39) in **10** and **12**. However, there were not enough data available to determine another pK_a. Ultimately, the trend of a decreased pK_a of a tertiary amine (like that of **10** and **12**) being lower than that of a secondary amine (DPA and IDA) is consistent with trends that have been observed across other series of amines.[114]

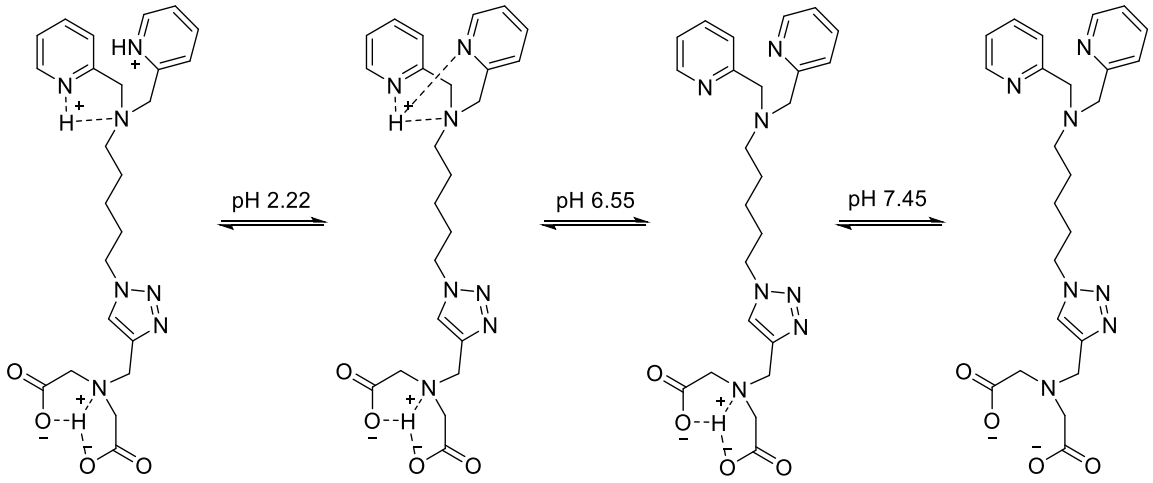

Figure 2.12. Proposed structures of protonation states of Compound 12.

It is important to determine the pK_a of **10** and **12** because the charge of the ligand at physiological pH can be used to gauge how well it can cross the cell membrane. If a species is negatively charged, it would be more difficult for it to pass through the cell membrane without utilizing cellular transport mechanisms. Compounds **10** and **12** are negatively charged at physiological pH. These two ligands both have a pK_a at approximately physiological pH (7.31 and 7.45 for **10** and **12** respectively), so it is expected that a mixture of -1 and -2 charged species will exist for each of these ligands at pH 7.4. The alkyne precursor to **10** and **12** (i.e. Compound **8**) would be expected to have a pK_a similar to the IDA component of ligands **10** and **12**, which would suggest that it would be negatively charged at physiological pH. The azide precursors to **10** and **12** (i.e. Compounds **3** and **5**) would also be expected to have pK_a values similar to those found to be associated with the DPA component of **10** and **12**. Therefore, **3** and **5** should both be neutral at physiological pH.

2.4. **Conclusions**

The pre-click precursors (**3**, **5**, and **8**) were successfully synthesized, but the TPEN analogue **13** has proven to be a difficult target to obtain. The protocol for HPLC purification of the target (**13**) has shown that Compounds **5**, and **6** can both be observed. There is significant separation between the potential product peaks and impurities that would allow for HPLC purification (Figure 2.3). Each of the pre-click targets (Compounds **5**, and **6**)

have distinct, sharp peaks in the chromatograms which suggest that in the future, HPLC would be an excellent method for isolating high purity pre-click products. Figure 2.3 shows that the crude reaction mixture of the TPEN analogue (**13**) has a different retention time from either of its pre-click precursors (**5** and **6**).

The DPA/IDA mixed targets were synthesized, and have a stoichiometric ratio of 2:1 ligand to copper binding under the current conditions (using Cu(II) in a solution of pH 7.4 PBS). The Job's plot appears to resemble a weakly binding complex (as observed by a curved maximum of the plot rather than a sharp maximum).[107] It is also possible that there may be a mixture of stoichiometries or competing equilibria with phosphate in the buffer. At this point, it is uncertain if this is the type of complex that would be formed *in situ* because the oxidation state of the copper catalysing the CuAAC is Cu(I), whereas the copper added during the Job's plot is Cu(II), and the local environment of the CuAAC might allow for the catalytic copper ion to be chelated differently than the pre-formed ligand chelating adventitious copper in solution.

There were found to be three exchangeable protons for each of the click targets as determined by NMR pH titrations. For Compound **10**, these values were 3.21 ± 0.09, 5.59 ± 0.03, and 7.53 ± 0.05, and for Compound **12**, these values were 2.22 ± 0.06, 6.55 ± 0.03, and 7.45 ± 0.02. These pK_a values are important because they describe the charge of the ligands (**10** and **12**) at physiological pH. A neutral or positively charged species will likely pass through the cell membrane more easily in comparison to a negatively charged species.

Chapter 3.

Design of a Biomimetic Analogue to CusF

DFT calculations[83] and structures completed by Tim Storr. PyMol structures drawn by Ryan Clarke.

3.1. Introduction

Nature has always been an inspiration for chemists. Understandably, to attain selectivity of a catalytic process, or the detection of a given analyte, chemists have investigated biologically-inspired systems. These biological mimics are classified as "biomimetic," and the applications of biomimetics in the field of chemistry range from medicinal[115] to agricultural[116] to polymers[117] to affinity chromatography.[118]

Copper is an abundant, and biologically essential metal and, as mentioned in Chapter 1, there are numerous ways for copper to be incorporated into biological systems. Although essential for life, one can only accumulate a certain amount of copper before it becomes toxic. The regulation of copper is tightly controlled, and effects of dysregulation can lead to significant toxicity.[10] In Chapter 1, the effects of dysregulation with respect to human biology was discussed, but other organisms also require copper. Since the goal of this thesis is to develop a copper chelator that will effectively remove copper from hepatocytes, using the concept of biomimetics to design a new ligand to bind copper could be a viable method of achieving this goal. A biomolecule from *Escherichia coli* that is known to bind copper was chosen as the inspiration for scaffolding a new ligand to bind to Cu(I). This biomolecule is a protein called cation efflux system protein CusF (CusF).[119] It is a component of the system responsible for trafficking copper in *E. coli* (CusF K_d: 2.72 ± 2 μM).[120] This system is called the CusCFBA Cu(I)/Ag(I) resistance system that is a part of a greater family of metalloresistance systems responsible for effluxing Cu(I) and Ag(I) in Gram negative bacteria.[121] The Cu-binding site is composed of a histidine at residue 36, and two methionine residues at 47 and 49 (Figure 3.1).[122] These three residues are

responsible for Cu(I) binding, although tryptophan residue 44 is hypothesized to interact with copper through its π-electrons.[122]

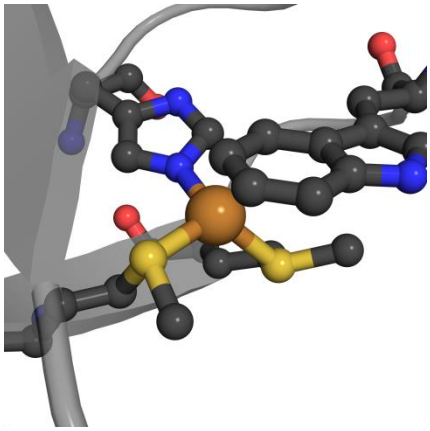

Figure 3.1. Active site of CusF with Cu(I) bound to two Met residues, and a His residue with an adjacent Trp residue (PDB: 2VB2).

To synthesize a biomimetic analogue of the metal-binding site shown in Figure 3.1, modeling was first performed. The methionine residues were replaced by ethyl methyl thioethers, and the histidine residue was replaced by an imidazole. To continue with the theme of click chemistry, these two components should then “click” together to form a triazole in the presence of copper (Scheme 3.1). Triazoles have aromatic character,[123] and in this case, the triazole is used as an analogue to tryptophan, at least with respect to the π-electron interactions.

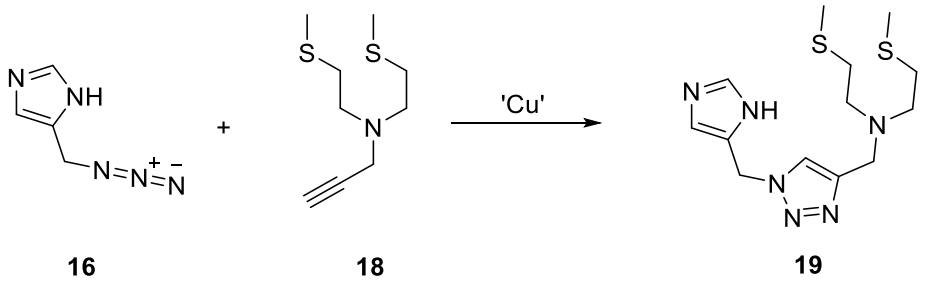

16 18 19

Scheme 3.1. Azide-appended imidazole, and alkyne-appended bis-ethylmethyl thioether click together to form an analogue of CusF copper binding site.

The resulting compound is predicted to have a high affinity for Cu(I) which is the oxidation state of copper that CusF binds.[120] This is also the oxidation state of copper that is known to be catalytically active for CuAAC,[124] and the oxidation state of copper that is predominant within cells.[125] Furthermore, Cu(I) is also responsible for Fenton-like chemistry,[25] and since this ligand should effectively bind Cu(I), levels of ROS should decrease. It is expected that Cu(I) will bind to the ligand in the manner shown in Figure 3.2.

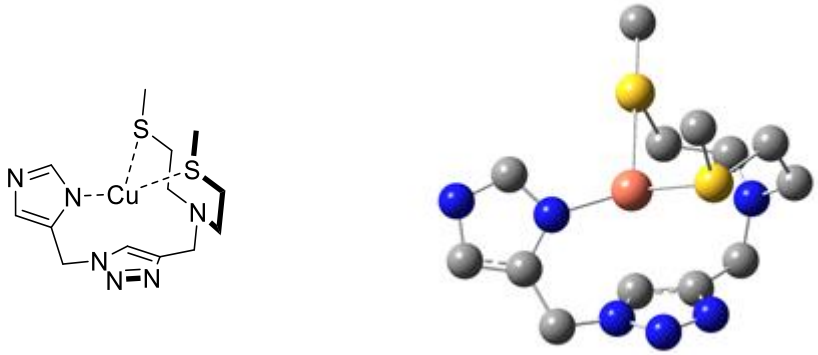

Figure 3.2. Perspective of Cu-19 with DFT prediction of Cu-19 (calculated with the uB3LYP functional of the 6-31g(d) basis set). Grey: carbon, blue: nitrogen, yellow: sulfur, copper: copper.

3.2. Experimental

Caution: The synthesis of compounds with pendent azides can be hazardous. Azides are known to be sensitive to friction and temperature, and are potentially explosive. Handle with care, and keep in solution whenever possible. All ^{1}H and ^{13}C NMR are compiled in the Appendix (Figures S.44 – S.49).

3.2.1. Synthesis

(1*H*-imidazol-4-yl)methanol hydrochloride (14)

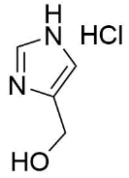

The reagent 4(5)-(hydroxymethyl)imidazole (1.000 g, 10.2 mmol) was dissolved into concentrated HCl (11.65 M, 1.025 g, 10.2 mmol). After dissolving, H_2O was removed *in vacuo* to afford the product. Yield: 1.443 g (100 % conversion).^{1}H NMR (MeOD): 8.885 (d, 1H, *J* = 1.4 Hz), 7.475 (m, 1H), 4.68 (d, 2H, *J* = 0.8 Hz). ^{13}C NMR (MeOD): 135.41, 135.20, 117.21, 54.80.

4-(chloromethyl)-1*H*-imidazole hydrochloride (15)

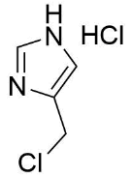

This synthesis differs from the literature protocol by dissolving 4(5)-(hydroxymethyl)imidazole hydrochloride into neat $SOCl_2$ and stirring at room temperature rather than dissolving 4(5)-(hydroxymethyl)imidazole hydrochloride and $SOCl_2$ into benzene and refluxing.[126] The reagent 4(5)-(hydroxymethyl)imidazole hydrochloride (1.580 g, 11.74 mmol) was dissolved in $SOCl_2$ (1 mL). The reaction was stirred for two

hours at room temperature uncapped, the $SOCl_2$ had evaporated and a further 2 mL of $SOCl_2$ was added to allow the reaction to continue. The vessel was closed and stirred at room temperature for ~16 hours. The remainder of the $SOCl_2$ was removed *in vacuo* to afford **15**. Yield: 1.388 g (88 %). ^{1}H NMR (MeOD): 8.97 (s, 1H), 7.65 (s, 1H), 4.82 (s, 2H). ^{13}C NMR (MeOD): 136.50, 131.82, 119.28, 34.50.

4-(azidomethyl)-1*H*-imidazole (16)

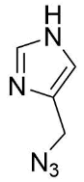

This compound was made as described in literature.[127] The reagent 4(5)-(chloromethyl)imidazole hydrochloride (0.530 g, 3.44 mmol) was dissolved in DMF (5 mL). Sodium azide (0.671 g, 10.3 mmol) was added to the solution and then stirred at room temperature for ~19 hours. Water (5 mL) and EtOAc (5 mL) were added to the solution. A 5 % $NaHCO_3$ solution (5 mL) was then added to the mixture to separate the organic and aqueous layers. The organic layer was collected and washed with water (2 x 5 mL). The organic layer was dried using $MgSO_4$, filtered and concentrated *in vacuo*. Yield: 0.187 g (44 %). ^{1}H NMR (MeOD): 7.70 (s, 1H), 7.14 (s, 1H), 4.28 (s, 2H). ^{13}C NMR (MeOD): 137.30, 134.76, 118.30, 47.96. IR (solution in MeOD): 2104 cm^{-1} (s, N_3), ESI (+)-MS m/z (M+1): 124.06.

bis(2-(methylthio)ethyl)amine (17)

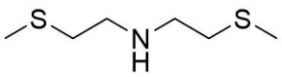

The synthesis of this product was attempted in two ways. One as previously described in the literature,[128] and another substituting the NaSMe salt with a ~15 % NaSMe solution in H_2O purchased from TCI-America (M0096). The reagent bis(2-chlorethyl)amine hydrochloride (1.589 g, 8.89 mmol) was added to a ~15 % solution of NaSMe in water (10 mL, ~1.5 g, ~21.42 mmol), and allowed to stir for20.5 hours. An

extraction using DCM (2 x 10 mL) was performed, and then the combined organic layers were dried using $MgSO_4$. The solid was filtered, and the product was concentrated *in vacuo*. Yield: 0.736 g (50 %). ^{1}H NMR ($CDCl_3$): 2.80 (t, 4H, *J* = 6.5 Hz), 2.62 (t, 4H, *J* = 6.5 Hz), 2.07 (s, 6H), 1.72 (s, 1H). ^{13}C NMR ($CDCl_3$): 47.64, 34.43, 15.35. ESI (+)-MS m/z (M+1 (25 %)): 166.07.

_N,N_-bis(2-(methylthio)ethyl)prop-2-yn-1-amine (18)

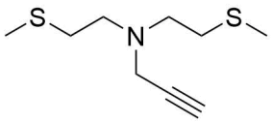

The reagent bis(2-(methylthio)ethyl)amine (0.113 g, 0.681 mmol) was dissolved in MeCN (1 mL) and 80 % propargyl bromide in toluene (76 µL, 0.081 g, 0.68 mmol) was added. The solution began to form a precipitate, which redissolved upon addition of trimethylamine ($N(Et)_3$) (69 µL, 0.050 g, 0.49 mmol). The reaction was stirred overnight (18.5 hours) at room temperature. The reaction mixture was concentrated *in vacuo*, and purified using silica gel chromatography. Eluent: 1 % MeOH in DCM. Yield: 0.068 g (49 %). ^{1}H NMR ($CDCl_3$): 3.44 (d, 2H, *J* = 2.2 Hz), 2.74 (dd, 4H, *J* = 8.6, 6.2 Hz), 2.58 (t, 4H, *J* = 8.6, 6.2 Hz), 2.19 (t, 1H, *J* = 2.2 Hz), 2.10 (s, 6H). ^{13}C NMR ($CDCl_3$): 78.27, 73.39, 53.13, 42.02, 32.17, 15.87. IR (neat): 2102 cm^{-1} (w, -CCH), ESI (+)-MS m/z (M+1): 204.09.

_N_-((1-((1_H_-imidazol-5-yl)methyl-1_H_-1,2,3-triazol-4-yl)methyl)-2-(methylthio)-_N_-(2-(methylthio)ethyl)ethan-1-amine (19)

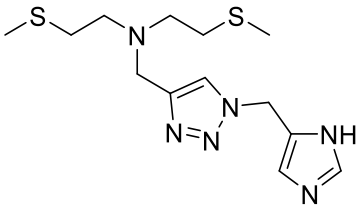

The reagent 4-(azidomethyl)-1*H*-imidazole (0.050 g, 0.405 mmol) and *N*,*N*-bis(2-(methylthio)ethyl)prop-2-yn-1-amine (0.082 g, 0.403 mmol) were dissolved in MeCN (1 mL). CuI (0.080 g, 0.420 mmol) was added and the mixture was sonicated to help dissolve CuI, and then diisopropylethylamine (350 µL, 0.260 g, 2.01 mmol) was added. The

reaction was stirred for 3 days at room temperature. Compound not isolated. ESI (+)-MS m/z (M+Cu (20 %)): 389.07.

3.3. Results and Discussion

3.3.1. Design and Synthesis

The design of the tridentate, triazole-containing ligand **19** was based upon the copper-binding site of CusF. Two methionines, a histidine, and a tryptophan are located at the copper-binding site of CusF.[120] The two thioethers of the methionine residues and the imidazole of the histidine residue bind to Cu(I) in a trigonal planar fashion[122] and a tryptophan lies parallel below this trigonal plane (Figure 3.1). It is hypothesized that the tryptophan interacts with the metal ion via π-electron interactions.[129] It is the simplicity of this binding site that inspired the development of a CuAAC product, where one component could represent histidine, while the second component represents the methionines and the triazole that binds these components together could be analogous to the tryptophan (Figure 3.2). DFT calculations performed by Dr. Tim Storr showed that the binding geometry of this target molecule to be similar to that of CusF (Figure 3.1). It was decided that the most facile synthetic method for Compound **19** would be the histidine analogue as an imidazole azide (**16**), and a bis-thioether alkyne (**18**) (Scheme 3.1). A transformation of the hydroxyl group of 4(5)-(hydroxymethyl)imidazole to yield a chloride leaving group which could then be transformed into an azide to afford the pre-click target **16.** The acid salt was prepared first so the thionyl chloride would react with the primary alcohol instead of simply affording the hydrochloride salt. This is summarized in Scheme 3.2.

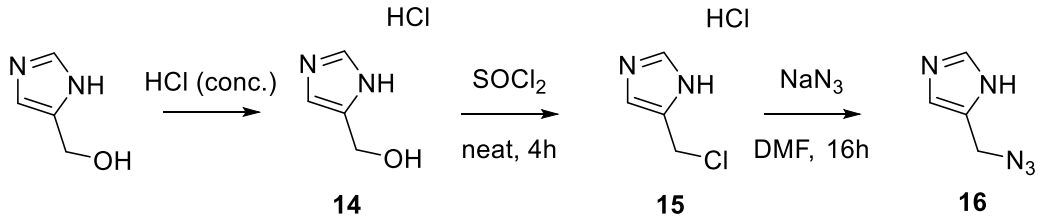

Scheme 3.2. Synthesis of 16, the His 36 analogue of CusF.

It is possible to combine the two steps by dissolving 4(5)-(hydroxymethyl)imidazole into neat thionyl chloride, and stirring for ~16 hours. Although there was 100 %

consumption of starting material as determined by ^{1}H NMR, there were approximately 10-15 % impurities that could not be identified. The bis-thioether amine (**17**) was synthesized from bis(2-chlorethyl)amine hydrochloride via reaction with sodium methylthiolate as a 15 % aqueous solution for 21 hours (Scheme 3.3). This forms the analogue for the two methionine residues (Met 47, Met 49).[122]

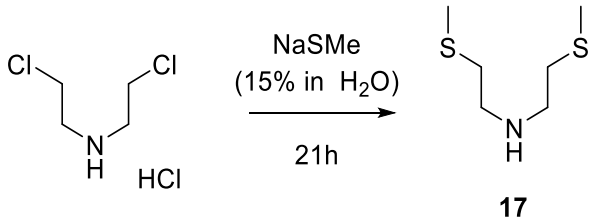

17

Scheme 3.3. Synthesis of 17 the Met 47, Met 49 analogue of CusF.

Propargyl bromide was reacted with the amine (**17**) tethering the two methionine residue analogues to afford the second half of the pre-click targets (**18**) (Scheme 3.4). The overall synthesis of the alkyne contained moderate yields, side-products, and was difficult to purify.

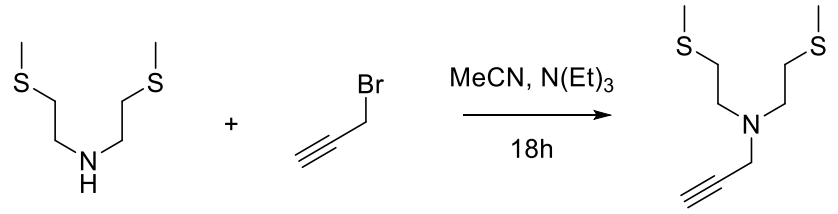

17 **18**

Scheme 3.4. Synthesis of Met 47, Met 49 CusF analogue with pendent alkyne.

The synthesis of **17** had a tendency of forming mixed products that could not easily be separated via column chromatography due to streaking of the product mixture on silica gel. Compound **17** has been reported, but the purification process involves distillation at 120 ^{o}C and 0.03 mbar pressure.[128] Attempts to replicate this purification procedure led to little success with most of the reaction mixture reacting further to go from a light brown oil to a dark brown oil. Only a small amount of product could be isolated using this purification method. The low yield and associated difficulty in purification could be due to competing reactions. Since this reaction is basic, there are three potential nucleophiles present

(hydroxide (from aqueous solution), sulfide and secondary amine), and they are all activated (i.e. sufficiently nucleophilic for S_N2 reactions at the chlorine-bound carbon). Therefore, numerous side reactions could occur.

The number of proton and carbon NMR resonances observed in the associated spectra support a mixture of products (Figure S.49). For example, there are numerous carbon peaks rather than the three that should be present for **17**, and there are additional proton resonances that should not be present. There are additional peaks in the mass spectrum (Figure S.50) of the product mixture observed that support by-product formation. Performing the reaction as described in the literature (i.e. using NaSMe as a salt rather than 15 % aqueous solution)[128] still leads to side-products (Figure S.51). It may be useful to attempt this reaction using a large excess of the sulfide, to reduce by-product formation by nucleophilic attack of the secondary amine. Another amendment to this synthesis could be to protect the secondary amine with a Boc group. This would inhibit some by-product formation by deactivating the amine. After formation of Boc-protected **17**, the protecting group could be removed and then reacted with propargyl bromide. Addition of the alkyne also appears to be a low-yielding step, but column chromatography allows for purification.

Attempts to isolate **19** were unsuccessful (Scheme 3.1). The concentration of the click materials were too low to observe the reaction via IR spectroscopy. Workup for the product has included Chelex® to bind excess copper as well as an attempted extraction with a basic EDTA solution. Although, chelation using basic-EDTA did remove the copper from the reaction mixture, and there was evidence of **19** formation by mass spectrometry (Figure S.52), the target (**19**) did not appear to be isolable via column chromatography. An alternative method to synthesize Compound **19** using different reaction conditions by dissolving the reactants in *i*-PrOH, and dissolving $CuSO_4 \cdot 5H_2O$ and ascorbic acid in water was also performed. Mixing the solutions together, and allowing the reaction mixture to stir at room temperature (RT) did appear to lead to the formation of the desired product, albeit with oxidation of the target as confirmed by mass spectrometry (ESI (+)-MS m/z M-1+Cu+O (50 %): 405.06). Compounds **18** and **19** both appear to be prone to oxidation as observed by mass spectrometry, likely at the sulfur. Consequentially, this must be considered when using these materials for subsequent reactions and experiments.

Performing this reaction under an inert atmosphere, such as nitrogen or argon may inhibit oxidation from occurring.

3.4. Conclusions

There were difficulties in synthesizing **17** which may be associated with side-reactions. This was supported by NMR and mass spectrometry data. The click product (**19**) was not isolated, however, the click precursors (**16** and **18**) could be isolated, but further optimization to improve the yield of **18** is required. The click product (**19**) was found to have been synthesized as a Cu(I) complex (as well as an oxidized ligand-Cu(I) complex) via mass spectrometry.

Chapter 4.

In Vitro Modeling of Wilson's Disease

4.1. Introduction

Wilson's disease affects the brain and liver, but the primary site for this disease is the liver.[29] A number of cell models have been used to study Wilson's disease including HEK293,[130] HepG2,[131] and WIF-B9.[68] For this research, it was determined that HepG2 would be the most appropriate cell line to use due to its ubiquity as a liver cell model[132] and literature precedence for use in Wilson's disease studies.[131, 133] It was previously established that copper concentrations in HepG2 cells increase significantly when incubated with Cu-enriched media.[131, 133] It is important to be aware of the limitations of using HepG2 when modelling Wilson's disease. HepG2 is an immortalized cell line (i.e. a cell line that will grow and divide indefinitely, provided it is given nutrients and space)[134] derived from a hepatocarcinoma from a 15-year old Caucasian male.[135] It is important to consider that this is a cancer cell line. Therefore, many cellular processes have been altered including genetic stability and metabolism.[136] In spite of these differences, it is still necessary to do what is possible to model this disease in the laboratory without relying on primary tissue samples of Wilson's disease patients. A new Wilson's disease model has been developed by knocking out ATP7B in the HepG2 cell line.[137]

For these studies, the most important part of modelling this disease is to increase the copper concentration in the liver cells to at least five times the basal concentration of the liver (from 50 µg Cu / g dry weight to 250 µg Cu / g dry weight),[52] since that is one criterion for Wilson's disease[52] and is considered to be the best available test for diagnosis of Wilson's disease.[138] The biological component of this project is based upon determining the background copper levels in HepG2 liver cells, and then growing the cells in copper-rich media to significantly increase intracellular copper levels. This would then be considered the diseased-state. From here, the cells would be treated with the drug candidates, and the copper levels would be measured. Success would be to demonstrate that the copper concentrations have been reduced compared to a negative control with

statistical significance. Ideally, the co-incubated pro-drugs would chelate all of the excess copper, and the copper levels would return to the basal concentration.

Copper concentration is typically reported as nmol Cu / mg protein,[133, 139] therefore it is necessary to measure the total protein content, and the copper content of a given sample. This circumvents cell counting, which then reduces the amount of error in reporting concentration with respect to number of cells. Protein concentration in this thesis are reported as a concentration in mg/mL, as determined by a Bradford assay. The copper concentration are reported in ppb as determined by inductively coupled plasma atomic emission spectroscopy (ICP-AES). The Bradford assay was performed in triplicate to quantify the protein concentration in the cells, and ICP-AES was performed in triplicate to quantify the copper concentration in the cells. By combining these values, the copper concentration can be reported in nmol Cu / mg protein.

4.2. **Experimental**

4.2.1. Cell Growth

HepG2 cells ordered from American Type Culture Collection (ATCC) (HB-8065) were stored in vapour phase nitrogen after receiving the shipment. These cells were grown in 10 mL of Dulbecco's Modified Eagle's Media (DMEM) (ATCC: 30-2002) and 10 % fetal bovine serum (FBS) (ATCC: 30-2020) in a 37 ^{o}C incubator using 5 % CO_2 air. The media was replaced every 3-5 days. Once the area of the flask had complete coverage by cells (i.e, 100 % confluent), they were then harvested. To harvest the cells after reaching maximal confluency, the media was removed from the cells and the cells were washed once with sterilised pH 7.4 PBS, then the saline solution was removed and the cells were incubated in approximately 3-5 mL of 1X Trypsin/ 0.37 mM EDTA solution (ATCC: 30-2101) or TrypLE (ThermoFisher Scientific: 12605-010) in the 37 °C incubator. Cells and trypsin media were removed and transferred to a 15 mL Falcon tube before transferring to microfuge tubes for pelleting and removing media.

The suspensions were spun down at 13 600 rpm for 2 minutes. The trypsin media was removed, and the pellet was washed twice with chilled pH 7.4 PBS. The cells were

then lysed using 500 µL of chilled lysis buffer. This buffer was prepared from pH 7.4 PBS, 0.1 % Triton X100, and 2 mM phenylmethanesulfonyl fluoride (PMSF). The PMSF was dissolved in isopropanol as a 100X stock and added to the PBS and Triton mixture just prior to usage. The mixture was homogenised with vigorous shaking. The mixture was held on ice for approximately 30-40 minutes with shaking every 10 minutes to ensure the mixture homogeneity. After this period of 30-40 minutes, the mixture was diluted two-fold using chilled PBS, then spun down in a centrifuge at 14 000 rpm at 4 ^{o}C for 10 minutes. The lysate supernatant was removed and stored in the freezer for use in future experiments.

4.2.2. Bradford Assay

The procedure for the Bradford assay was performed as described in the manual.[140] All measurements were performed in triplicate using a 96-well plate, and a bovine serum albumin (BSA) standards kit supplied in the Bradford reagent pack (OZ Biosciences: BA00100). The assay was performed using pH 7.4 PBS as the blank/diluent, 10 µL of blank, followed by 10 µL of each standard for a total of 8 standards ranging from 0 mg/mL to 1.500 mg/mL protein, and cell lysates were tested at 1X, 2X, 4X, and 8X dilutions. After addition of all standards and cell lysates (including dilutions), 140 µL of Bradford reagent from the Bradford reagent pack was added to each of these wells. Triton X-100 (which was used to lyse the cells) does not interfere with this assay at the concentration it is present in after the cell lysis protocol (0.05 %).[140] The mixtures were allowed to incubate for approximately 30 minutes. The mixtures were measured in a 96-well plate reader (Biotek Synergy 4 Multi-Mode Microplate Reader) using 595 nm as the absorption wavelength.

4.2.3. ICP-AES

Preparation of the cell lysate for measurement of copper using ICP-AES (Model: Horiba Jobin-Yvon Ultima 2) required the lysate to be diluted 2X using concentrated nitric acid to digest all of the proteins, and solubilize the metal ions. This mixture was allowed to sit for approximately 40 hours before being diluted 25X (using 2 % nitric acid) to dilute the acid to an appropriate concentration (4 % nitric acid) for instrumental analysis.

Standards were made using a stock solution of 1.000 ± 0.001 mg/L copper in nitric acid (Sigma Aldrich: 38996), and diluted using 2 % nitric acid in Millipore water.

4.2.4. Copper Doping and Chelation

The copper-histidine solution was prepared in ratios as previously described in the literature.[133, 139] To make the copper-enriched media, $CuSO_4 \cdot 5H_2O$ and histidine were prepared in a solution (1:10 ratio) which was then added to the media with a copper concentration of 100 µM. It is known that incubation of HepG2 cells with 100 µM copper and 1mM histidine is generally considered non-toxic[133, 141] up to approximately six weeks of exposure.[141] The solution was sterilized in a biosafety cabinet using a sterile filter. During copper-enrichment experiments, the cells were incubated in Cu-His enriched media for 24 hours. These cells were washed twice with PBS to remove any remaining copper-enriched media. These cells were then exposed to 100 µM of D-penicillamine, **5**, **8**, **10**, or 50 µM of **5** and **8** co-incubated (Figure 4.1), or PBS as a vehicle control. These solutions were prepared by dissolving the reagents in PBS to a concentration of 20 mM (with the exception of DPA-azide (**5**), which was prepared to a concentration of 10 mM because it required a small amount of HCl (~0.5 mL of 10 % HCl used) to solubilize it in PBS). These were then passed through a sterile filter into DMEM to produce a 10X solution. The final media was composed of 80 % standard DMEM, 10 % FBS, and 10 % 10X drug solution. The cells were then incubated for 24 hours before being washed and harvested as described. All conditions were performed in triplicate. Analysis of the products in the media after incubation was performed by HPLC as previously described in Section **2.2.4**.

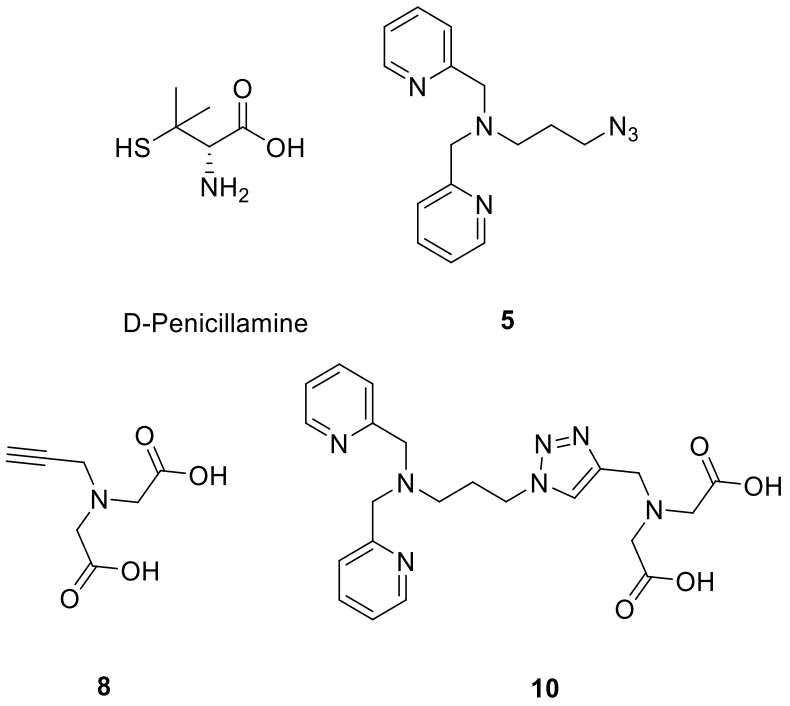

Figure 4.1. Structures of D-penicillamine, 5, 8, and 10 used in cell assays.

4.3. Results and Discussion

4.3.1. Bradford Assay

The Bradford assay was chosen since it is easy to perform and it has been used in literature for quantification of protein in whole cell lysates.[133, 139] This assay depends upon the chemical change of Coomassie Brilliant Blue G-250 (Figure 4.2) which changes from a maximum absorbance of 465 nm to 595 nm depending on the local environment of the molecule.[142] First, the dye is deprotonated, and interacts with the protein surface residues.[143] The assay was performed in triplicate.

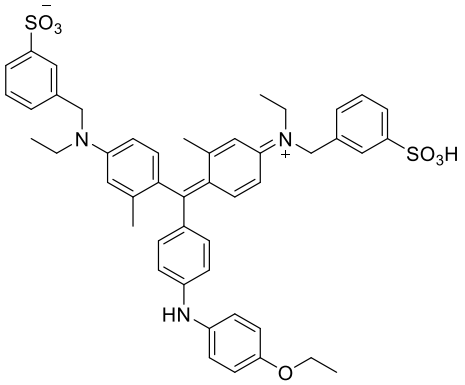

Figure 4.2. Structure of Coomassie Brilliant Blue G-250 in neutral form, the reagent responsible for the colourimetric response in the Bradford assay.

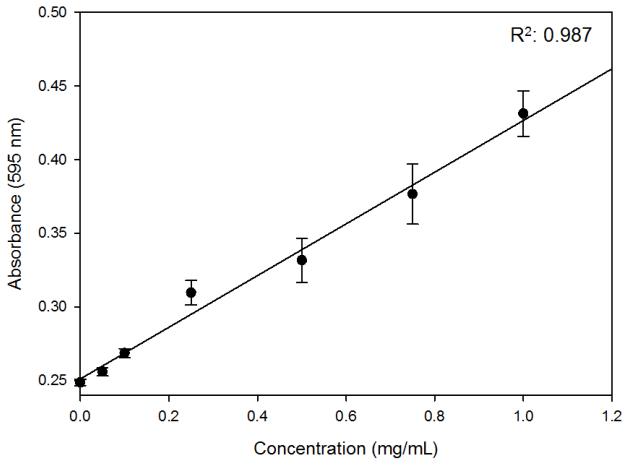

Figure 4.3. Bradford Assay calibration to determine protein content of cells under the treatment of 100 μM of Compound 10 using BSA.

The standards used for this assay are at concentrations of 0, 50, 100, 250, 500, 750, 1000, and 1500 μg/mL of BSA. The points used for the assay are only in the range where there is a linear relationship between protein concentration and absorbance (Figure 4.3). The data point at 1500 μg/mL could not be used because it no longer showed a linear relationship with the remainder of the curve. The unknown samples were diluted 2X, 4X, and 8X to ensure that at least one of the dilutions would fall within the linear range of the assay.

4.3.2. ICP-AES

The measurement of copper concentration can be performed by a number of instrumental techniques such as atomic absorption spectrometry (AAS), ICP-AES, and total reflection X-ray fluorescence spectroscopy (TXFS). Initially, AAS was investigated as a method to determine the copper concentration in HepG2 cells, but it became evident that the results obtained on the AAS (AI 1200 Atomic Absorption/Plasma Emission Spectrometer) were not reproducible because of a systematic drift in standard concentration values. It was determined that this drift existed when the standard concentrations were unable to be reproduced after generating the standard curve. It is likely due to the instrument having a working concentration range too high for the concentrations required by the experiments.

ICP-AES has lower detection limits than that of the AAS (AAS detection limit: 3 ppb, ICP-AES detection limit: 0.3 ppb).[144] Four spectral lines that were monitored on the ICP-AES were 223.008 nm, 224.700 nm, 324.750 nm, and 324.758 nm. The wavelengths with the most intense absorptions were 324.750 nm and 324.758 nm. The instrument can measure the standards at each of these spectral lines in the same experiment, allowing for the selection of a spectral line that provides the data with the least amount of error and/or the largest response. In this study, the line at 324.758 nm was used for measuring the copper concentrations of the samples because it had the lowest error and largest response in comparison to the other spectral lines. The standards used to evaluate the reliability of the standards ranged from 20 ppb to 100 ppb. The standards used to evaluate copper concentrations within the cells ranged from 20 ppb to 200 ppb. Attempted standards at 2 ppb, 5 ppb, and 10 ppb began to show a shift in the maximum peak of the 324.750 nm and 324.758 nm spectral lines. This suggested that there was a problem with the instrument's detection of copper at this concentration using these lower energy lines. The response at 223.008 nm and 224.700 nm was not strong enough to provide reliable measurements at these lower concentrations.

Three sets of experiments were performed on the ICP-AES. The first of which was to confirm that there was no significant systematic drift in the instrument as it ran the standards, and the standards could reliably reproduce the prepared concentrations. The second was to test the lower limit of the working range for this instrument to produce

reliable data and to measure the increase in copper concentration in HepG2 cells with incubation in media consisting of 100 μM copper and 1 mM His (Table 4.1). The standards for this experiment were made at 2, 20, and 100 ppb. The 2 ppb standard proved to be unreliable, and no different than the sample blank. From the 20 ppb standard, two samples of copper solution were made: 5 ppb, and 10 ppb. The measurements of the 5 ppb sample ranged from 6-12 ppb depending on the spectral line observed, and the measurements of the 10 ppb sample ranged from 11-19 ppb depending on the spectral line observed. The 20 ppb standard was tested, and it had a range of 19-22 ppb depending on the spectral line observed.

Table 4.1. Determining the lower working limit of ICP-AES for copper using four different spectral lines: 223.008 nm, 224.700 nm, 324.750 nm, and 324.758 nm.

Copper Conc.	223.008 nm		224.700 nm		324.750 nm		324.758 nm	
	Measure (ppb)	RSD (%)	Measure (ppb)	RSD (%)	Measure (ppb)	RSD (%)	Measure (ppb)	RSD (%)
Blank	6	9.04	1	42.73	8	3.63	8	1.58
2 ppb	7	10.81	3	7.49	5	4.36	5	7.19
5 ppb	9	10.40	6	5.81	12	1.19	12	3.00
10 ppb	13	4.50	11	6.53	19	1.37	18	2.56
20 ppb	22	6.92	19	6.17	22	2.03	22	2.01

This experiment found the lower working limit of the instrument to be at approximately 20 ppb despite the theoretical limit being 0.3 ppb for copper.[144] Since the calibration curve set up for this experiment included the 2 ppb point (which was unreliable), this slightly skewed the measurements of the 20 ppb standard. The intensities of the 223.008 nm and 224.700 nm spectral lines were too low for the instrument to provide reliable readings, hence the higher %RSD values. Even if the measured readings were inaccurate for the 324.750 nm and 324.754 nm spectral lines, the measurements were consistent, which provided lower %RSD values.

Table 4.2. Evaluation of the copper concentrations in HepG2 cells grown in the absence of copper-enriched media, and in the presence of copper-enriched media.

Growth Condition		223.008 nm		224.700 nm		324.750 nm		324.754 nm	
		Measure (ppb)	RSD (%)	Measure (ppb)	RSD (%)	Measure (ppb)	RSD (%)	Measure (ppb)	RSD (%)
-Cu	S1	5	20.59	1	39.74	2	6.93	2	2.46
	S2	7	13.52	1	25.35	7	18.56	6	1.55
	S3	6	2.61	1	47.27	6	5.24	6	2.03
+Cu	S1	136	1.67	134	2.52	196	3.03	195	1.30
	S2	141	3.58	142	1.31	201	1.47	202	1.58
	S3	154	0.94	153	1.83	228	0.20	226	1.06

The cells that were grown in unenriched copper media and enriched copper media were also evaluated for their copper concentrations (Table 4.2). The untreated cells sample did not have a copper concentration above the lower working limit of the instrument, whereas the Cu-His treated sample had concentrations greater than the reliable standards used (20 ppb – 100 ppb). The wide variation between the spectral lines of 223.008 nm and 224.700 nm with 324.750 nm and 324.754 nm is likely due to the observation of the peak signal shifting at 324.750 nm and 324.754 nm if the concentration of the standard was too low. Although no values could be determined from this experiment, the data suggests that there is a significant difference between the two growth conditions (i.e. copper enrichment versus no copper enrichment). These samples would be evaluated again in the next experiment on the ICP-AES with a new series of standards.

The third experiment on the ICP-AES tested the untreated and the Cu-His treated cell samples to evaluate their copper concentrations, as well as test conditions that will further be discussed in section **4.3.3**. In this experiment, only one of the samples of the untreated condition fell below the lowest standard. The other two samples of the untreated cells were found to have a copper concentration of 18 ± 17 nmol Cu / mg protein. There is a great amount of error associated with the untreated cells. The two samples that were in range of the calibration curve were 7.48, and 23.4 nmol Cu / mg protein. It is possible that there was copper contamination of at least one of the samples since there is a great increase in copper concentration from when these samples were tested and reported in Table 4.2 and those reported in Table S.1. The Cu-His treated cells were found to exhibit a concentration of 43 ± 9.8 nmol Cu / mg protein. Previous literature reported an increase in intracellular copper by approximately 30-fold,[133, 141] from 1.30 nmol Cu / mg protein to about 37 nmol Cu / mg protein,[133] which differs from the results of this experiment (Table 4.3). Calculations for error propagation utilize the root-mean-square error method as seen in Equation 4.1, and an example calculation can be seen in Equation 4.2 for the error propagation of the incubation of Cu-His treated cells with Compound **5** (see Section 4.2.4 for details).

$$\frac{\delta z}{z} = \sqrt{\left(\frac{\delta a}{a}\right)^2 + \left(\frac{\delta b}{b}\right)^2 \ldots \left(\frac{\delta y}{y}\right)^2} \qquad \textbf{Equation 4.1}$$

$$\partial z = 26.9 \frac{nmol\ Cu}{mg\ protein} \sqrt{\left(\frac{2.66}{24.2}\right)^2 + \left(\frac{-1.65}{28.6}\right)^2 + \left(\frac{-1.01}{27.9}\right)^2} = 3.48 \frac{nmol\ Cu}{mg\ protein} \qquad \textbf{Equation 4.2}$$

Since there is variability between the samples of each condition that is dependent upon sample preparation (e.g. differences in number of cells collected while growing cells in triplicate of the copper enriched media condition), all samples are individually calculated for their copper concentration, and then sample triplicates are averaged. Raw data can be found in Table S.1.

Table 4.3. Difference in levels of copper in HepG2 cells with and without 100 µM:1mM Cu/His media compared to the literature.

	No Copper (nmol Cu / mg protein)	Copper-enriched (nmol Cu / mg protein)
Arredondo *et al*., Am. J. Physiol. Gastrointest. Liver. Physiol. 2004[133]	1.30 ± 0.5	36.4 ± 4
Work in this thesis	18.1 ± 17.5	43.1 ± 9.8

4.3.3. Copper Loading and Chelation in Cells

There were six conditions that were tested. The negative control was PBS at pH 7.4. This served as the vehicle for the compounds, and allows for the measurement of how much copper is naturally excreted from the copper enriched cells over a 24 hour incubation period. The positive control for this experiment was the addition of D-penicillamine, which is the most common drug for the treatment of Wilson's disease.[29] This chelator is known to remove copper, therefore it is expected that incubating the disease model with this drug should reduce copper levels within the cells. Since the proposition for this treatment is a co-treatment of two compounds (**5** and **8**) that are activated upon reaching a high copper concentration (i.e. the cellular environment of the hepatocytes of Wilson's disease patients), both components of the click target compound (**10**) must be tested for their independent efficacies. The treatments are the target components (Compounds **5** and **8**), the click target (Compound **10**) and a co-incubation of each of the two pre-click components (Compounds **5** and **8**). The condition using a co-incubation of **5** and **8** would ideally be the treatment used to treat this disease, since they are both tridentate chelators that should click together to form a hexadentate chelator that would then form a complex with the endogenous copper in the liver.

Table 4.4. Concentration of copper in HepG2 cells that have been incubated for 24 hours in a 100 μM solution of Cu-His (1:10 Cu:His ratio), then treated with 100 μM of D-penicillamine, Compound 5, Compound 8, Compound 10, or 50 μM Compound 5 + 50 μM Compound 8 for 24 hours.

Test Condition	Copper Concentration (nmol Cu / mg protein)	Relative Concentration in comparison to control
Control	33 ± 27	1.00 ± 0.80
D-Pen	38.2 ± 16	1.15 ± 0.47
5	26.9 ± 3.5	0.81 ± 0.11
8	32.7 ± 6.1	0.99 ± 0.18
10	37.0 ± 2.9	1.12 ± 0.09
5 + **8**	30.4 ± 4.4	0.92 ± 0.13

Overall, the results of the Table 4.4 and Figure 4.4 show that there is no statistical difference between any of the test conditions and the negative control. A major source of error in this experiment was in determining the protein concentration of the cells. The variation in protein content (2.02 to 6.25 mg / mL) is likely a combination of the number of cells collected and lysed, and an effect of the treatment condition. Most of the protein concentrations were between 2.5 and 3.5 mg/mL, in which variability can be attributed to collecting cells from the tissue culture flasks. The two highest protein concentration values were 4.07 and 6.25 mg/mL, which both were a part of the negative control treatment condition. It is unclear how this occurred, but these results make it clear that further work must be performed to reproduce the negative control in order to confirm the efficacy of any of the chelators in removing copper from the cell model.

D-penicillamine was chosen as a positive control for this experiment because it is the front line treatment for Wilson's disease, but it was not validated in the experiments performed in this thesis. It has been suggested that in *in vitro* studies, D-penicillamine may not effectively remove copper from cells.[137] Dosing for D-penicillamine is 0.75-1.5 g per day.[29] This suggests that it may take a prolonged high dose (up to two years) for this compound to be effective.[29] Both approved drugs (D-penicillamine and trientine) should be evaluated in this cell model to establish a positive control before attempting to evaluate the efficacy of any of the compounds designed in this thesis.

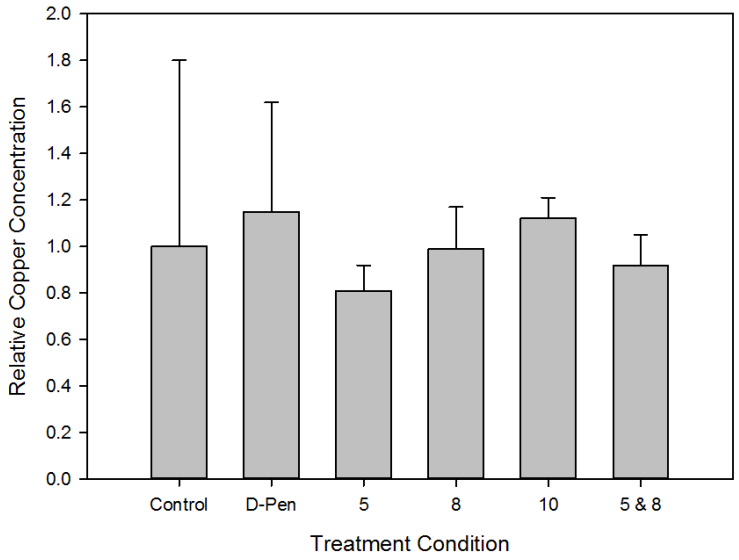

Figure 4.4. Relative copper concentrations in HepG2 cells after 24 hour incubation in 100 μM Cu-His (1:10 ratio) media, then 24 hour incubation with 100 μM D-penicillamine, Compound 8, Compound 5, Compound 10, or 50 μM Compound 5 and 50 μM Compound 8 normalized to 1.00 relative to control.

The only difference (as determined by error bars not overlapping) in this experiment was between Compound **5** and Compound **10**. All that can be drawn from this is that Compound **5** appears to remove more copper from this disease model than Compound **10**. In the absence of an appropriate negative control, no strong conclusions can be made about this experiment. This experiment to establish a disease model, and treat via incubation of the model chelators has not provided any strong evidence for the efficacy of Compounds **5**, **8**, and **10** in removing copper from the disease model, but it has

provided a useful protocol for how to approach the efficacy of chelators in removing copper from copper-loaded cells.

In a preliminary experiment to determine the species present after incubation with both the azide and alkyne precursors, the media and the cell lysates were subjected to HPLC analysis. A 200 μL sample of the lysate and two 300 μL samples of media from the co-incubation of azide and alkyne was filtered using a 3kDa molecular weight cut off filter and spinning in a centrifuge at 8230 rpm for 8 minutes. This filtrate was then investigated by mass spectrometry (ESI-MS). Unfortunately, this experiment did not provide any insight on the speciation of the co-incubated pro-drugs, and it could be that the products were below the detection limit of the instrument. Neither Compound **5** nor Compound **8** were observed.

These samples were then investigated using high performance liquid chromatography (HPLC). The sample containing the lysate did not appear to have a peak associated with click product whereas the chromatogram of the media showed a peak at a retention time of 1.04 minutes which matches the retention time of a sample of the click product (Figure 4.5). This matching of peaks suggests that **10** was formed, but it is inconclusive of whether the product was formed in the cells and then excreted, or if the alkyne and azide molecules were clicked together in the media. Overall, it appears that the click product may be present in the media, but the exact concentration cannot be determined.

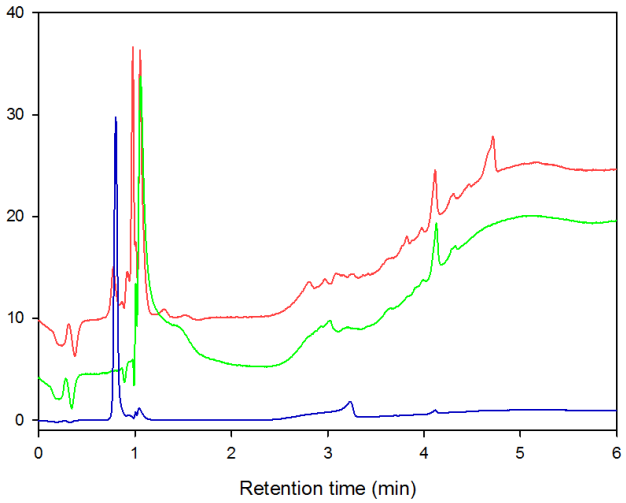

Figure 4.5. **HPLC chromatograms. (Red): media of 50 μM Compound 5 and 50 μM Compound 8 co-incubation with copper-loaded HepG2 cells. (Green): 100 μM of 10. (Blue): cell lysate of 50 μM Compound 5 and 50 μM Compound 8 co-incubation with copper-loaded HepG2 cells (See Experimental Section: 2.2.4 for HPLC conditions).**

4.4. Conclusions

HepG2 cells were used as an *in vitro* model of Wilson's disease. The Wilson's disease model was established by incubating for 24 hours in a media enriched with 100 μM $CuSO_4 \cdot 5H_2O$ and 1 mM histidine. This increased the concentration from 18.1 ± 17.5 nmol Cu / mg protein to 43 ± 9.8 nmol Cu / mg protein, which is a similar value to that was previously reported (36.4 ± 4 nmol Cu / mg protein).[133] Large errors associated with measuring the copper concentrations in the copper-free and copper-enriched media incubations of HepG2 cells have limited any conclusion regarding copper loading, and the rate of efflux of copper over a 24 hour period (Tables 4.3 and 4.4). Potential reasons for the large error associated with the copper-free condition observed in Table 4.3 may be due to copper contamination during preparation for the ICP-AES. Table 4.2 showed that this sample originally had copper levels below the standard, so in repeating the analysis, the results compiled in Table 4.3 (when compared to Table 4.2) would suggest that there was a preparation error. D-penicillamine was measured to have copper levels at 115 ± 47 % of the buffer condition. Compounds **5** and **8** (Figure 4.1) were measured to have copper concentrations relative to buffer of 81 ± 11 %, and 99 ± 18 %, respectively. The

co-incubation of compound **5** and **8** was measured to have copper concentrations relative to buffer of 92 ± 13 %. The click compound **10** also did not significantly reduce copper loading in the disease model with respect to the buffer only condition at 112 ± 9 %. The cell lysate and media from the alkyne and azide co-incubation condition were tested by mass spectrometry with no observation of click product (**10**) or either component (**5** and **8**) visible in the mass spectrometry spectra. There was no evidence in the HPLC chromatogram of compound **10** in the lysate, but a peak on the HPLC chromatogram of the media suggests that **10** may be present. There did not appear to be any of either of the azide (**5**) or alkyne (**8**) components in the media or lysate.

Chapter 5.

Future Work

5.1. Synthesis

Chapter 2 discussed the synthetic methodology and synthesis of two ligands, **10** and **12** (Figure 5.1). These compounds were synthesized in lieu of the target TPEN analogue **13** (Figure 5.1) due to the difficulty of its isolation. Ultimately, the reaction mixture for target **13** had a retention time on the HPLC which differed from compounds **5** and **6** (Figure 2.3), which offers a potential avenue for purification. The triazole **13** contains a propyl chain from the reaction of **5** with **6**, so the pentyl derivative reacted from compounds **3** and **6** would be the next TPEN derivative to synthesize. The next step in this part of the project will be to collect the HPLC fraction thought to be associated with compound **13** and characterise it using ^{1}H NMR, ^{13}C NMR and mass spectrometry. The pK_a values of **13** would be determined as described in Section **2.2.3**. It is important to know the charge of this compound at physiological pH because that affects how well it can cross the cell membrane. To determine metal-ligand stoichiometry of **13**, a Job's plot analysis would be performed as it had been for compounds **10** and **12** as described in Section **2.2.2**.

Since each of these ligands are meant to act as chelators within hepatocytes, there are a number of different metals such as copper, iron, and zinc that could be complexed. It would be useful to quantify the stability constants for the ligands (Figure 5.1) with each of these metals. Competition assays with ligands, such as D-penicillamine and trientine, can also provide relative binding affinities for these ligands. If these compounds prove to have binding affinities comparable with D-penicillamine or trientine or higher, perhaps they could prove to be comparable or have greater efficacy than D-penicillamine or trientine in removing copper from the liver, and treating Wilson's disease.

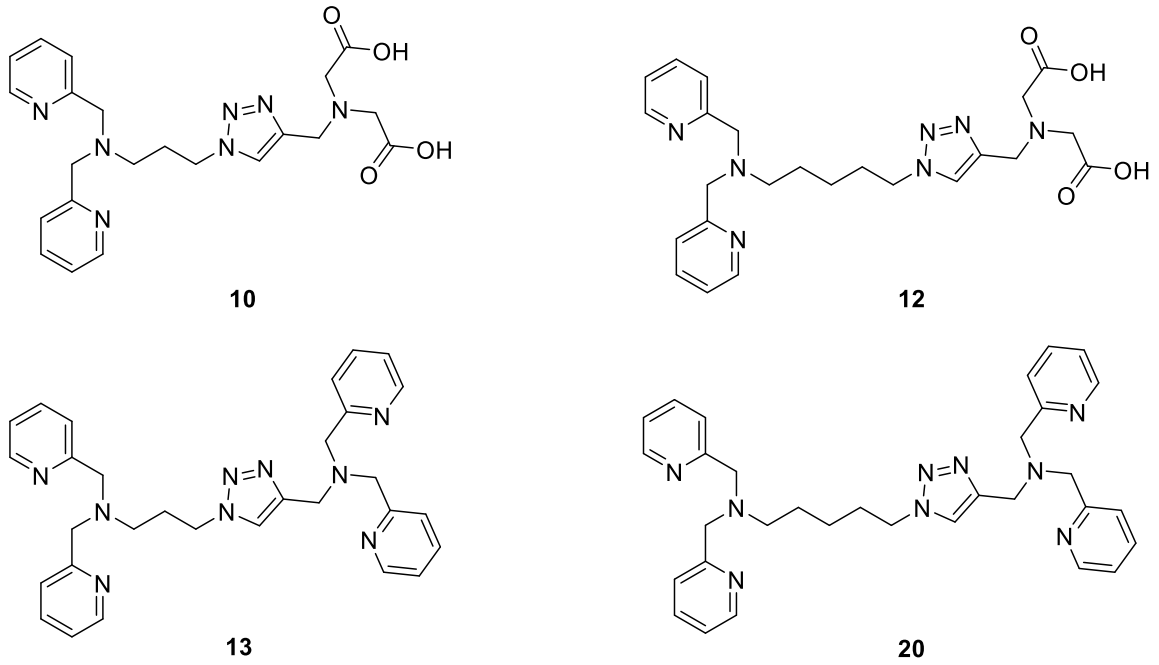

Figure 5.1. Structures of the propyl and pentyl mixed acid/pyridine ligands (Compounds 10 and 12) and propyl and pentyl TPEN derivatives (Compounds 13 and 20).

The future work for the synthesis of the CusF analogue has been outlined; **19** must be isolated and characterized before continuing further experimentation. HPLC is one of the methods that can be used for isolating the target. Upon isolation, a Job's plot analysis to determine the stoichiometry of the ligand:copper interaction and a variable pH NMR experiment to determine the pK_a of **19** need to be performed. Furthermore, it will be useful to determine its binding affinity for Cu(I).

5.2. **Biological Studies**

Up to this point, a protocol has been established to evaluate the efficacy of Compounds **5**, **8**, and **10** in removing copper from the HepG2 cell model. These compounds (**5**, **8**, **10**) must still be evaluated for their toxicity. The other pre-click compounds (**3**, **6**, **16**, **18**), and triazole targets (**13**, **19**, **20**) (Figure 5.2) must also be evaluated for their efficacy in reducing copper loading and for their toxicities. The toxicity should be determined for both copper-free and copper-enriched conditions. A colorimetric differentiation of viability such as propidium iodide should be used, then sorted through

fluorescence activated cell sorting (FACS) to afford accurate cell viability results. The use of a 3-(4,5-dimethylthiazol-2-yl)-2,5-diphenyltetrazolium bromide (MTT) assay might not provide reliable results in the copper-enriched conditions because the high copper concentration within the cells may interfere with this type of assay.[145] Furthermore, it has been observed that the HepG2 cells tend to clump together into clusters, which could introduce significant error to an MTT assay.

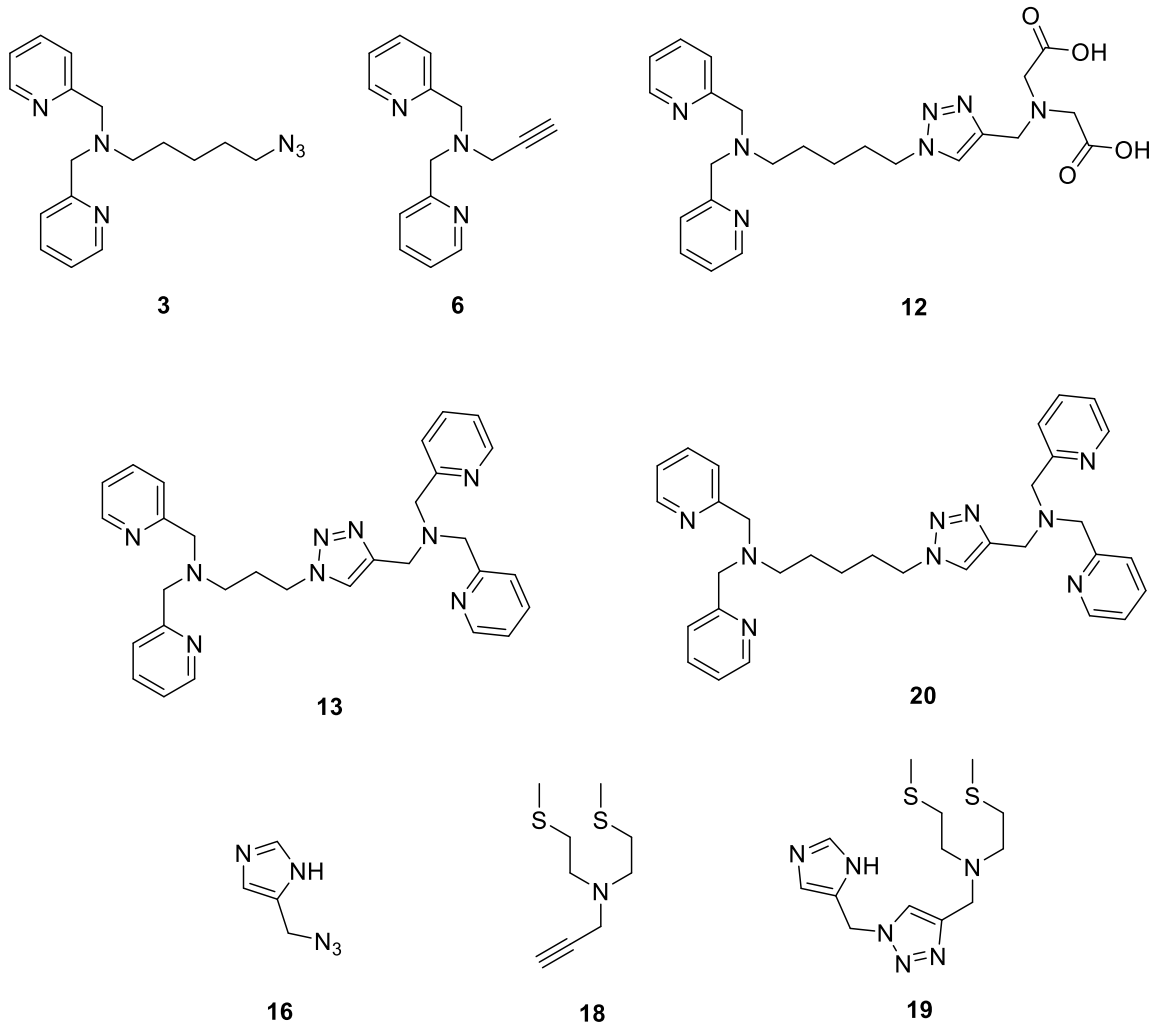

Figure 5.2. Structures of compounds that still have to be evaluated for their efficacy in reducing copper levels in the Wilson's disease cell model: Compounds 3, 6, 12, 13, 20, 16, 18, and 19.

After it has been determined that these compounds in Figures 5.1 and 5.2 are non-toxic at concentrations effective at removing copper from the cellular disease model, collaboration with laboratories that have access to an appropriate animal model of Wilson's disease must be established. The typical animal model for Wilson's disease is the Long-Evans Cinnamon rat because this model exhibits excessive copper accumulation in their livers.[146-147] Although, this model is only appropriate for observing hepatological effects of Wilson's disease since neurological effects that are associated with Wilson's disease are not commonly observed.[146] Other major differences between this rat model and a Wilson's disease patient is that the rat model is much more prone to liver cancer than a Wilson's disease patient,[146-147] and the rat model typically has a defective immune system (low serum IgG, and depleted T cell levels).[146] Despite these clinical differences, Long Evans Cinnamon rats are known to respond to chelation therapy; copper can be effectively removed from this rat model using D-penicillamine[146] and trientine.[148] Therefore, it is reasonable to use these rats as an animal model for evaluating the efficacy of the chelators that have been synthesized in this thesis.

Another potential therapy using the chelators developed herein, is to form zinc complexes of the click precursors (e.g. compounds **5** and **8**). Since zinc is used as an effective treatment for limiting copper uptake, future experiments could be to characterize the pre-click ligands as zinc complexes. Therefore, these complexes could be used as a drug to deliver zinc, which should help with limiting copper uptake by reducing copper absorption into the intestine,[51] and also limiting off-target effects of the pre-click ligands interfering with the homeostasis of other endogenous metals such as iron or zinc before reaching the liver. It has previously been shown that combination therapy of trientine and zinc has been effective in treating Wilson's disease,[149] but this therapy was not performed as a trientine-zinc salt. The efficacy of a chelator-zinc salt has yet to be reported.

References

1. Jones, M. R.; Duncan, D.; Storr, T., Introduction to Ligand Design in Medicinal Inorganic Chemistry. In *Ligand Design in Medicinal Inorganic Chemistry*, Storr, T., Ed. John Wiley & Sons Ltd.: Chichester, West Sussex, PO19 8SQ, United Kingdom, 2014; pp 1-8.

2. Vallee, B. L.; Auld, D. S., *Biochemistry* **1990,** *29* (24), 5647-59.

3. Lipscomb, W. N.; Sträter, N., *Chem. Rev.* **1996,** *96* (7), 2375-2434.

4. Klug, A.; Schwabe, J. W., *FASEB J.* **1995,** *9* (8), 597-604.

5. Quinlan, K. G.; Verger, A.; Yaswen, P.; Crossley, M., *Biochim. Biophys. Acta* **2007,** *1775* (2), 333-40.

6. Carrillo, N.; Ceccarelli, E. A., *Eur. J. Biochem.* **2003,** *270* (9), 1900-15.

7. Siletsky, S. A.; Konstantinov, A. A., *Biochim. Biophys. Acta* **2012,** *1817* (4), 476-88.

8. Karp, G., In *Cell and Molecular Biology*, 5 ed.; John Wiley & Sons, Inc.: Hoboken, New Jersey, 2007; pp 112-114.

9. Sampson, V.; Alleyne, T., *Eur. J. Biochem.* **2001,** *268* (24), 6534-44.

10. Gaggelli, E.; Kozlowski, H.; Valensin, D.; Valensin, G., *Chem. Rev.* **2006,** *106* (6), 1995-2044.

11. Liochev, S. I.; Fridovich, I., *Free Radic. Biol. Med.* **2010,** *48* (12), 1565-9.

12. Ramsden, C. A.; Riley, P. A., *Bioorg. Med. Chem.* **2014,** *22* (8), 2388-95.

13. Holm, L.; Saraste, M.; Wikstrom, M., *EMBO J.* **1987,** *6* (9), 2819-23.

14. Hofacker, I.; Schulten, K., *Proteins* **1998,** *30* (1), 100-7.

15. Fridovich, I., *Annu. Rev. Biochem.* **1995,** *64*, 97-112.

16. Shin, D. S.; Didonato, M.; Barondeau, D. P.; Hura, G. L.; Hitomi, C.; Berglund, J. A.; Getzoff, E. D.; Cary, S. C.; Tainer, J. A., *J. Mol. Biol.* **2009,** *385* (5), 1534-55.

17. Ramirez, D. C.; Gomez Mejiba, S. E.; Mason, R. P., *Free Radic. Biol. Med.* **2005,** *38* (2), 201-14.

18. Rolff, M.; Schottenheim, J.; Decker, H.; Tuczek, F., *Chem. Soc. Rev.* **2011,** *40* (7), 4077-98.

19. Zumdahl, S. S.; DeCoste, D. J., In *Chemical Principles*, 7 ed.; Brooks/Cole, Cengage Learning: Belmont, California, United States of America, 2013; p A24.

20. Anderson, G. J., *IUBMB life* **2001,** *51* (1), 11-17.

21. Bou-Abdallah, F., *Biochim. Biophys. Acta* **2010,** *1800* (8), 719-31.

22. Weiss, G.; Gordeuk, V. R., *Eur. J. Clin. Invest.* **2005,** *35 Suppl 3*, 36-45.

23. Pieracci, F. M.; Barie, P. S., *Crit. Care Med.* **2006,** *34* (7), 1898-905.

24. Davies, K. J., *IUBMB life* **1999,** *48* (1), 41-7.

25. Stohs, S. J.; Bagchi, D., *Free Rad. Biol. Med.* **1995,** *18* (2), 321-336.

26. Vujic Spasic, M., *Front. Pharmacol.* **2014,** *5*.

27. Go, Y. M.; Jones, D. P., *Free Radic. Biol. Med.* **2011,** *50* (4), 495-509.

28. Langley, B.; Ratan, R. R., *J. Neurosci. Res.* **2004,** *77* (5), 621-9.

29. Das, S. K.; Ray, K., *Nat. Clin. Pract. Neurol.* **2006,** *2* (9), 482-93.

30. Das, S.; Levinson, B.; Whitney, S.; Vulpe, C.; Packman, S.; Gitschier, J., *Am. J. Hum. Genet.* **1994,** *55* (5), 883-9.

31. Kodama, H.; Murata, Y., *Pediatr. Int.* **1999,** *41* (4), 430-435.

32. Kodama, H.; Murata, Y.; Kobayashi, M., *Pediatr. Int.* **1999,** *41* (4), 423-9.

33. Tumer, Z.; Lund, C.; Tolshave, J.; Vural, B.; Tonnesen, T.; Horn, N., *Am. J. Hum. Genet.* **1997,** *60* (1), 63-71.

34. Kodama, H.; Fujisawa, C.; Bhadhprasit, W., *Curr. Drug Metab.* **2012,** *13* (3), 237-50.

35. Storr, T.; Merkel, M.; Song-Zhao, G. X.; Scott, L. E.; Green, D. E.; Bowen, M. L.; Thompson, K. H.; Patrick, B. O.; Schugar, H. J.; Orvig, C., *J. Am. Chem. Soc.* **2007,** *129* (23), 7453-63.

36. Montes, S.; Rivera-Mancia, S.; Diaz-Ruiz, A.; Tristan-Lopez, L.; Rios, C., *Oxid. Med. Cell Longev.* **2014,** *2014*, 147251.

37. Branch, T.; Girvan, P.; Barahona, M.; Ying, L., *Angew. Chem. Int. Ed. Engl.* **2015,** *54* (4), 1227-30.

38. Doraiswamy, P. M.; Finefrock, A. E., *Lancet Neurol.* **2004,** *3* (7), 431-4.

39. Dusek, P.; Roos, P. M.; Litwin, T.; Schneider, S. A.; Flaten, T. P.; Aaseth, J., *J. Trace Elem. Med. Biol.* **2015,** *31*, 193-203.

40. Penkowa, M.; Caceres, M.; Borup, R.; Nielsen, F. C.; Poulsen, C. B.; Quintana, A.; Molinero, A.; Carrasco, J.; Florit, S.; Giralt, M.; Hidalgo, J., *J. Neurosci. Res.* **2006,** *84* (7), 1452-74.

41. Schlief, M.; Gitlin, J., *Mol. Neurobiol.* **2006,** *33* (2), 81-90.

42. van den Berghe, P. V.; Klomp, L. W., *Nutr. Rev.* **2009,** *67* (11), 658-72.

43. Maryon, E. B.; Molloy, S. A.; Kaplan, J. H., *Am. J. Physiol. Cell Physiol.* **2013,** *304* (8), C768-79.

44. Dolgova, N. V.; Nokhrin, S.; Yu, C. H.; George, G. N.; Dmitriev, O. Y., *Biochem. J.* **2013,** *454* (1), 147-56.

45. Fatemi, N.; Sarkar, B., *Environ. Health Perspect.* **2002,** *110* (Suppl 5), 695-698.

46. Burkhead, J. L., Lutsenko, S., The Role of Copper as a Modifier of Lipid Metabolism. In *Lipid Metabolism*, Baez, R. V., Ed. InTech: 2013.

47. Wooton-Kee, C. R.; Jain, A. K.; Wagner, M.; Grusak, M. A.; Finegold, M. J.; Lutsenko, S.; Moore, D. D., *J. Clin. Invest.* **2015,** *125* (9), 3449-60.

48. Wilson, S. A. K., *Brain* **1912,** *34* (4), 295-507.

49. Vilensky, J. A.; Redman, K., *Ann. Emerg. Med.* **2003,** *41* (3), 378-83.

50. Ala, A.; Walker, A. P.; Ashkan, K.; Dooley, J. S.; Schilsky, M. L., *The Lancet* **2007,** *369* (9559), 397-408.

51. Brewer, G. J., *Expert Opin. Orphan Drugs* **2014,** *2* (12), 1245-1248.

52. Dalvi, A.; Padmanaban, M., *Dis. Mon.* **2014,** *60* (9), 450-9.

53. Association, E., *J. Hepatol. 56* (3), 671-685.

54. Strand, S.; Hofmann, W. J.; Grambihler, A.; Hug, H.; Volkmann, M.; Otto, G.; Wesch, H.; Mariani, S. M.; Hack, V.; Stremmel, W.; Krammer, P. H.; Galle, P. R., *Nat. Med.* **1998,** *4* (5), 588-93.

55. Karp, G., In *Cell and Molecular Biology*, 5 ed.; John Wiley & Sons, Inc.: Hoboken, New Jersey, 2007; pp 655-657.

56. Weinberg, R. A., In *The Biology of Cancer*, Taylor & Francis Group, LLC: New York, New York, 2007; pp 335-336.

57. Dalvi, A., *Dis. Mon.* **2014,** *60* (9), 460-4.

58. Ferenci, P., *Metab. Brain Dis.* **2004,** *19* (3-4), 229-39.

59. Santos Silva, E. E.; Sarles, J.; Buts, J. P.; Sokal, E. M., *J. Pediatr.* **1996,** *128* (2), 285-7.

60. Kim, B.; Chung, S. J.; Shin, H.-W., *J. Clin. Neurosci.* **2013,** *20* (4), 606-608.

61. Brewer, G. J.; Yuzbasiyan-Gurkan, V.; Johnson, V.; Dick, R. D.; Wang, Y., *Am. J. Med. Sci.* **1993,** *305* (4), 199-202.

62. Anderson, L. A.; Hakojarvi, S. L.; Boudreaux, S. K., *Ann. Pharmacoth.* **1998,** *32* (1), 78-87.

63. Czlonkowska, A.; Gajda, J.; Rodo, M., *J. Neurol.* **1996,** *243* (3), 269-73.

64. Brewer, G. J.; Askari, F.; Lorincz, M. T.; Carlson, M.; Schilsky, M.; Kluin, K. J.; Hedera, P.; Moretti, P.; Fink, J. K.; Tankanow, R.; Dick, R. B.; Sitterly, J., *Arch. Neurol.* **2006,** *63* (4), 521-7.

65. Hou, G.; Dick, R.; Zeng, C.; Brewer, G. J., *Transl. Res.* **2006,** *148* (6), 309-314.

66. Jullien, A. S.; Gateau, C.; Lebrun, C.; Kieffer, I.; Testemale, D.; Delangle, P., *Inorg. Chem.* **2014,** *53* (10), 5229-39.

67. Gateau, C.; Delangle, P., *Ann. N. Y. Acad. Sci.* **2014,** *1315*, 30-6.

68. Pujol, A. M.; Cuillel, M.; Jullien, A. S.; Lebrun, C.; Cassio, D.; Mintz, E.; Gateau, C.; Delangle, P., *Angew. Chem. Int. Ed. Engl.* **2012,** *51* (30), 7445-8.

69. Nakazato, K.; Tomioka, S.; Nakajima, K.; Saito, H.; Kato, M.; Kodaira, T.; Yatsuzuka, S.; Shimomura, Y.; Hiroki, T.; Motoyama, K.; Kodama, H.; Nagamine, T., *J. Trace Elem. Med. Biol.* **2014,** *28* (4), 441-7.

70. Faa, G.; Nurchi, V. M.; Ravarino, A.; Fanni, D.; Nemolato, S.; Gerosa, C.; Van Eyken, P.; Geboes, K., *Coord. Chem. Rev.* **2008,** *252* (10–11), 1257-1269.

71. Meldal, M.; Tornoe, C. W., *Chem. Rev.* **2008,** *108* (8), 2952-3015.

72. Kolb, H. C.; Finn, M. G.; Sharpless, K. B., *Angew. Chem. Int. Ed.* **2001,** *40* (11), 2004-2021.

73. Tornoe, C. W.; Christensen, C.; Meldal, M., *J. Org. Chem.* **2002,** *67* (9), 3057-64.

74. Bock, V. D.; Hiemstra, H.; van Maarseveen, J. H., *Eur. J. Org. Chem.* **2006,** *2006* (1), 51-68.

75. Struthers, H.; Spingler, B.; Mindt, T. L.; Schibli, R., *Chem. Eur. J.* **2008,** *14* (20), 6173-83.

76. Kluba, C. A.; Mindt, T. L., *Molecules* **2013,** *18* (3), 3206-26.

77. Kuang, G.-C.; Michaels, H. A.; Simmons, J. T.; Clark, R. J.; Zhu, L., *J. Org. Chem.* **2010,** *75* (19), 6540-6548.

78. Bevilacqua, V.; King, M.; Chaumontet, M.; Nothisen, M.; Gabillet, S.; Buisson, D.; Puente, C.; Wagner, A.; Taran, F., *Angew. Chem. Int. Ed.* **2014,** *53* (23), 5872-5876.

79. Uttamapinant, C.; Tangpeerachaikul, A.; Grecian, S.; Clarke, S.; Singh, U.; Slade, P.; Gee, K. R.; Ting, A. Y., *Angew. Chem. Int. Ed.* **2012,** *51* (24), 5852-5856.

80. Uttamapinant, C.; Sanchez, M. I.; Liu, D. S.; Yao, J. Z.; Ting, A. Y., *Nat. Protoc.* **2013,** *8* (8), 1620-34.

81. Chan, T. R.; Hilgraf, R.; Sharpless, K. B.; Fokin, V. V., *Org. Lett.* **2004,** *6* (17), 2853-2855.

82. Cho, Y. E.; Lomeda, R. A.; Ryu, S. H.; Lee, J. H.; Beattie, J. H.; Kwun, I. S., *Nutr. Res. Pract.* **2007,** *1* (1), 29-35.

83. Frisch, M. J.; Trucks, G. W.; Schlegel, H. B.; Scuseria, G. E.; Robb, M. A.; Cheeseman, J. R.; Scalmani, G.; Barone, V.; Mennucci, B.; Petersson, G. A.; Nakatsuji, H.; Caricato, M.; Li, X.; Hratchian, H. P.; Izmaylov, A. F.; Bloino, J.; Zheng, G.; Sonnenberg, J. L.; Hada, M.; Ehara, M.; Toyota, K.; Fukuda, R.; Hasegawa, J.; Ishida, M.; Nakajima, T.; Honda, Y.; Kitao, O.; Nakai, H.; Vreven, T.; Montgomery Jr., J. A.; Peralta, J. E.; Ogliaro, F.; Bearpark, M.; Heyd, J. J.; Brothers, E.; Kudin, K. N.; Staroverov, V. N.; Kobayashi, R.; Normand, J.; Raghavachari, K.; Rendell, A.; Burant, J. C.; Iyengar, S. S.; Tomasi, J.; Cossi, M.; Rega, N.; Millam, J. M.; Klene, M.; Knox, J. E.; Cross, J. B.; Bakken, V.; Adamo, C.; Jaramillo, J.; Gomperts, R.; Stratmann, R. E.; Yazyev, O.; Austin, A. J.; Cammi, R.; Pomelli, C.; Ochterski, J. W.; Martin, R. L.; Morokuma, K.; Zakrzewski, V. G.; Voth, G. A.; Salvador, P.; Dannenberg, J. J.; Dapprich, S.; Daniels, A. D.; Farkas, Ö.; Foresman, J. B.; Ortiz, J. V.; Cioslowski, J.; Fox, D. J., *Gaussian 09, revision D.01*. Gaussian Inc.: Wallingford, CT., 2009.

84. Lamas, G. A.; Goertz, C.; Boineau, R.; et al., *JAMA* **2013,** *309* (12), 1241-1250.

85. King-Shier, K. M.; Quan, H.; Mather, C.; Verhoef, M. J.; Knutson, M. L.; Ghali, W. A., *Int. J. Nurs. Stud.* **2012,** *49* (9), 1074-83.

86. Lamas, G. A.; Hussein, S. J., *Complement Ther. Clin. Pract.* **2006,** *12* (3), 213-5.

87. George, G. N.; Prince, R. C.; Gailer, J.; Buttigieg, G. A.; Denton, M. B.; Harris, H. H.; Pickering, I. J., *Chem. Res. Toxicol.* **2004,** *17* (8), 999-1006.

88. Šömen Joksić, A.; Katz, S. A., *J. Environ. Sci. Health A Tox. Hazard Substr. Environ. Eng.* **2015,** *50* (14), 1479-1488.

89. Weatherall, D. J.; Clegg, J. B., *Bull. World Health Organ.* **2001,** *79* (8), 704-12.

90. Mayo Clinic, Diseases and Conditions: Thalassemia. http://www.mayoclinic.org/diseases-conditions/thalassemia/basics/definition/con-20030316 (accessed December 9, 2015).

91. Origa, R. B., P.;Agus, A,; Crobu, G.; Defraia, E.; Dessi, C.; Leoni, G.; Muroni, P.P.; Galanelo, R., *Haematologica* **2005,** *90* (10), 1309-1314.

92. Kaur, D.; Andersen, J. K., *Aging cell* **2002,** *1* (1), 17-21.

93. Cherny, R. A.; Atwood, C. S.; Xilinas, M. E.; Gray, D. N.; Jones, W. D.; McLean, C. A.; Barnham, K. J.; Volitakis, I.; Fraser, F. W.; Kim, Y.; Huang, X.; Goldstein, L. E.; Moir, R. D.; Lim, J. T.; Beyreuther, K.; Zheng, H.; Tanzi, R. E.; Masters, C. L.; Bush, A. I., *Neuron* **2001,** *30* (3), 665-76.

94. Panza, F.; Solfrizzi, V.; Frisardi, V.; Imbimbo, B. P.; Capurso, C.; D'Introno, A.; Colacicco, A. M.; Seripa, D.; Vendemiale, G.; Capurso, A.; Pilotto, A., *Aging Clin. Exp. Res.* **2009,** *21* (6), 386-406.

95. Sampson, E. L.; Jenagaratnam, L.; McShane, R., *Cochrane Database Syst. Rev.* **2012,** *5*, Cd005380.

96. Birker, P. J. M. W. L.; Freeman, H. C., *J. Chem. Soc., Chem. Commun.* **1976,** (9), 312-313.

97. Martell, A. E., Smith, R. M., *Critical Stability Constants*. Plenum Press, London, 1974; Vol. 1: Amino Acids.

98. Várnagy, K.; Sóvágó, I.; Kozłowski, H., *Inorg. Chim. Acta* **1988,** *151* (2), 117-123.

99. Lacoste, R. G.; Marttel, A. E., *Inorg. Chem.* **1964,** *3* (6), 881-884.

100. Cherny, R. A.; Barnham, K. J.; Lynch, T.; Volitakis, I.; Li, Q.-X.; McLean, C. A.; Multhaup, G.; Beyreuther, K.; Tanzi, R. E.; Masters, C. L.; Bush, A. I., *J. Struct. Biol.* **2000,** *130* (2–3), 209-216.

101. Martell, A. E., Smith, R. M., *Critical Stability Constants*. Plenum Press, London, 1974; Vol. 2: Amines.

102. Saikia, B.; Saikia, P. P.; Goswami, A.; Barua, N. C.; Saxena, A. K.; Suri, N., *Synthesis* **2011,** *2011* (19), 3173-3179.

103. Lin, H.-Y.; Snider, B. B., *J. Org. Chem.* **2012,** *77* (10), 4832-4836.

104. Johnson, R. P.; Uthaman, S.; John, J. V.; Lee, H. R.; Lee, S. J.; Park, H.; Park, I.-K.; Suh, H.; Kim, I., *ACS Appl. Mat. Interfaces* **2015**.

105. Chaignon, J.; Stiriba, S.-E.; Lloret, F.; Yuste, C.; Pilet, G.; Bonneviot, L.; Albela, B.; Castro, I., *Dalton Trans.* **2014,** *43* (25), 9704-9713.

106. Wirth, T.; Pestel, G. F.; Ganal, V.; Kirmeier, T.; Schuberth, I.; Rein, T.; Tietze, P. L. F.; Sieber, P. S. A., *Angew. Chem. Int. Ed.* **2013,** *52* (27), 6921-6925.

107. Hill, Z. D.; MacCarthy, P., *J. Chem. Educ.* **1986,** *63* (2), 162.

108. Jones, M. R.; Service, E. L.; Thompson, J. R.; Wang, M. C. P.; Kimsey, I. J.; DeToma, A. S.; Ramamoorthy, A.; Lim, M. H.; Storr, T., *Metallomics* **2012,** *4* (9), 910-920.

109. Song, B.; Kurokawa, G. S.; Liu, S.; Orvig, C., *Can. J. Chem.* **2001,** *79* (5-6), 1058-1067.

110. Liu, S.; Edgar, K. J., *Biomacromolecules* **2015,** *16* (9), 2556-2571.

111. Yu-Gen, Z. J.-M., L., *Acta Phys. Chim. Sin.* **1992,** *8* (2), 251-254.

112. Horikoshi, R.; Funasako, Y.; Yajima, T.; Mochida, T.; Kobayashi, Y.; Kageyama, H., *Polyhedron* **2013,** *50* (1), 66-74.

113. Nakon, R.; Rechani, P. R.; Angelici, R. J., *J. Am. Chem. Soc.* **1974,** *96* (7), 2117-2120.

114. Sykes, P., In *A Guidebook to Mechanism in Organic Chemistry*, 6 ed.; Prentice Hall: 1996; pp 66-67.

115. Liu, G. X.; Fang, G. Q.; Xu, W., *Int. J. Mol. Sci.* **2014,** *15* (9), 15287-303.

116. Segall, Y., *J. Agric. Food Chem.* **2011,** *59* (7), 2845-56.

117. Drotleff, S.; Lungwitz, U.; Breunig, M.; Dennis, A.; Blunk, T.; Tessmar, J.; Gopferich, A., *Eur. J. Pharm. Biopharm.* **2004,** *58* (2), 385-407.

118. Melissis, S. C.; Rigden, D. J.; Clonis, Y. D., *J. Chromatogr. A* **2001,** *917* (1-2), 29-42.

119. UniProt UniProtKB - P77214 (CUSF_ECOLI). http://www.uniprot.org/uniprot/P77214 (accessed December 15, 2015).

120. Kittleson, J. T.; Loftin, I. R.; Hausrath, A. C.; Engelhardt, K. P.; Rensing, C.; McEvoy, M. M., *Biochemistry* **2006,** *45* (37), 11096-102.

121. Kim, E.-H.; Rensing, C.; McEvoy, M. M., *Nat. Prod. Rep.* **2010,** *27* (5), 711-719.

122. Xue, Y.; Davis, A. V.; Balakrishnan, G.; Stasser, J. P.; Staehlin, B. M.; Focia, P.; Spiro, T. G.; Penner-Hahn, J. E.; O'Halloran, T. V., *Nat. Chem. Biol.* **2008,** *4* (2), 107-109.

123. Clayden, J.; Greeves, N.; Warren, S.; Wothers, P., In *Organic Chemistry*, Oxford University Press: New York, 2008; pp 1148-1149.

124. Powers, A. R.; Ghiviriga, I.; Abboud, K. A.; Veige, A. S., *Dalton Trans.* **2015,** *44* (33), 14747-14752.

125. Konigsberger, L.-C.; Konigsberger, E.; Hefter, G.; May, P. M., *Dalton Trans.* **2015**.

126. Turner, R. A.; Huebner, C. F.; Scholz, C. R., *J. Am. Chem. Soc.* **1949,** *71* (8), 2801-2803.

127. Song, Y. J., Z. J.; Pandey, A.; Scarborough, R. M.; Scarborough, C. Factor xa inhibitors. US 20070259924 A1, 2007.

128. Blomenkemper, M.; Schröder, H.; Pape, T.; Hahn, F. E., *Inorg. Chim. Acta* **2012,** *390*, 143-147.

129. Loftin, I. R.; Blackburn, N. J.; McEvoy, M. M., *J. Biol. Inorg. Chem.* **2009,** *14* (6), 905-12.

130. Mufti, A. R.; Burstein, E.; Csomos, R. A.; Graf, P. C. F.; Wilkinson, J. C.; Dick, R. D.; Challa, M.; Son, J.-K.; Bratton, S. B.; Su, G. L.; Brewer, G. J.; Jakob, U.; Duckett, C. S., *Mol. Cell* **2006,** *21* (6), 775-785.

131. Urani, C.; Melchioretto, P.; Morazzoni, F.; Canevali, C.; Camatini, M., *Toxicol. in Vitro* **2001,** *15* (4-5), 497-502.

132. Delangle, P.; Mintz, E., *Dalton Trans.* **2012,** *41* (21), 6359-70.

133. Arredondo, M.; Cambiazo, V.; Tapia, L.; Gonzalez-Aguero, M.; Nunez, M. T.; Uauy, R.; Gonzalez, M., *Am. J. Physiol. Gastrointest. Liver Physiol.* **2004,** *287* (1), G27-32.

134. Webber, M. M.; Bello, D.; Quader, S., *The Prostate* **1996,** *29* (6), 386-94.

135. ATCC Hep G2 [HEPG2] (ATCC® HB-8065™). http://www.atcc.org/Products/All/HB-8065.aspx#characteristics (accessed October 18, 2015).

136. Hanahan, D.; Weinberg, R. A., *Cell* **2011,** *144* (5), 646-674.

137. Chandhok, G.; Schmitt, N.; Sauer, V.; Aggarwal, A.; Bhatt, M.; Schmidt, H. H., *PLoS One* **2014,** *9* (6), e98809.

138. Ferenci, P.; Steindl-Munda, P.; Vogel, W.; Jessner, W.; Gschwantler, M.; Stauber, R.; Datz, C.; Hackl, F.; Wrba, F.; Bauer, P.; Lorenz, O., *Clin. Gastroenterol. Hepatol.* **2005,** *3* (8), 811-8.

139. Gonzalez, M.; Tapia, L.; Alvarado, M.; D. Tornero, J.; Fernandez, R., *J. Anal. At. Spectrom.* **1999,** *14* (5), 885-888.

140. Bio-Rad Quick Start™ Bradford Protein Assay. http://www.bio-rad.com/webroot/web/pdf/lsr/literature/4110065A.pdf (accessed October 18, 2015).

141. Jiménez, I.; Aracena, P.; Letelier, M. E.; Navarro, P.; Speisky, H., *Toxicol. in Vitro* **2002,** *16* (2), 167-175.

142. Bradford, M. M., *Anal. Biochem.* **1976,** *72* (1), 248-254.

143. Compton, S. J.; Jones, C. G., *Anal. Biochem.* **1985,** *151* (2), 369-374.

144. ThermoElemental, AAS, GFAAS, ICP or ICP-MS? Which technique should I use? An elementary overview of elemental analysis. Thermo Elemental: Franklin, Massachusetts, 2001.

145. Semisch, A.; Hartwig, A., *Chem. Res. Toxicol.* **2014,** *27* (2), 169-71.

146. Terada, K.; Sugiyama, T., *Pediatr. Int.* **1999,** *41* (4), 414-8.

147. Li, Y.; Togashi, Y.; Sato, S.; Emoto, T.; Kang, J. H.; Takeichi, N.; Kobayashi, H.; Kojima, Y.; Une, Y.; Uchino, J., *J. Clin. Invest.* **1991,** *87* (5), 1858-61.

148. Iseki, K.; Kobayashi, M.; Ohba, A.; Miyazaki, K.; Li, Y.; Togashi, Y.; Takeichi, N., *Biopharm. Drug Dispos.* **1992,** *13* (4), 273-83.

149. Askari, F. K.; Greenson, J.; Dick, R. D.; Johnson, V. D.; Brewer, G. J., *J. Lab. Clin. Med.* **2003,** *142* (6), 385-90.

Appendix.

Supplementary Data

Figure S.1 Determining the bond angle of the N-C bond of DPA-C3-triazole-DPA.

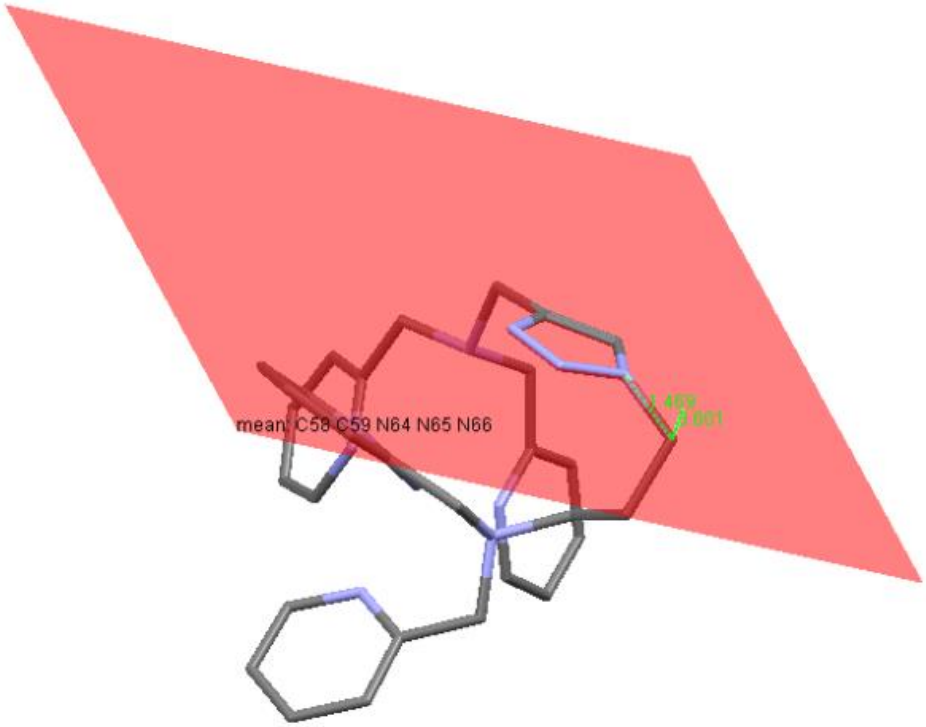

Sin(θ) = opp/hyp

Sin(θ) = 0.601/1.469

θ = 26.8^{o}

Figure S.2. Determining the bond angle of the N-C bond of DPA-C5-triazole-DPA.

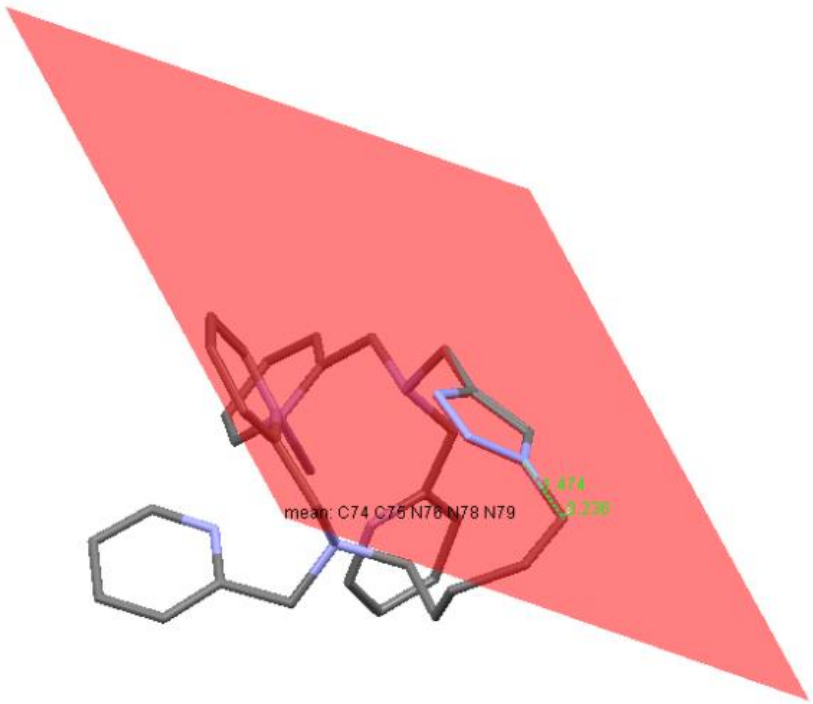

Sin(θ) = opp/hyp

Sin(θ) = 0.236/1.474

θ = 10.2^{o}

Figure S.3. ^{1}H and ^{13}C NMR of 1,5-diazidopentane.

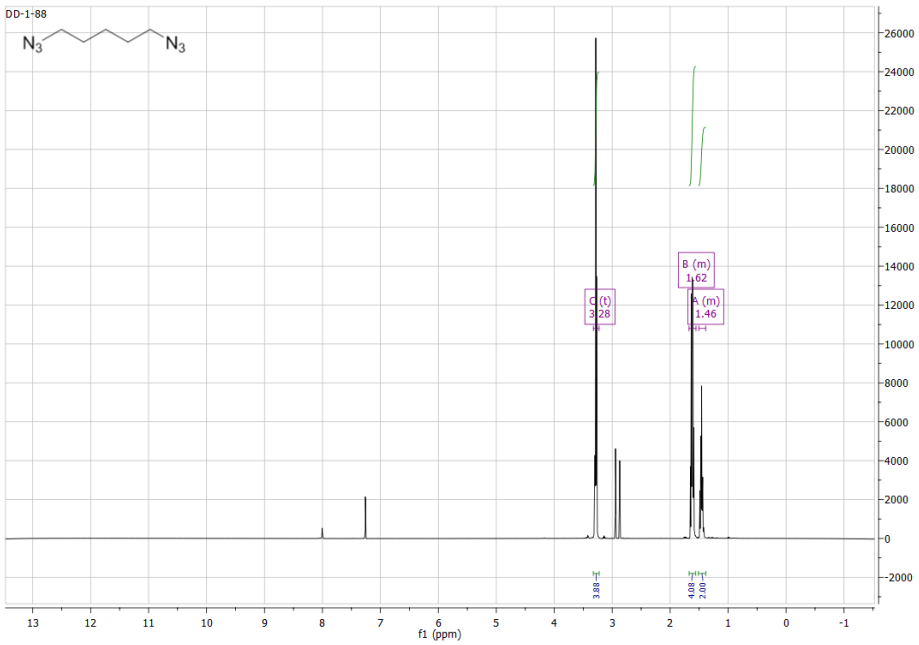

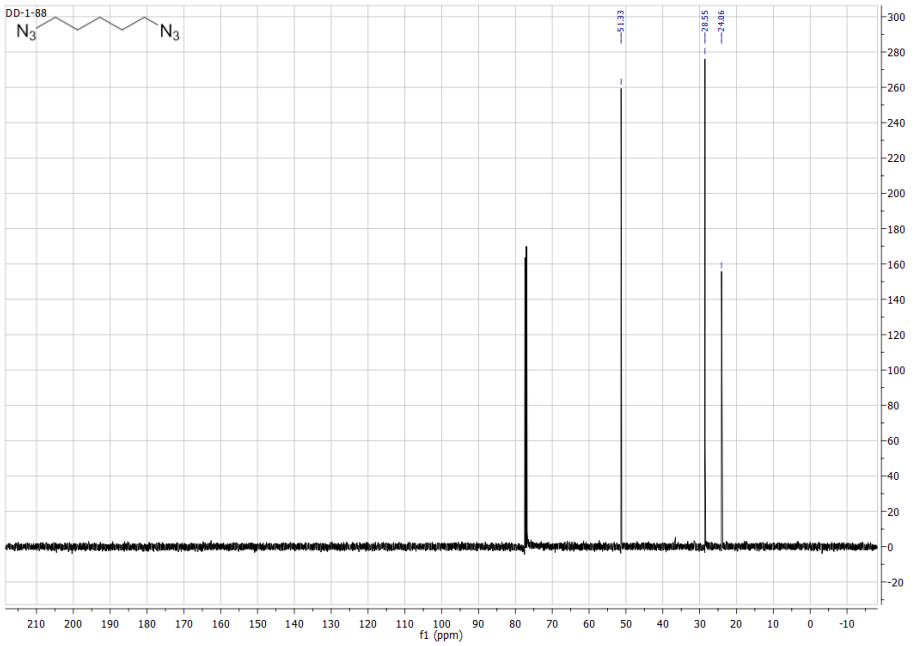

Figure S.4. ^{1}H and ^{13}C NMR of 1-amino-5-azidopentane.

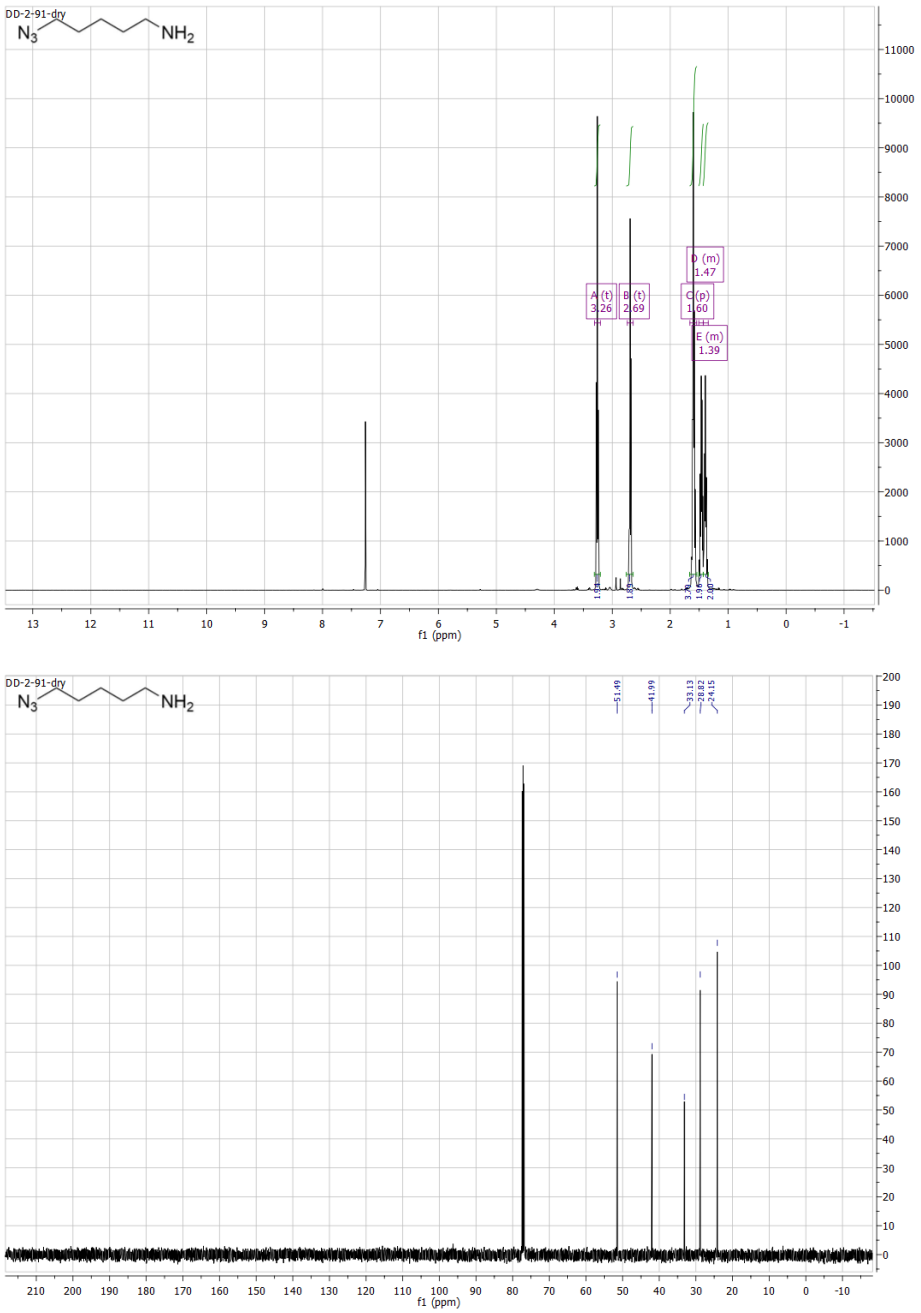

Figure S.5. **^{1}H and ^{13}C NMR of 5-azido-*N*,*N*-bis(pyridin-2-ylmethyl)pentan-1-amine.**

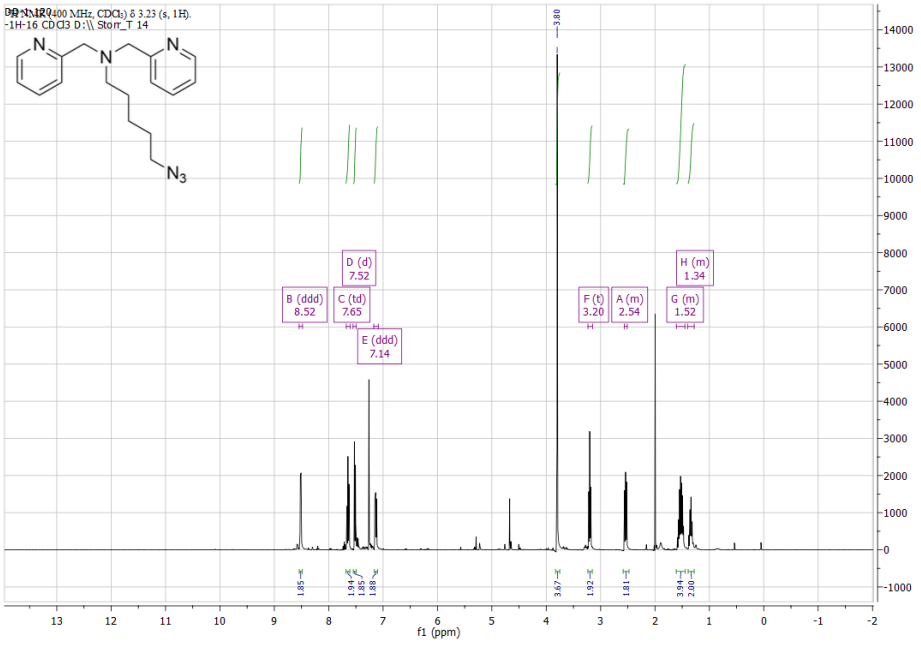

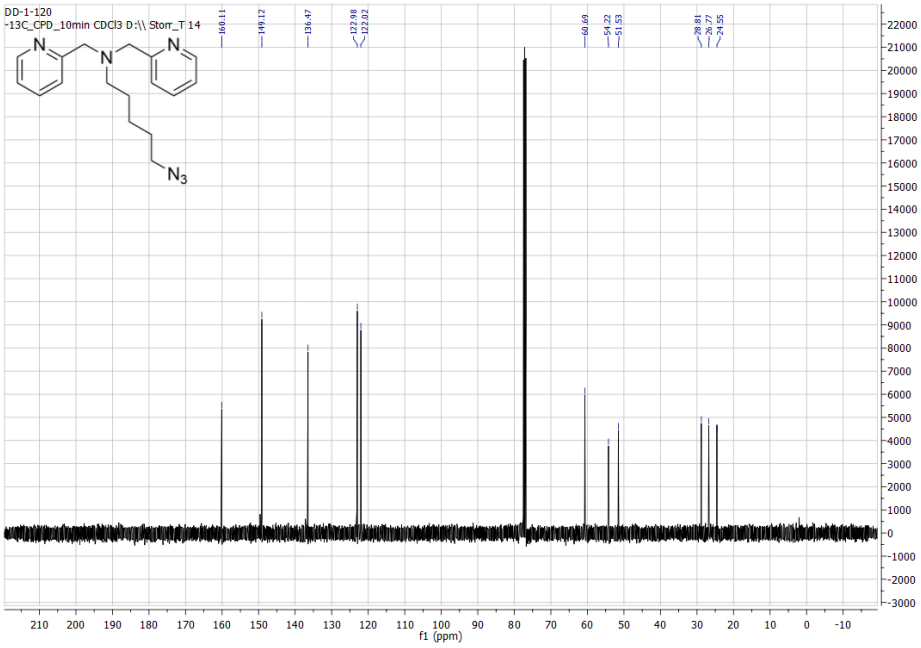

Figure S.6. ^{1}H and ^{13}C NMR of 1-amino-3-azidopropane.

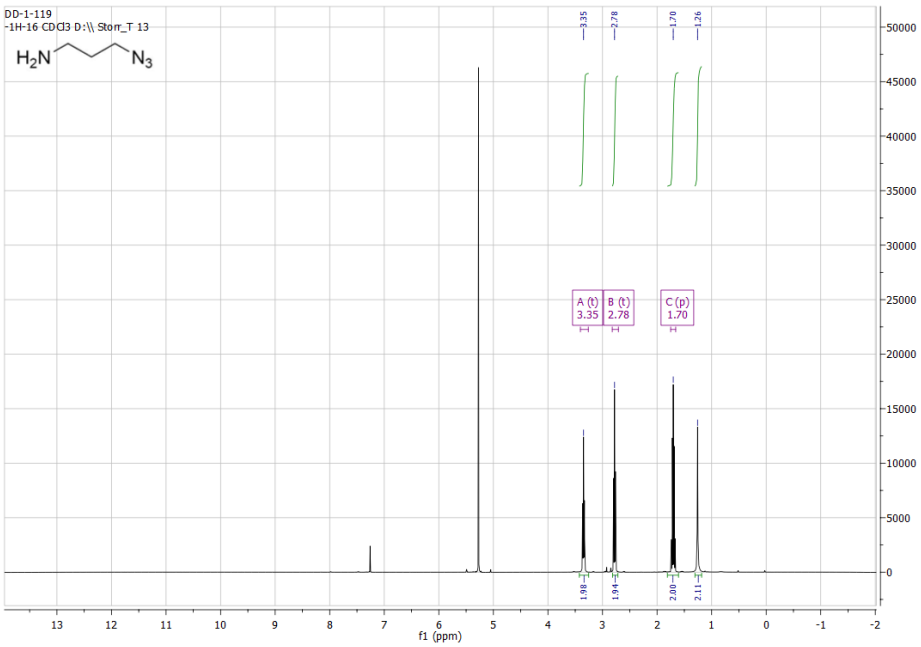

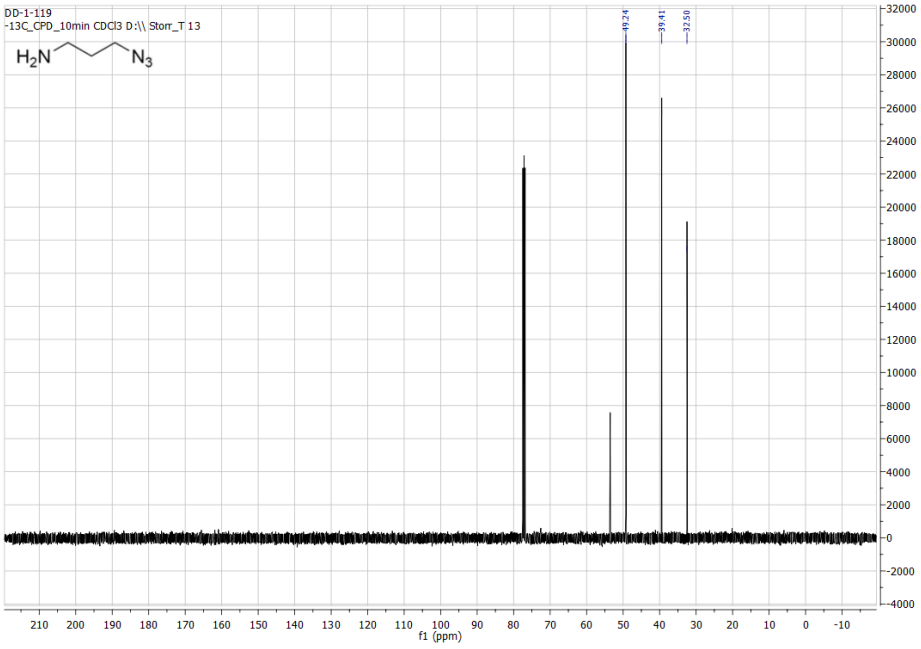

Figure S.7. **^{1}H and ^{13}C NMR of 3-azido-*N*,*N*-bis(pyridin-2-ylmethyl)propan-1-amine.**

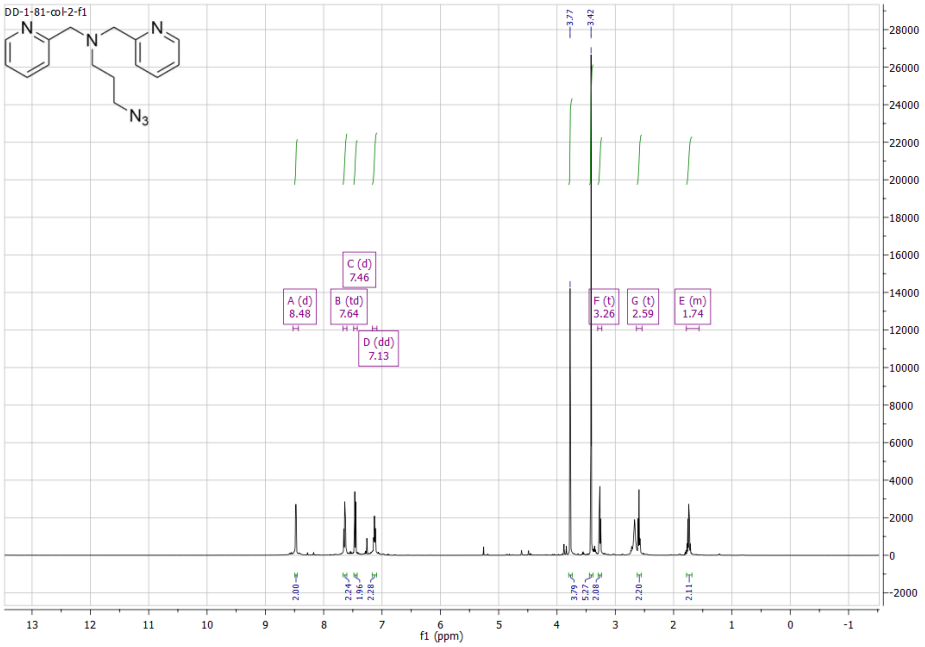

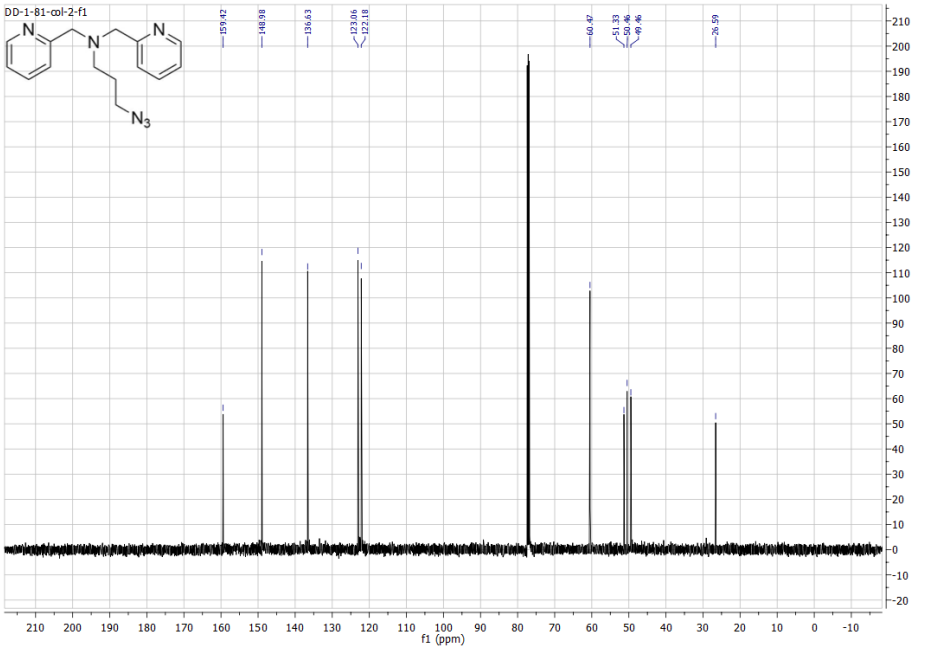

Figure S.8. ^{1}H and ^{13}C NMR of *N*,*N*-bis(pyridin-2-ylmethyl)prop-2-yn-1-amine.

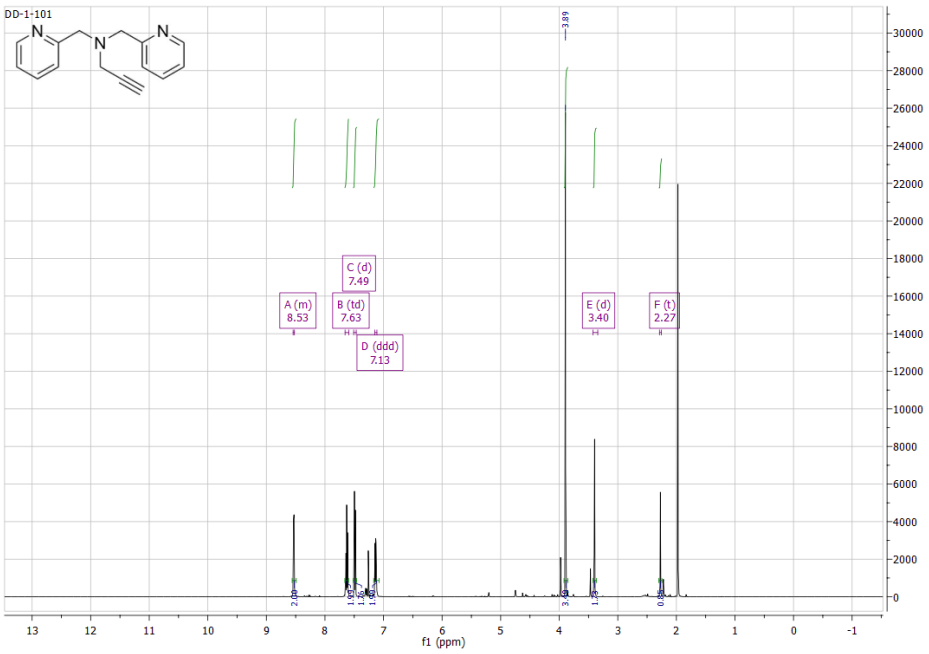

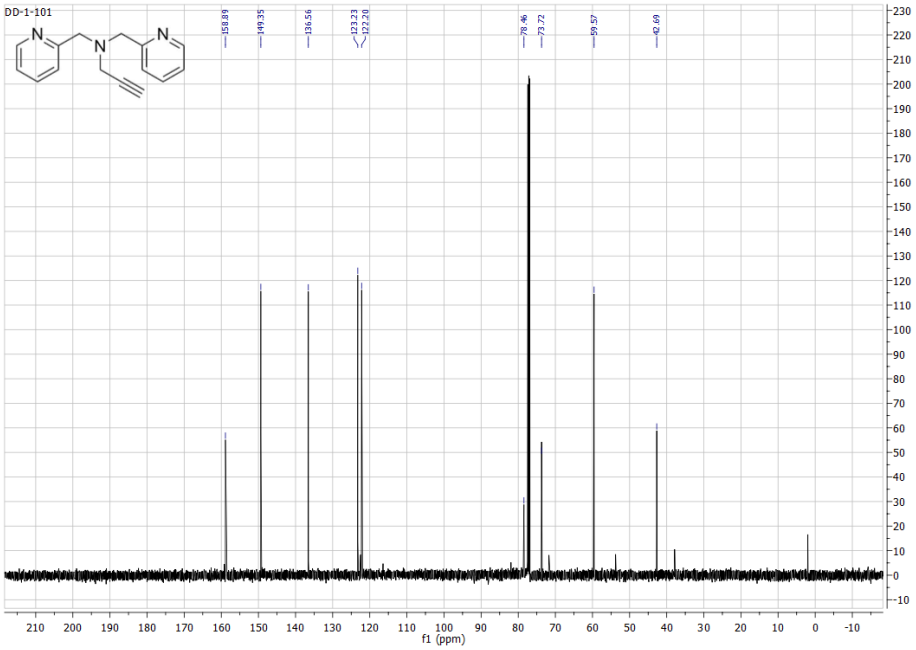

Figure S.9. **^{1}H and ^{13}C NMR of di-*tert*-butyl 2,2'-(prop-2-yn-1-ylazanediyl) diacetate.**

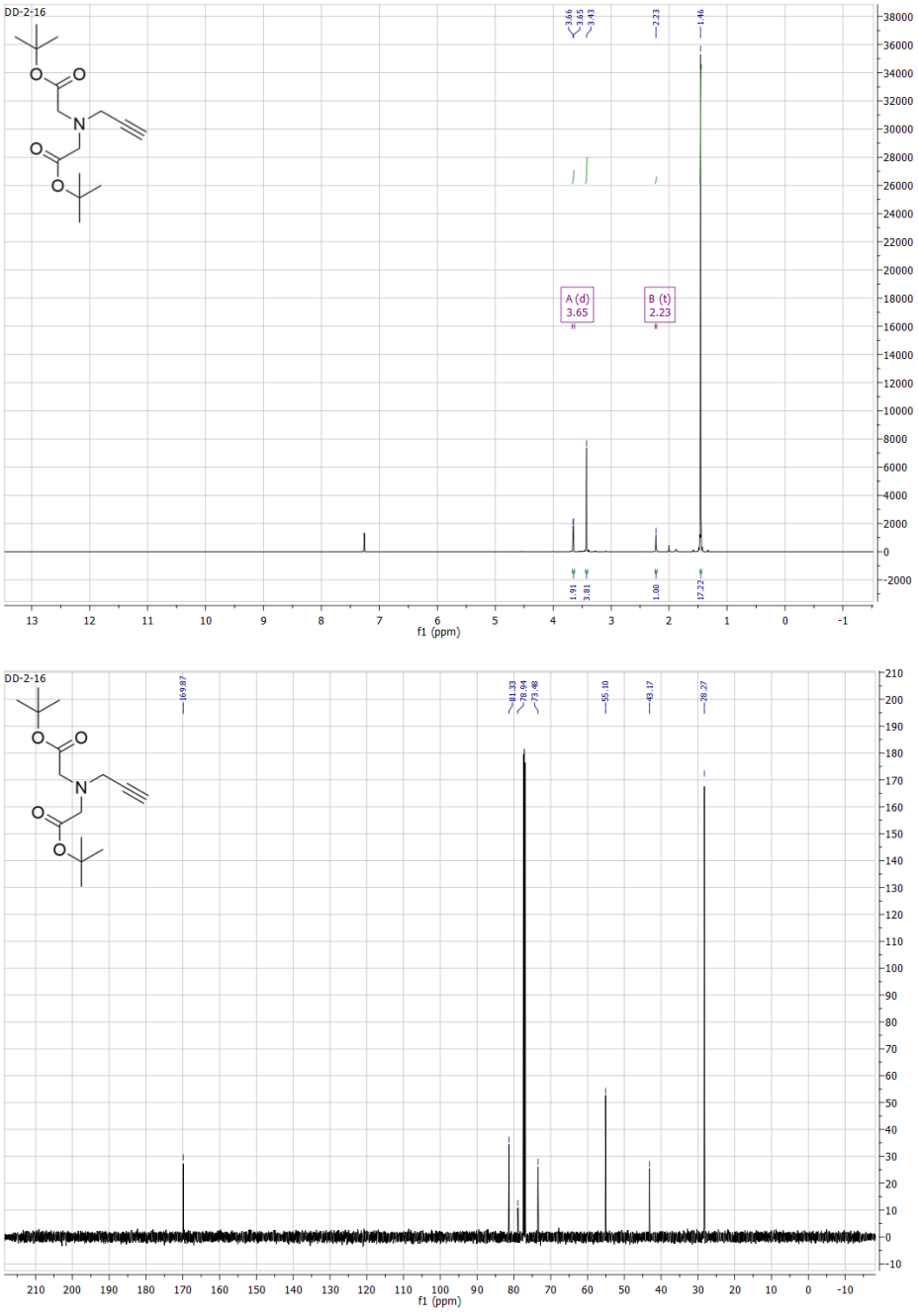

Figure S.10. ^{1}H and ^{13}C NMR of 2,2'-(prop-2-yn-1-ylazanediyl) diacetate.

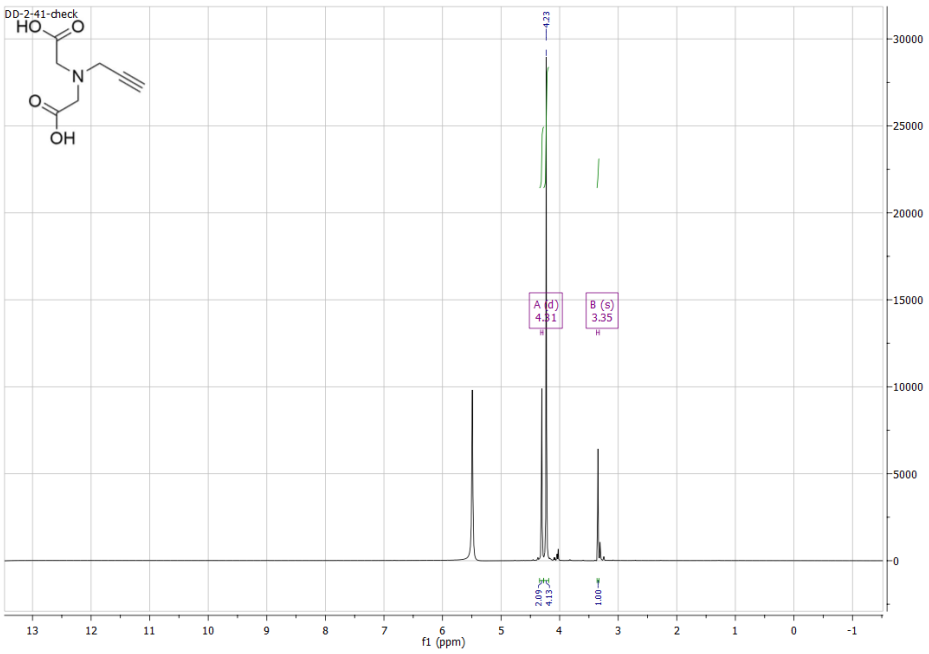

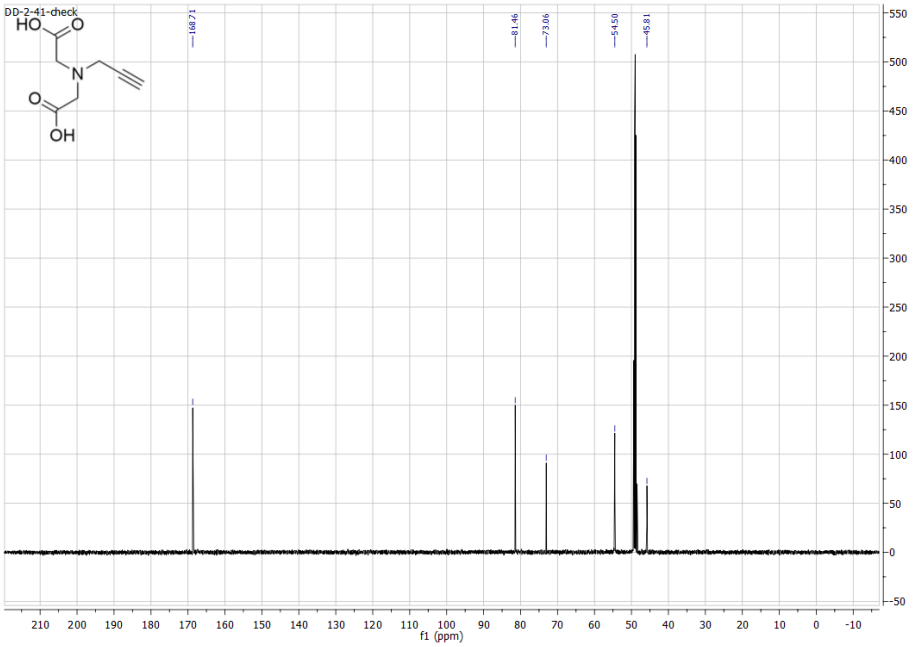

Figure S.11. **^{1}H and ^{13}C NMR of di-*tert*-butyl 2,2'-(((1-(3-(bis(pyridin-2-ylmethyl)amino)propyl)-1*H*-1,2,3-triazol-4-yl)methyl)azanediyl)diacetate.**

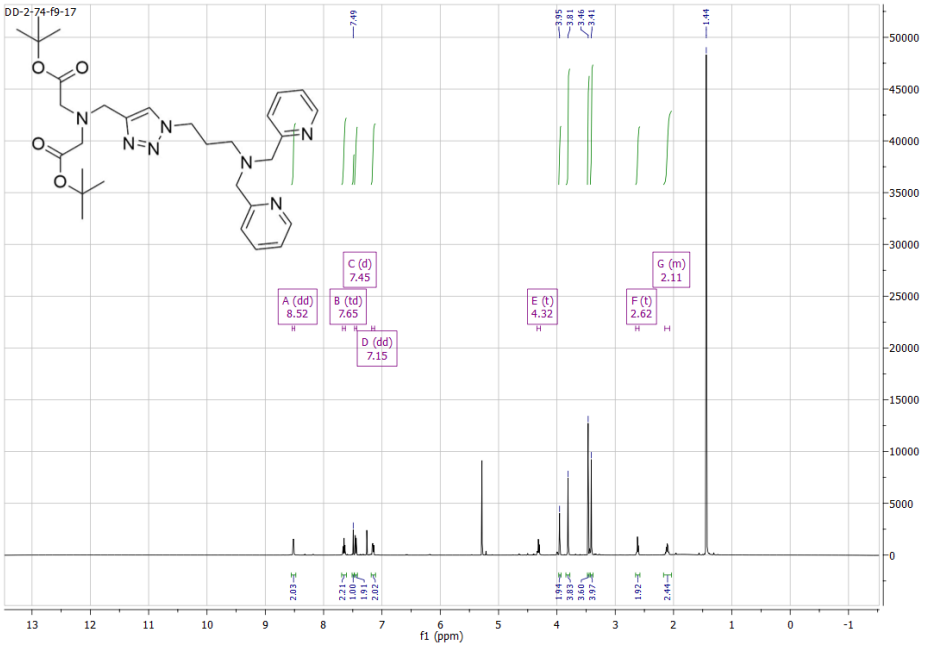

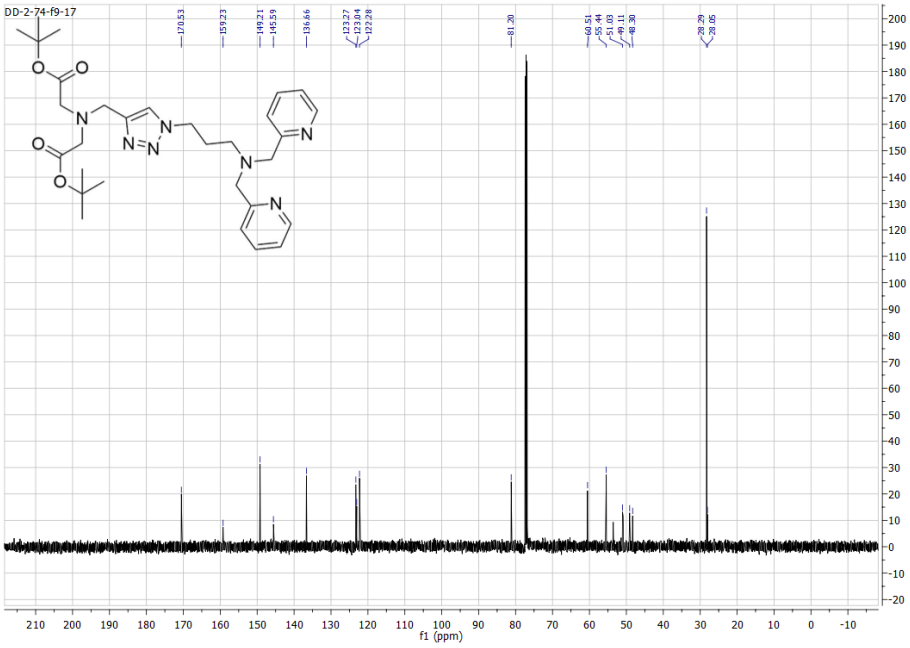

Figure S.12. ^{1}H and ^{13}C NMR of 2,2'-(((1-(3-(bis(pyridin-2-ylmethyl)amino)propyl)-1*H*-1,2,3-triazol-4-yl)methyl)azanediyl)diacetic acid.

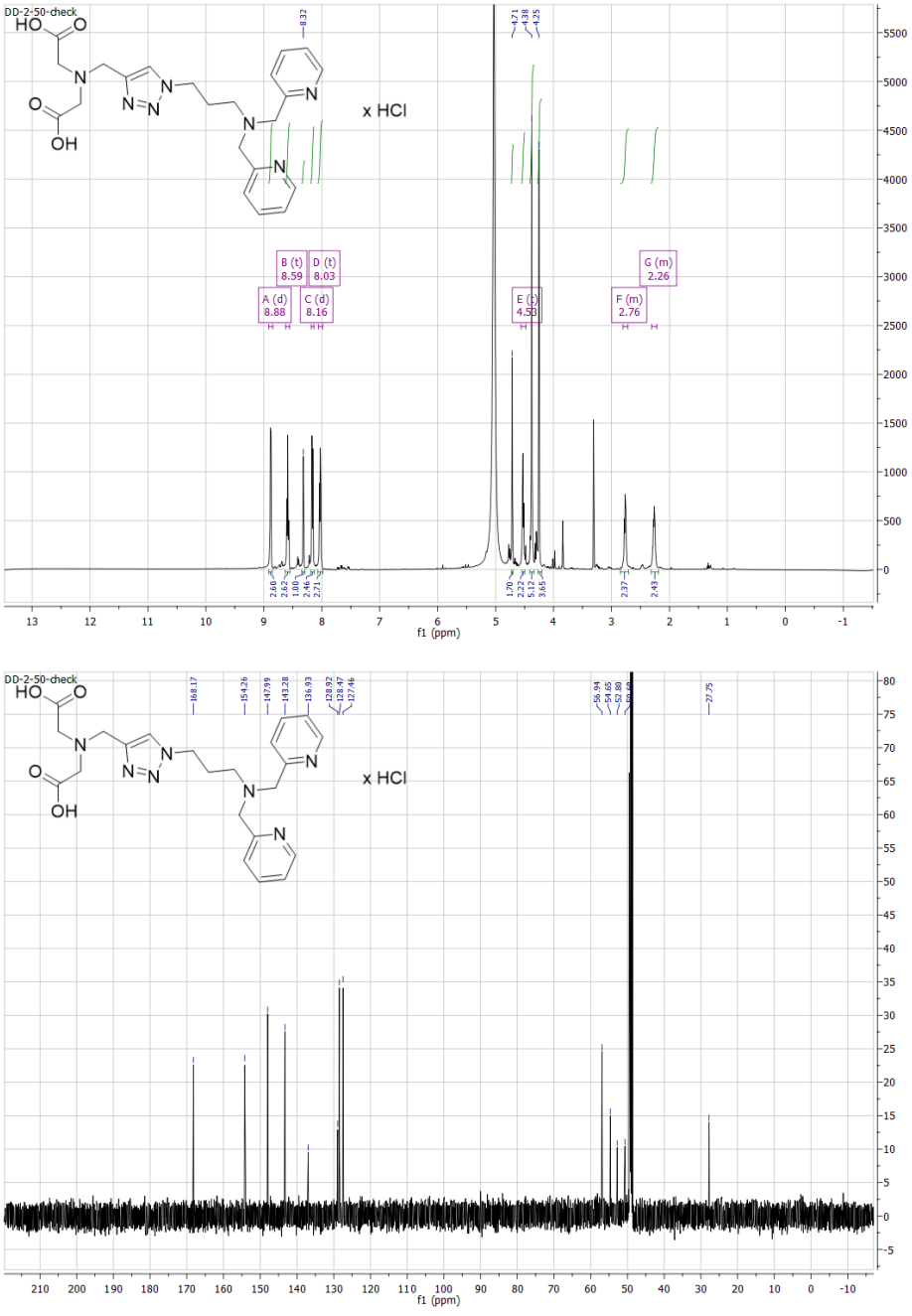

Figure S.13. ^{1}H and ^{13}C NMR of di-*tert*-butyl 2,2'-(((1-5-(bis(pyridin-2-ylmethyl)amino)pentyl)-1*H*-1,2,3-triazol-4-yl)methyl)azanediyl diacetate.

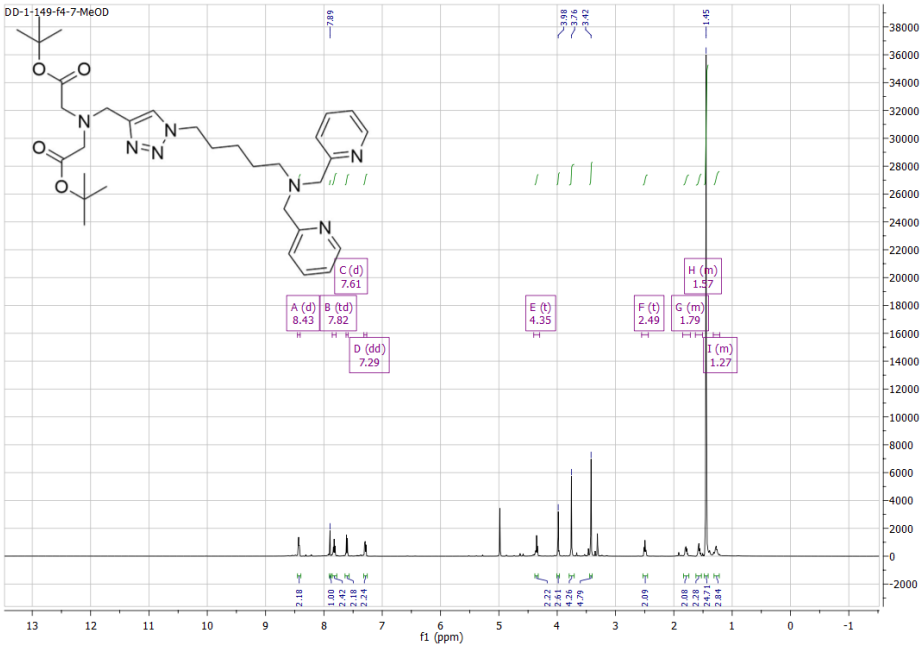

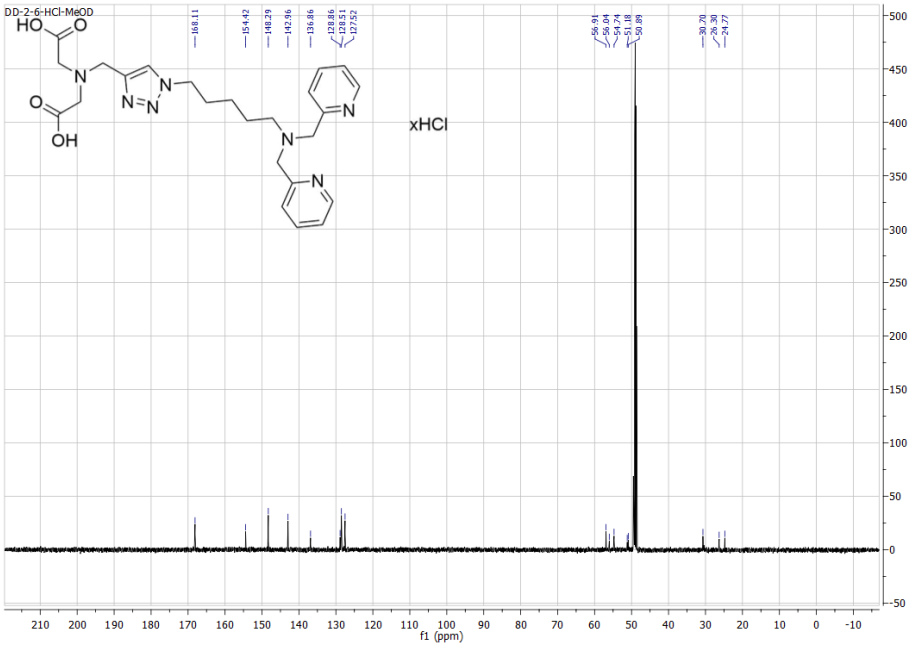

Figure S.14. ^{1}H and ^{13}C NMR of 2,2'-(((1-(5-(bis(pyridin-2-ylmethyl)amino)pentyl)-1*H*-1,2,3-triazol-4-yl)methyl)azanediyl)diacetic acid.

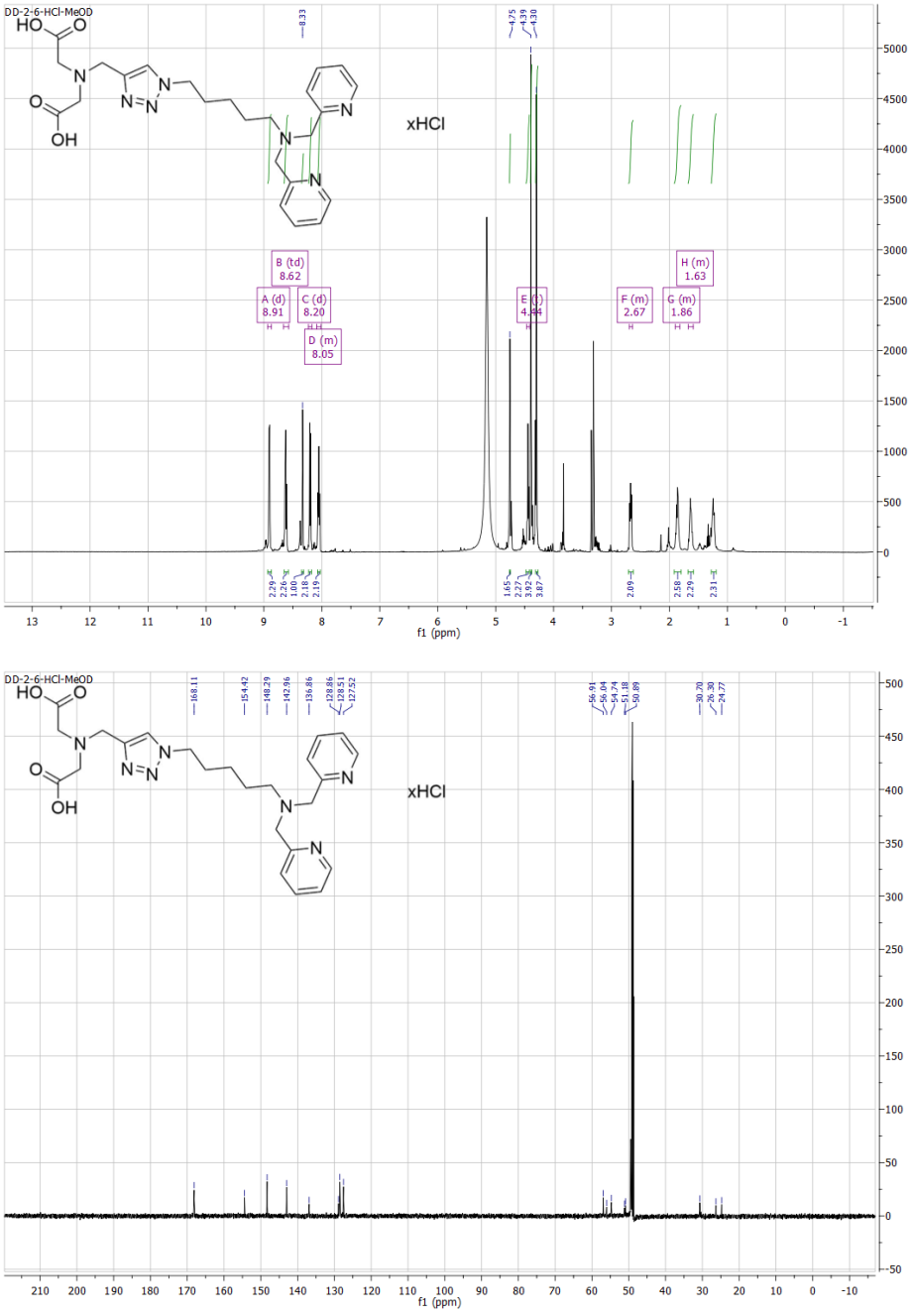

Figure S.15. MS spectrum of reaction mixture of Compound 13.

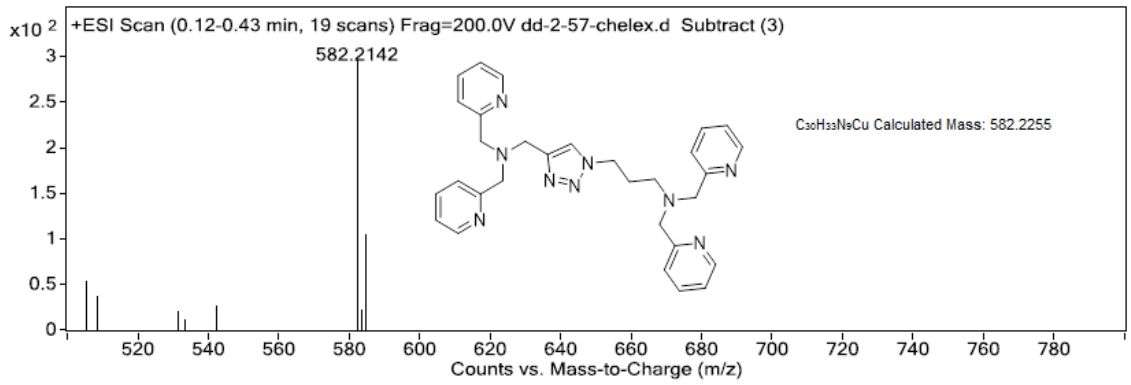

Figure S.16. Job's plot of Compound 10 using lines of best fit to find stoichiometric ratio of L:M.

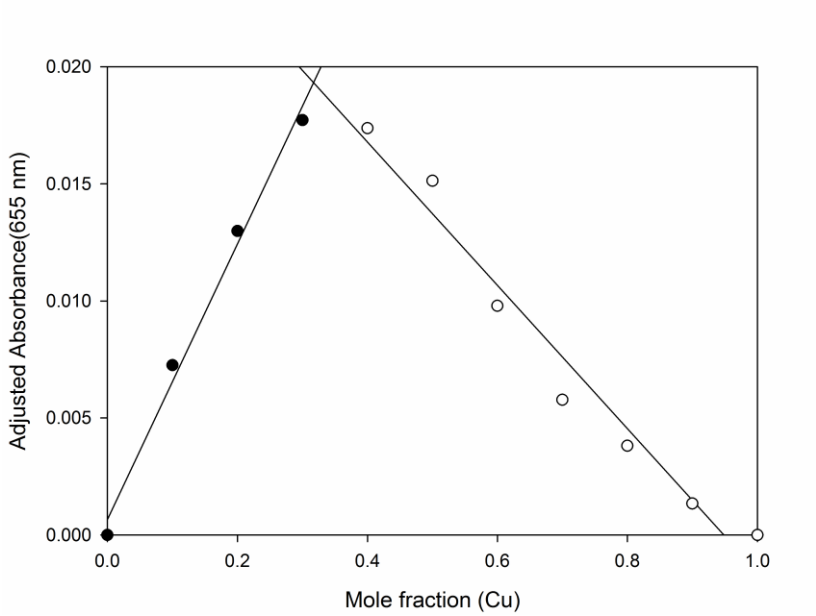

Figure S.17. Job's plot of Compound 12 using lines of best fit to find stoichiometric ratio of L:M.

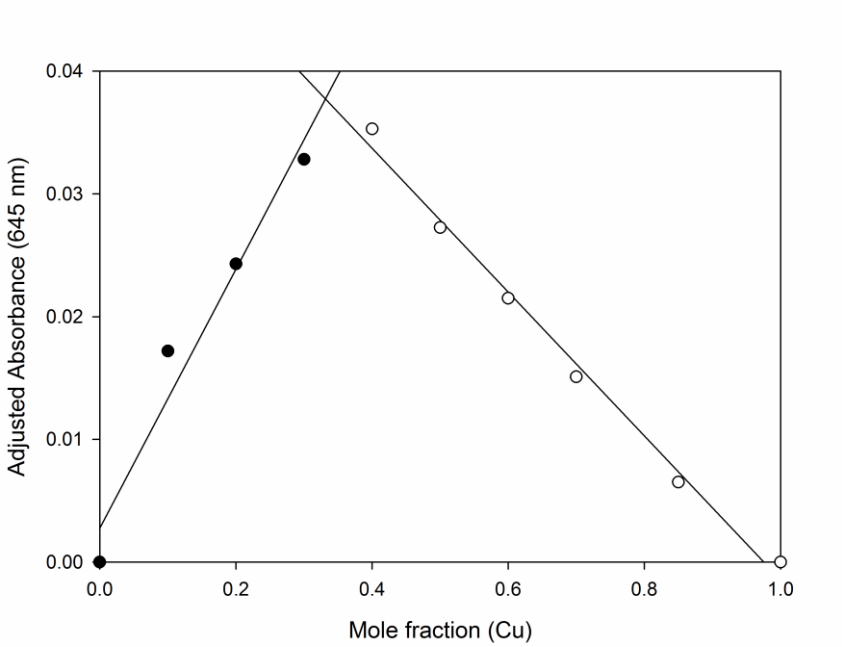

Figure S.18. Compound 10 with calculated pK_a values for all resonances and associated R^2 values.

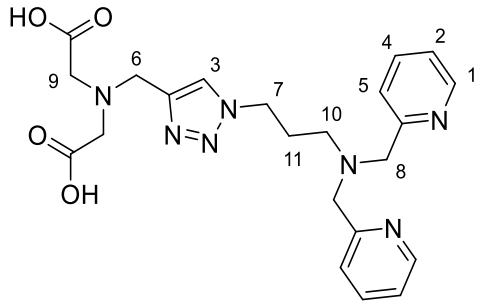

Peak	Calculated pK_a	R^2-value
1	4.34 ± 0.13	0.9928
2	3.65 ± 0.08	0.9957
3	7.44 ± 0.09	0.9933
4	3.54 ± 0.07	0.9959
5	3.79 ± 0.11	0.9946
6	7.98 ± 0.04	0.9971
7	6.60 ± 0.16	0.9842
8	3.18 ± 0.03, 6.00 ± 0.02	0.9994, 0.9991
9	7.98 ± 0.06	0.9948
10	3.15 ± 0.10, 6.08 ± 0.03	0.9910, 0.9982,
11	3.15 ± 0.14, 6.10 ± 0.07	0.9850, 0.9930

Figure S.19. pH dependent NMR shift and associated sigmoidal fits for Compound 10 Resonance H_1.

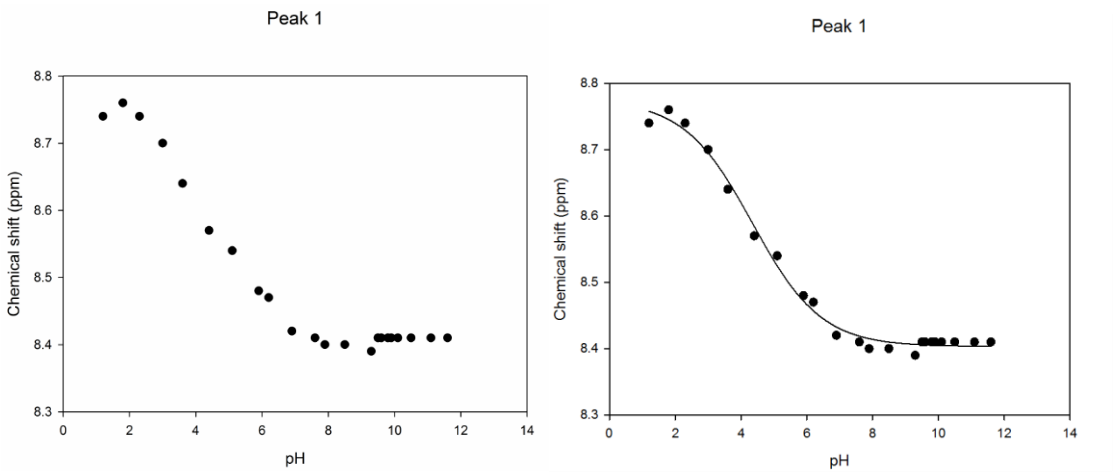

Figure S.20. pH dependent NMR shift and associated sigmoidal fits for Compound 10 Resonance H_2.

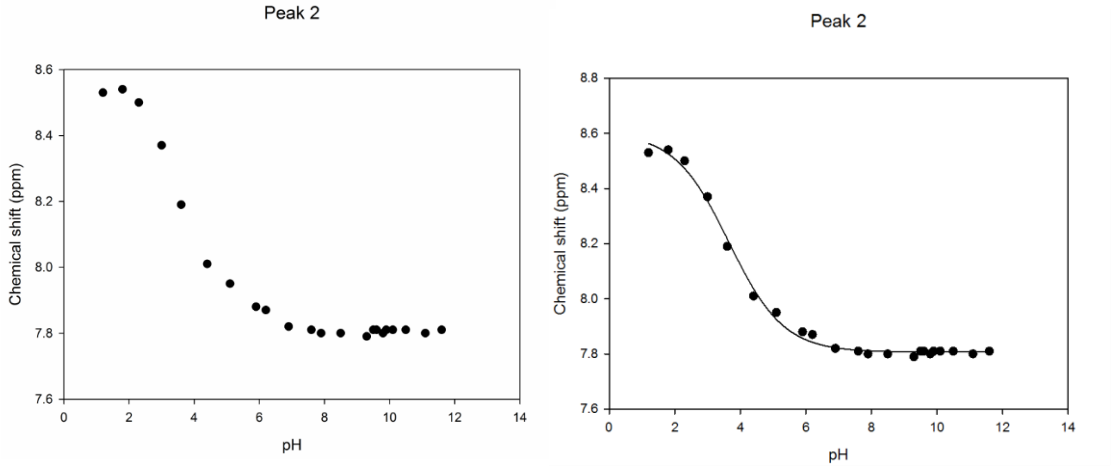

Figure S.21. pH dependent NMR shift and associated sigmoidal fits for Compound 10 Resonance H_3.

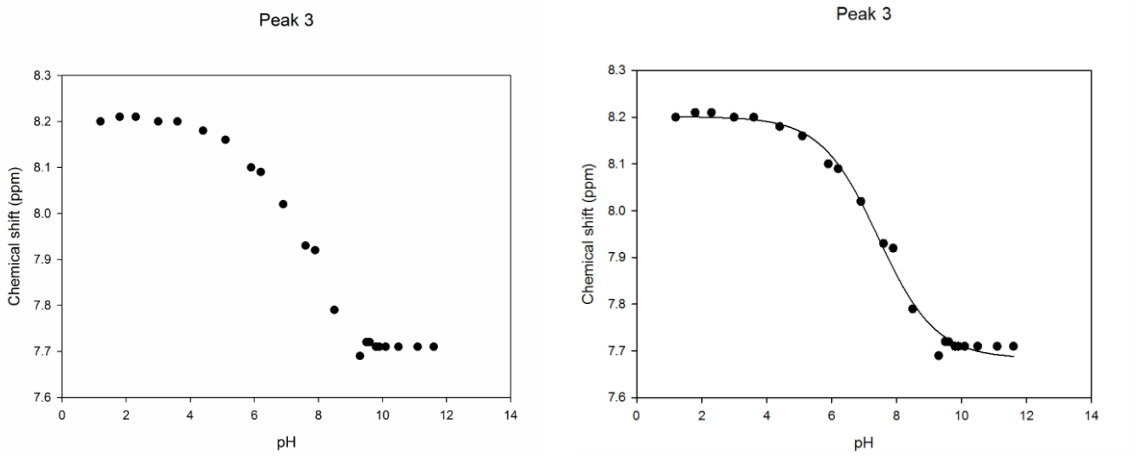

Figure S.22. pH dependent NMR shift and associated sigmoidal fits for Compound 10 Resonance H_4.

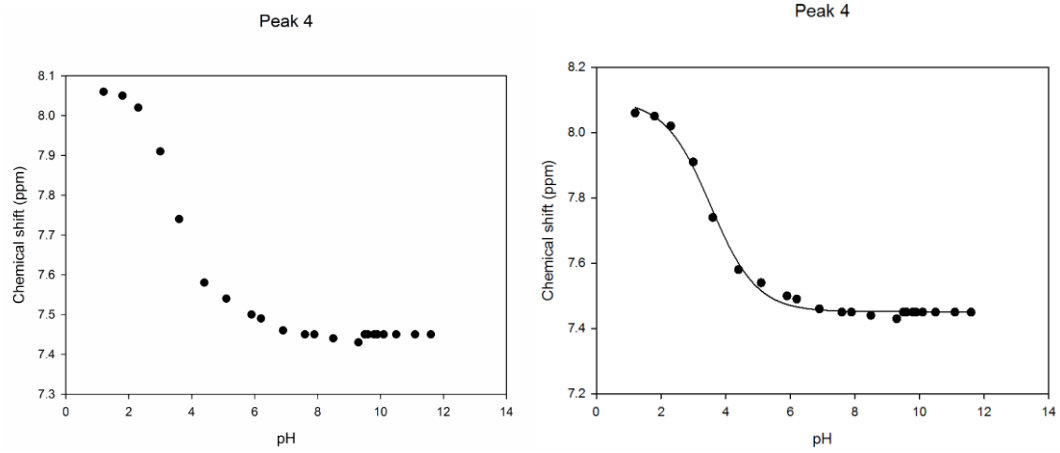

Figure S.23. pH dependent NMR shift and associated sigmoidal fits for Compound 10 Resonance H_5.

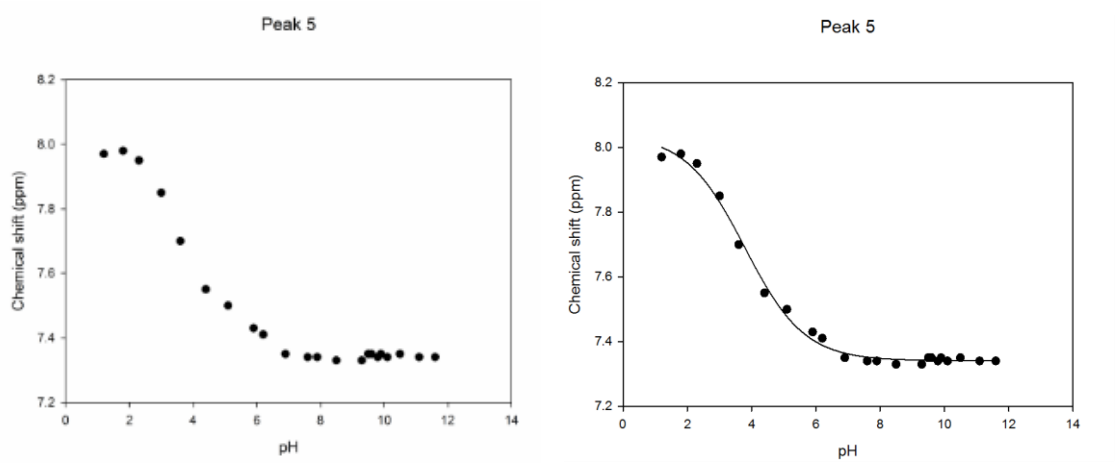

Figure S.24. pH dependent NMR shift and associated sigmoidal fits for Compound 10 Resonance H_6.

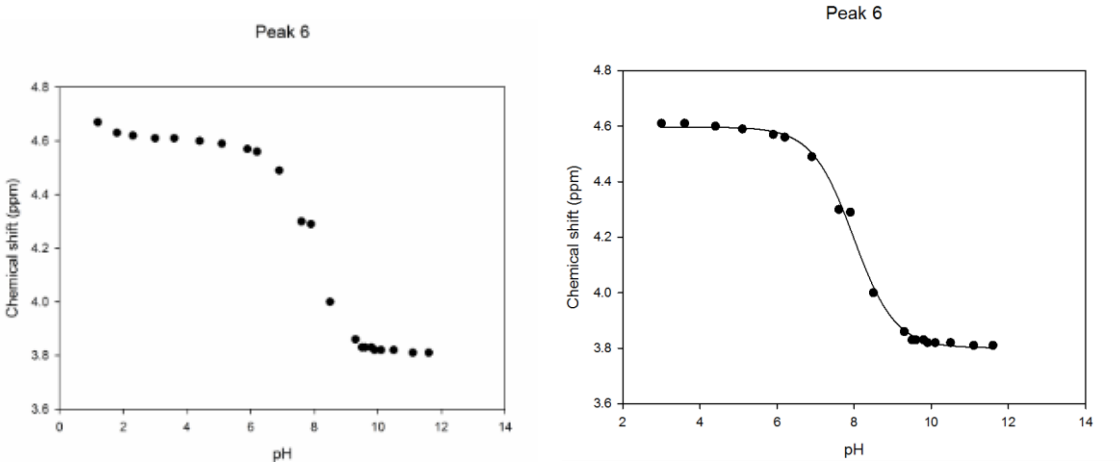

Figure S.25. pH dependent NMR shift and associated sigmoidal fits for Compound 10 Resonance H_7.

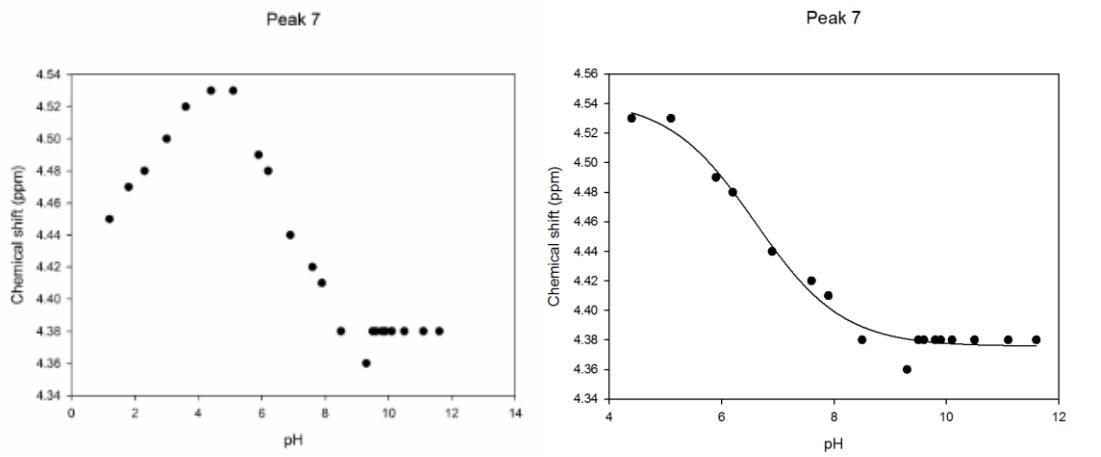

Figure S.26. pH dependent NMR shift and associated sigmoidal fits for Compound 10 Resonance H_8

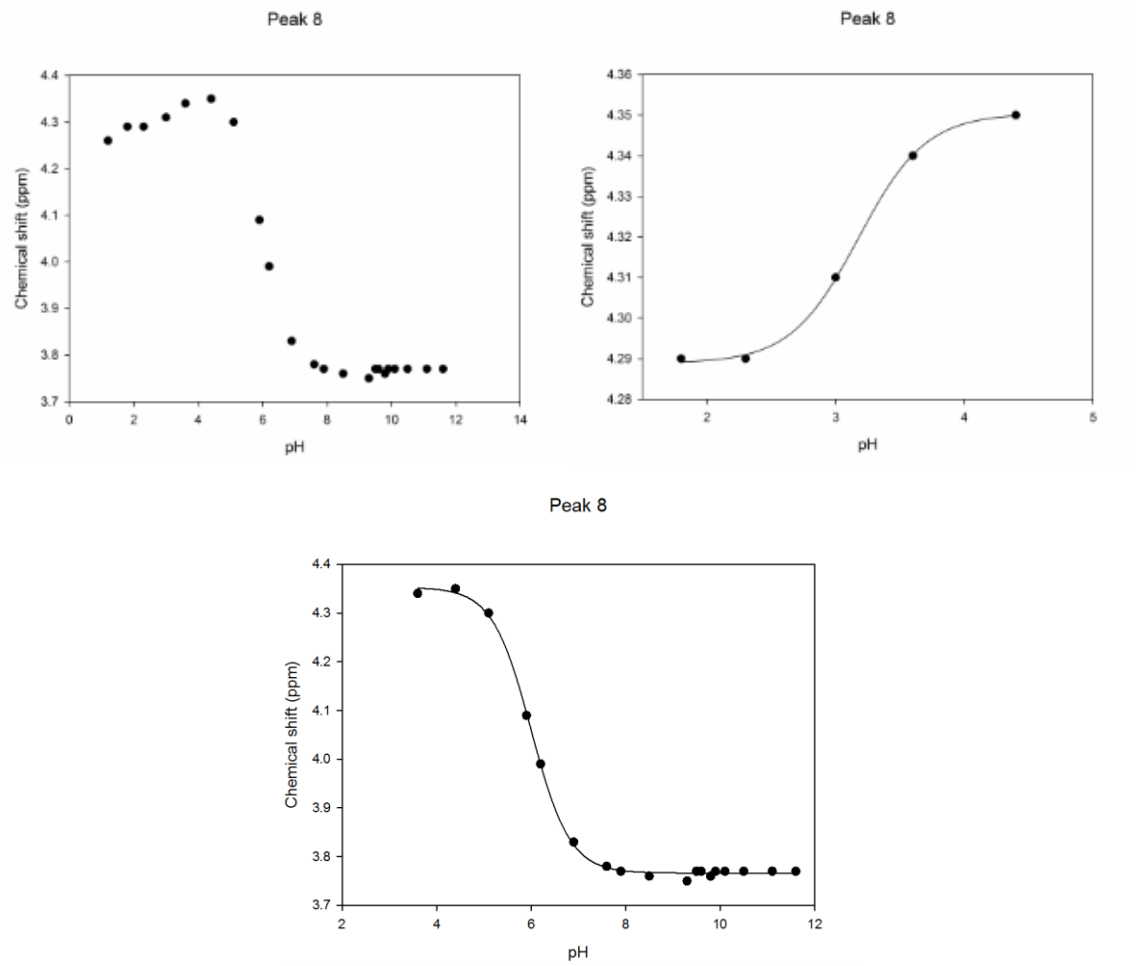

Figure S.27. pH dependent NMR shift and associated sigmoidal fits for Compound 10 Resonance H_9.

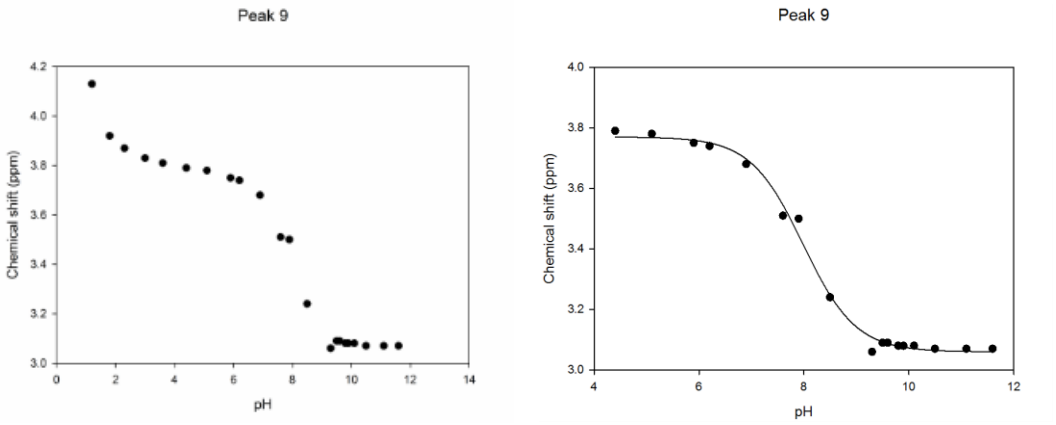

Figure S.28. pH dependent NMR shift and associated sigmoidal fits for Compound 10 Resonance H_{10}.

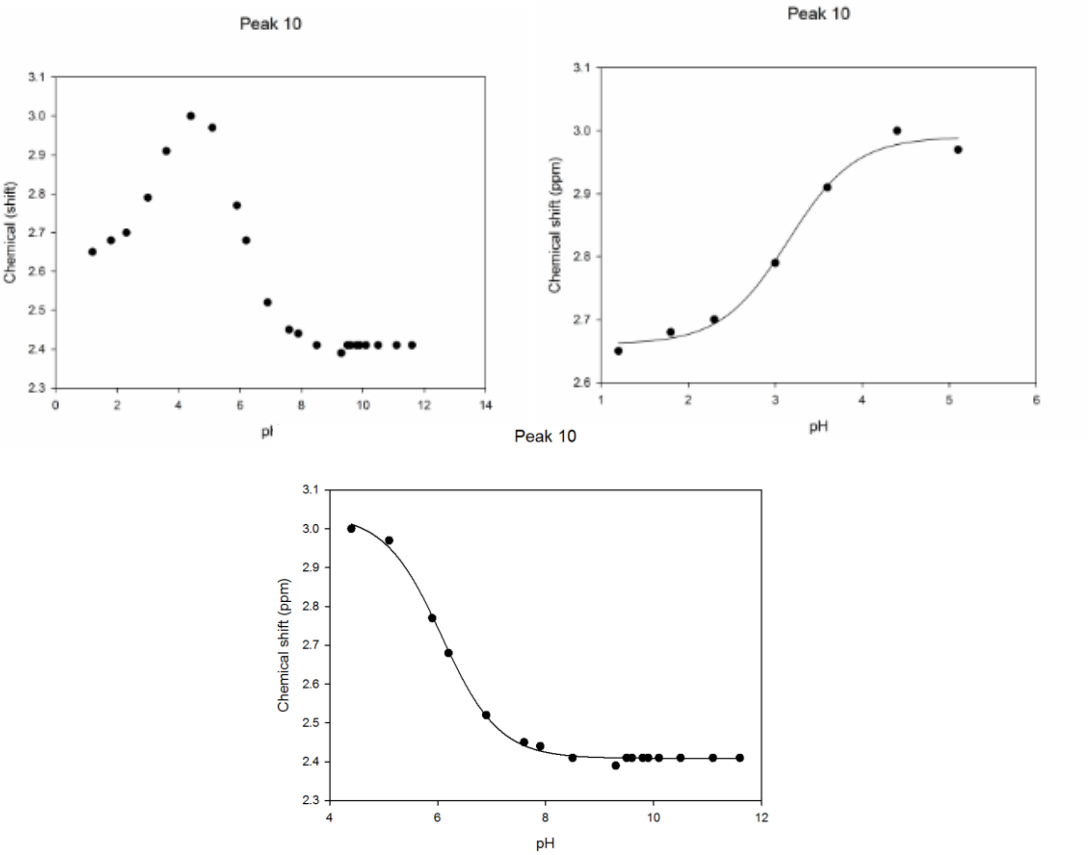

Figure S.29. pH dependent NMR shift and associated sigmoidal fits for Compound 10 Resonance H_{11}.

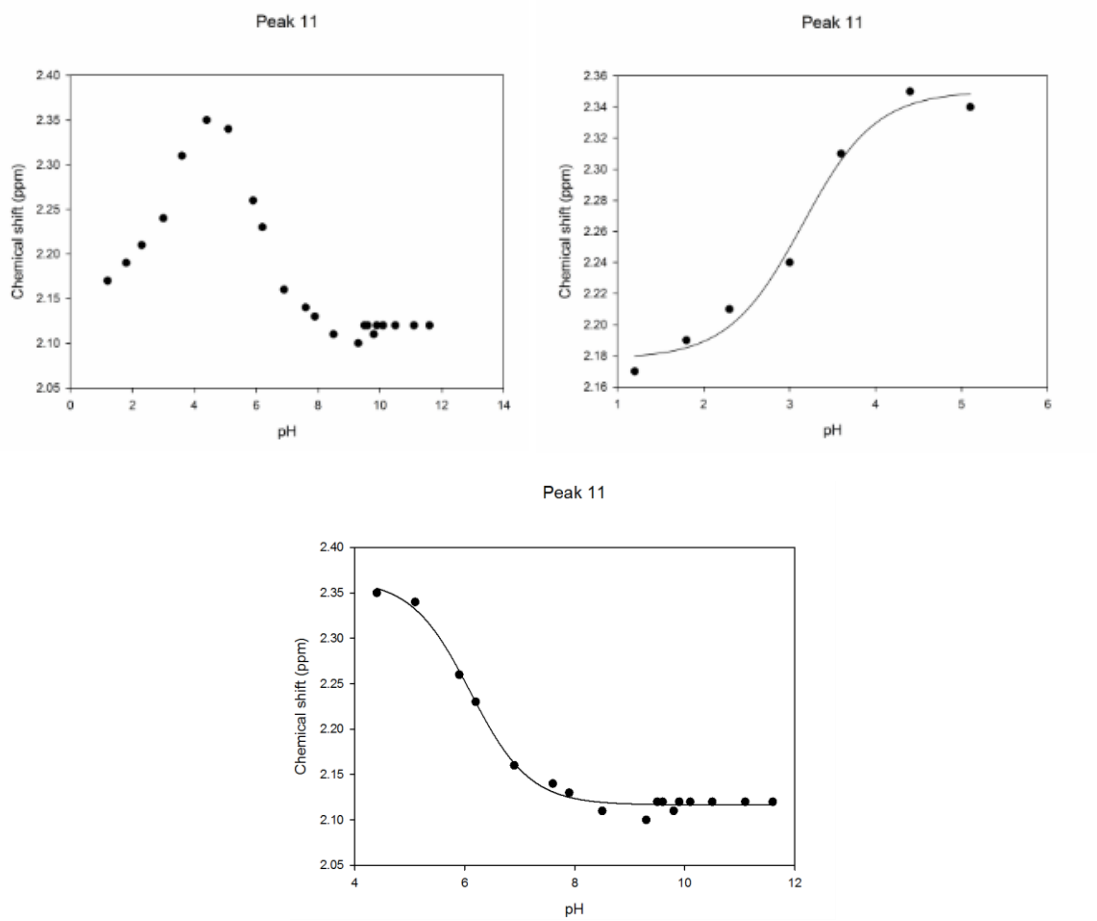

Figure S.30. Compound 12 with calculated pK_a values for all resonances and associated R^2 values.

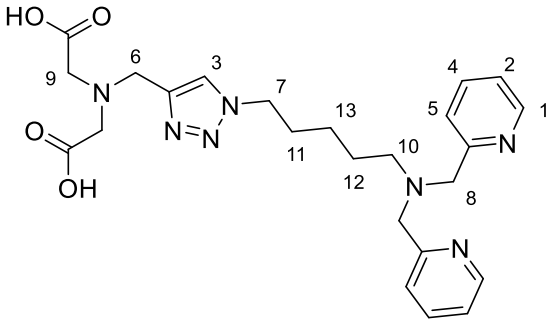

Peak	Calculated pK_a	R^2-value
1	2.76 ± 0.09, 7.05 ± 0.05	0.9905, 0.9968
2	2.69 ± 0.04, 7.14 ± 0.07	0.9994, 0.9907
3	7.40 ± 0.04	0.9962
4	2.66 ± 0.04, 7.44 ± 0.09	0.9993, 0.9926
5	2.64 ± 0.07, 7.11 ± 0.03	0.9974, 0.9988
6	7.99 ± 0.02	0.9992
7	2.39 ± 0.14, 7.45 ± 0.05	0.9937, 0.9978
8	2.60 ± 0.08, 7.10 ± 0.03	0.9953, 0.9989
9	8.01 ± 0.02	0.9993
10	2.62 ± 0.08, 7.10 ± 0.03	0.9962, 0.9989
11	2.59 ± 0.11, 7.28 ± 0.04	0.9911, 0.9978
12	2.74 ± 0.05, 7.08 ± 0.05	0.9977, 0.9968
13	N/A	N/A

Figure S.31. pH dependent NMR shift and associated sigmoidal fits for Compound 12 Resonance H_1.

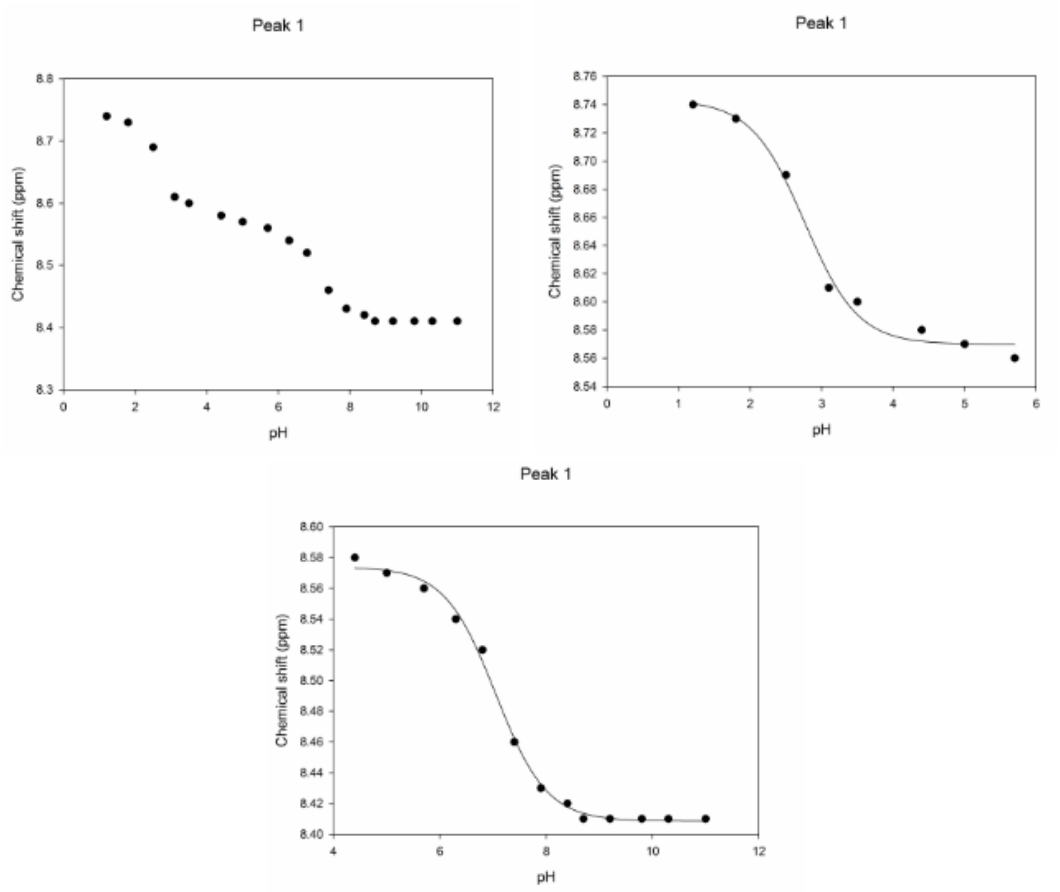

Figure S.32. pH dependent NMR shift and associated sigmoidal fits for Compound 12 Resonance H_2.

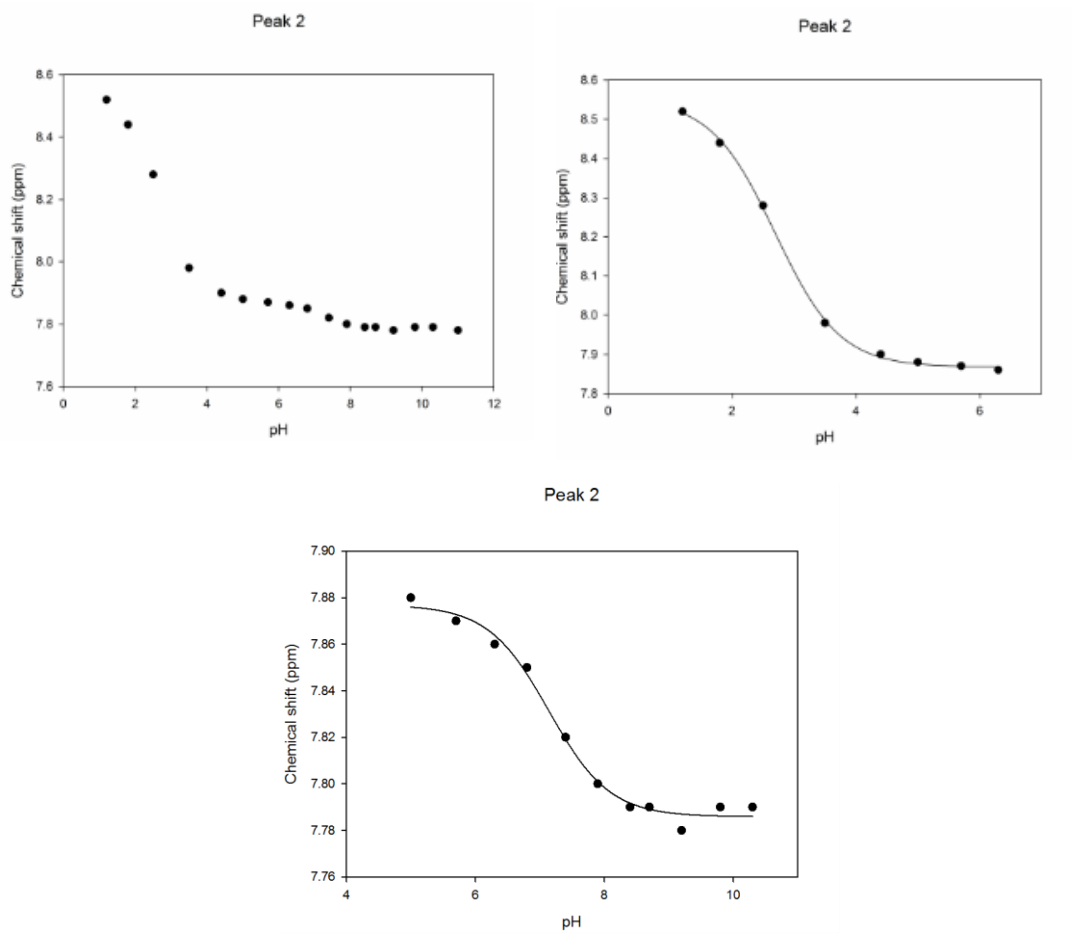

Figure S.33. pH dependent NMR shift and associated sigmoidal fits for Compound 12 Resonance H_3.

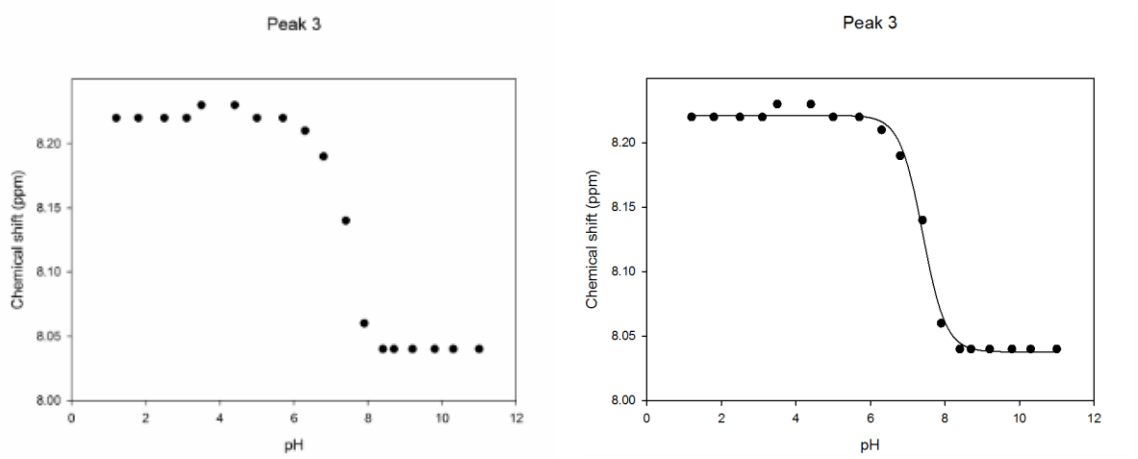

Figure S.34. pH dependent NMR shift and associated sigmoidal fits for Compound 12 Resonance H_4.

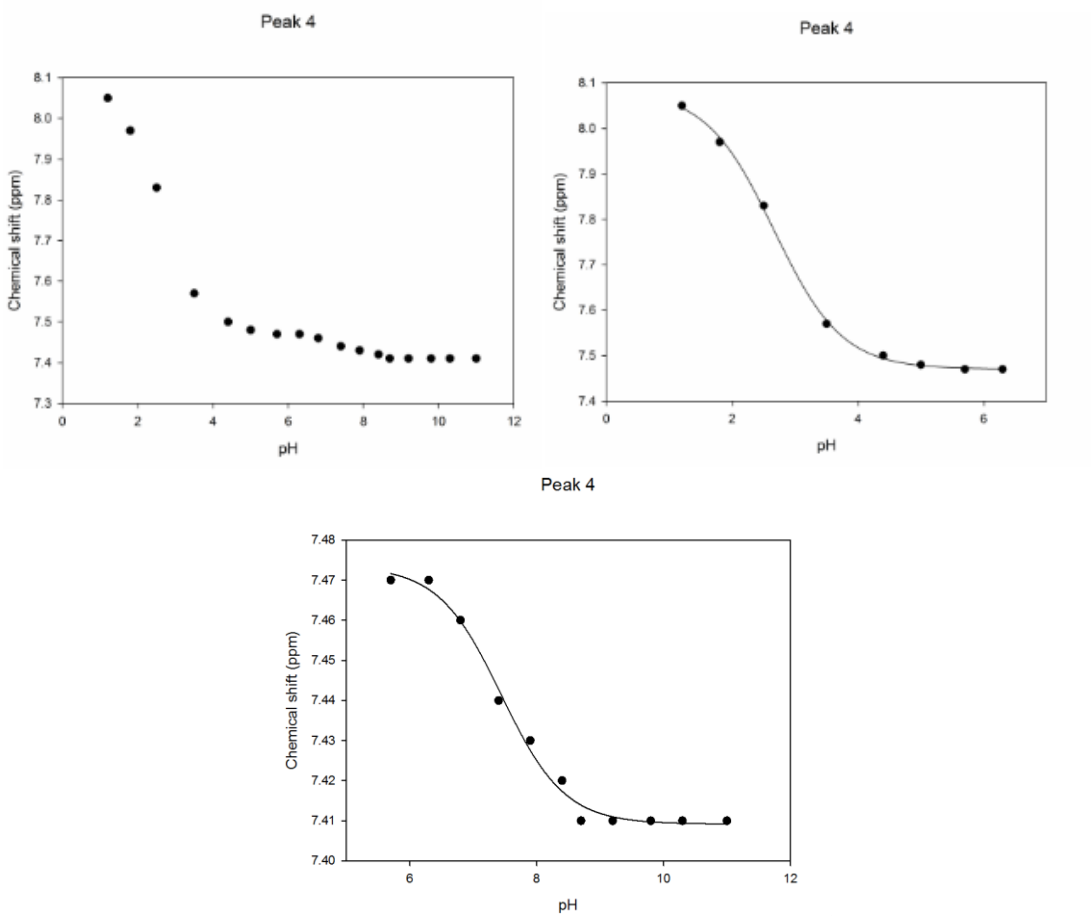

Figure S.35. pH dependent NMR shift and associated sigmoidal fits for Compound 12 Resonance H_5.

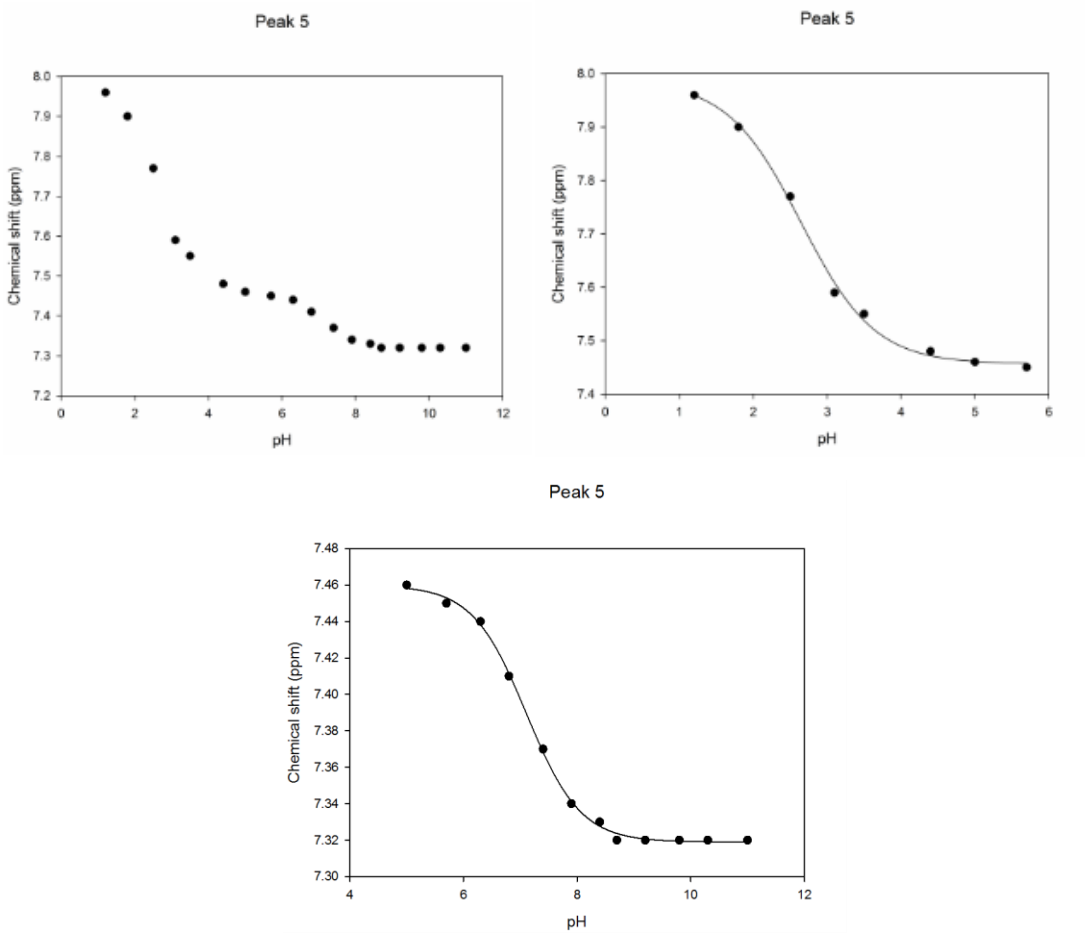

Figure S.36. pH dependent NMR shift and associated sigmoidal fits for Compound 12 Resonance H_6.

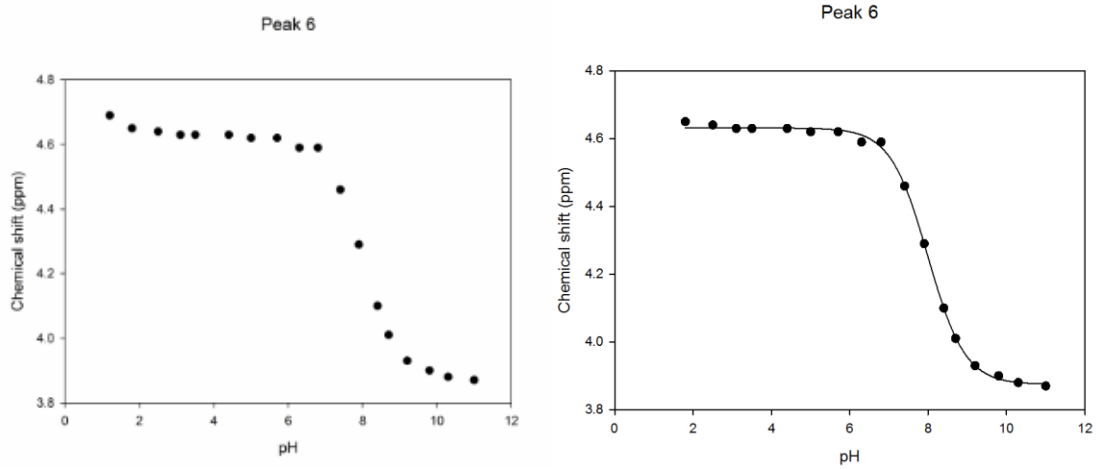

Figure S.37. pH dependent NMR shift and associated sigmoidal fits for Compound 12 Resonance H_7.

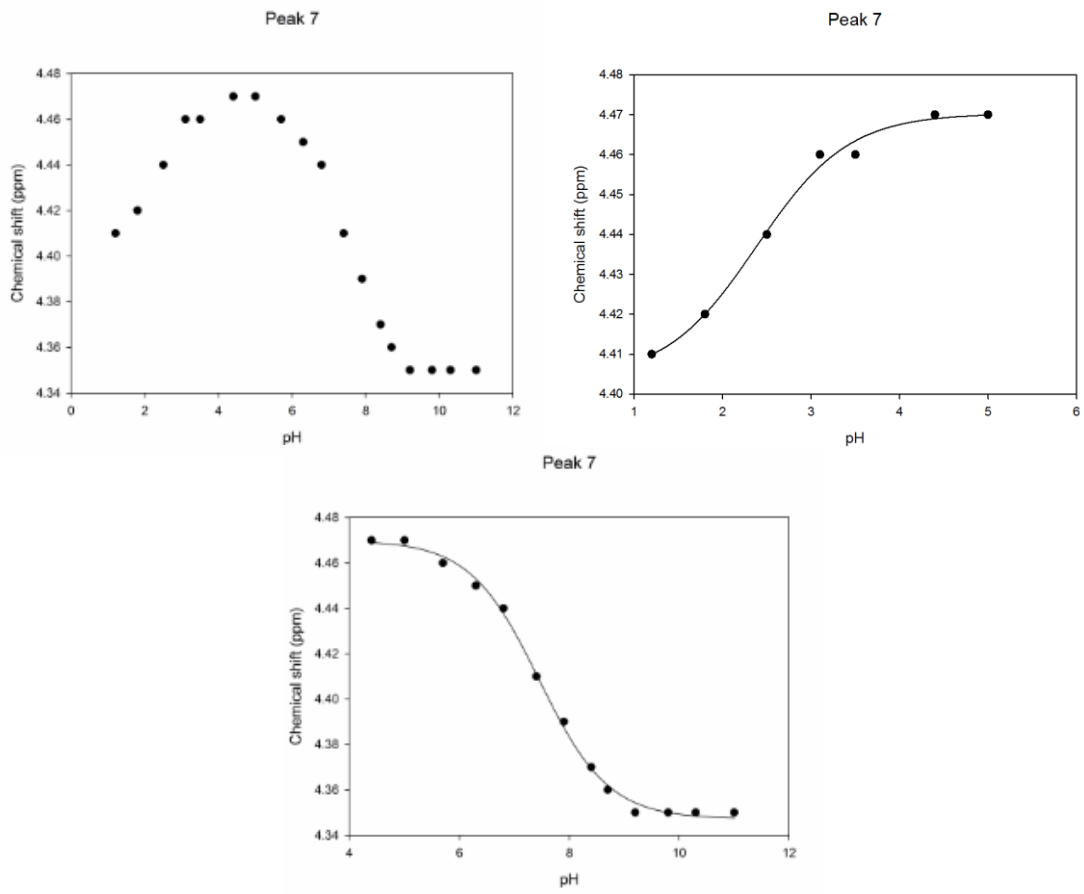

Figure S.38. pH dependent NMR shift and associated sigmoidal fits for Compound 12 Resonance H_8.

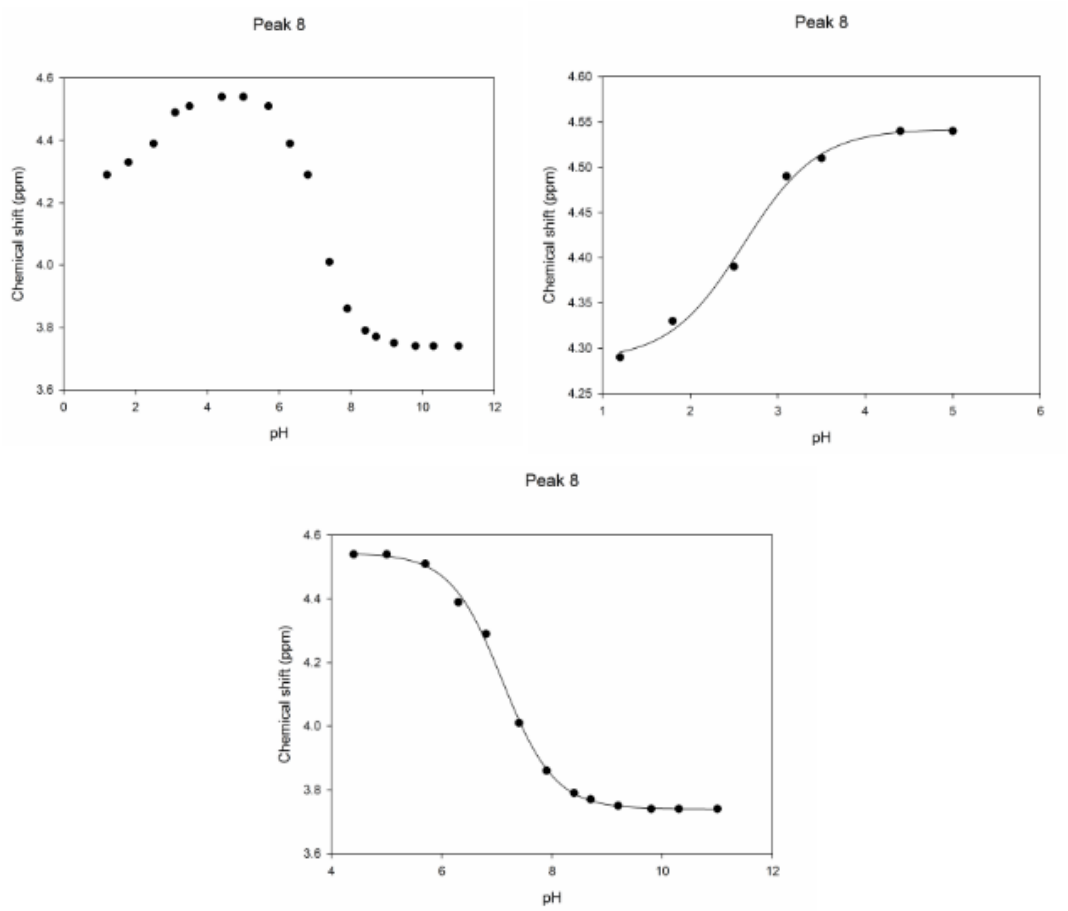

Figure S.39. pH dependent NMR shift and associated sigmoidal fits for Compound 12 Resonance H_9.

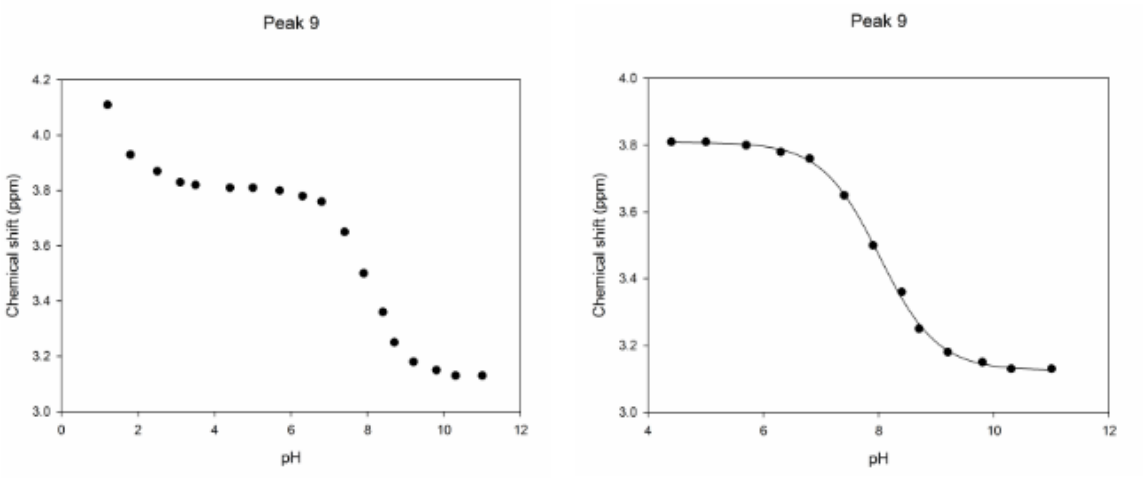

Figure S.40. pH dependent NMR shift and associated sigmoidal fits for Compound 12 Resonance H_{10}.

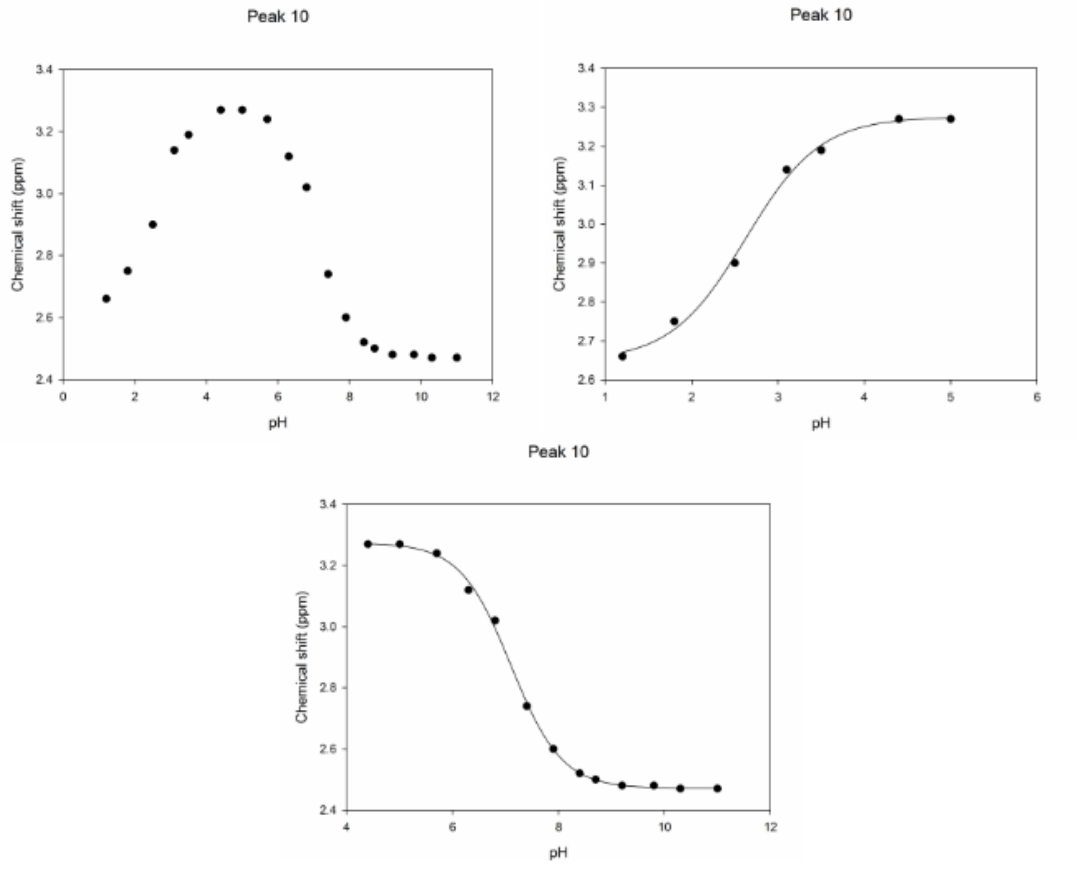

Figure S.41. pH dependent NMR shift and associated sigmoidal fits for Compound 12 Resonance H_{11}.

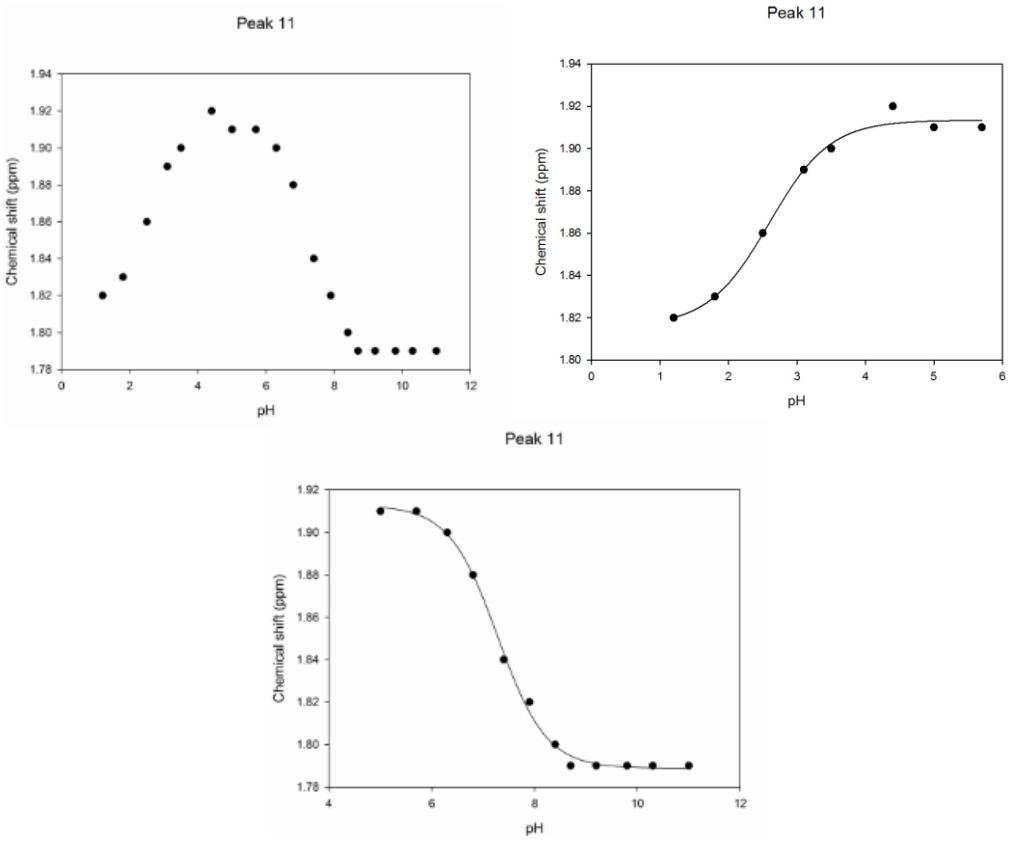

Figure S.42. pH dependent NMR shift and associated sigmoidal fits for Compound 12 Resonance H_{12}.

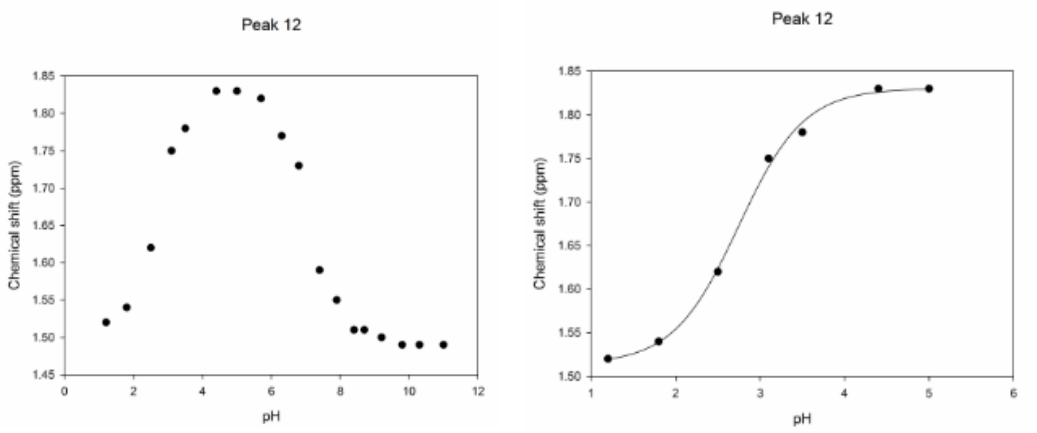

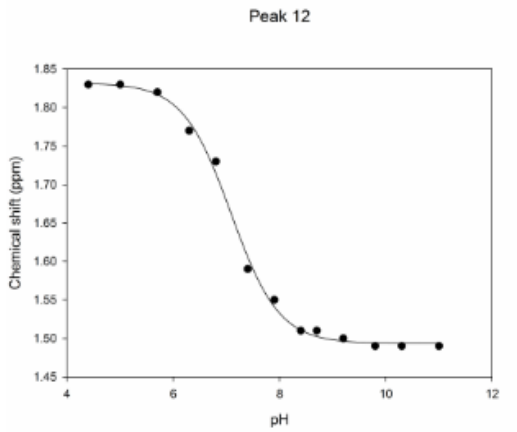

Figure S.43. pH dependent NMR shift and associated sigmoidal fits for Compound 12 Resonance H_{13}

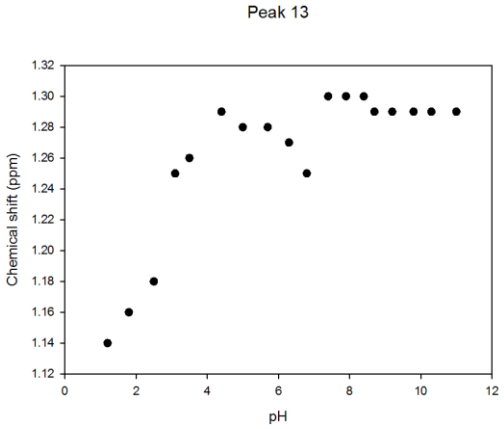

Figure S.44. ^{1}H and ^{13}C NMR of (1*H*-imidazol-4-yl)methanol hydrochloride.

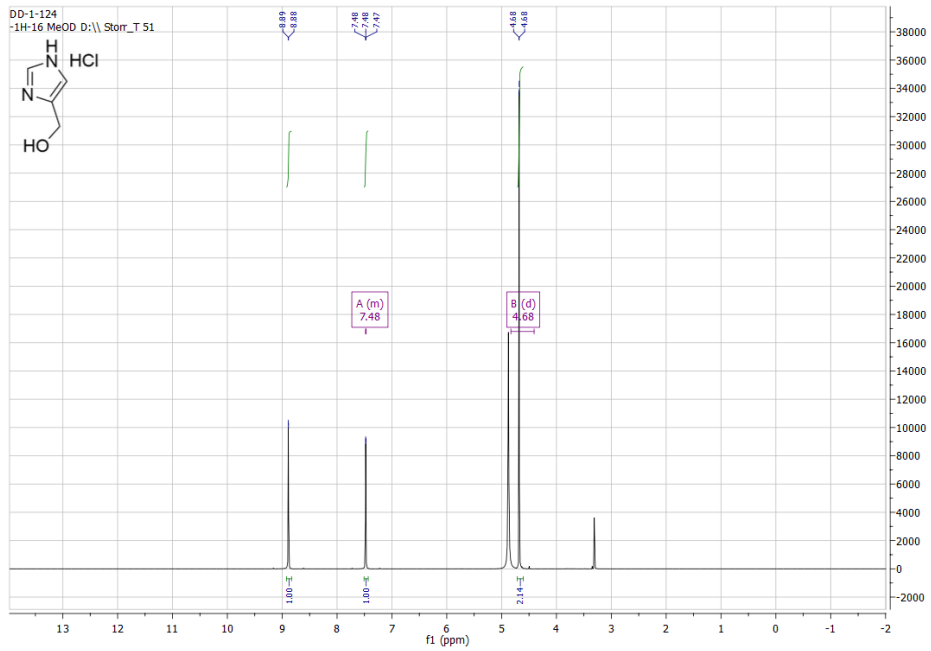

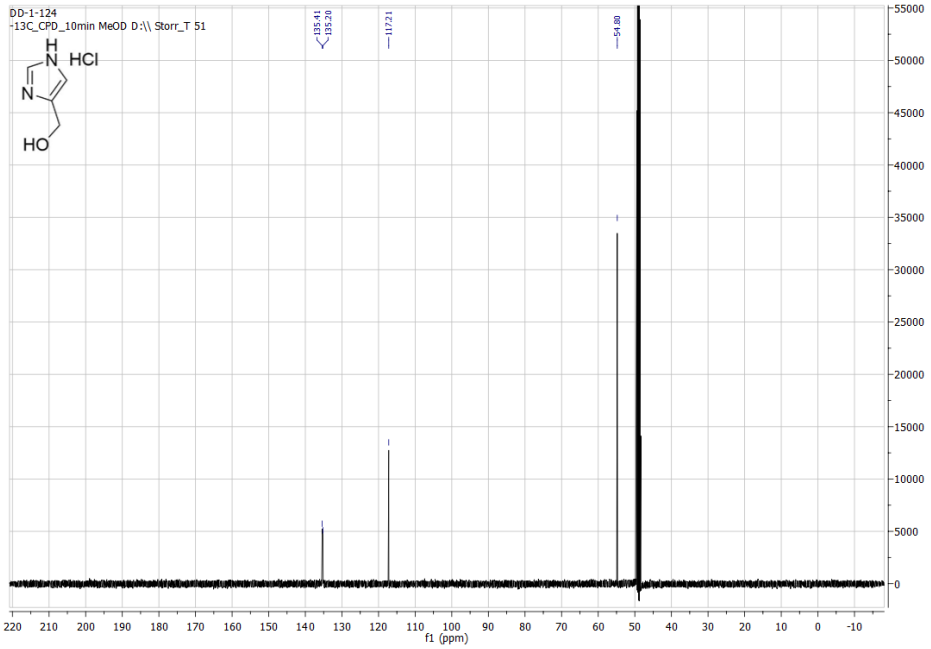

Figure S.45. ^{1}H and ^{13}C NMR of 4-(chloromethyl)-1*H*-imidazole hydrochloride.

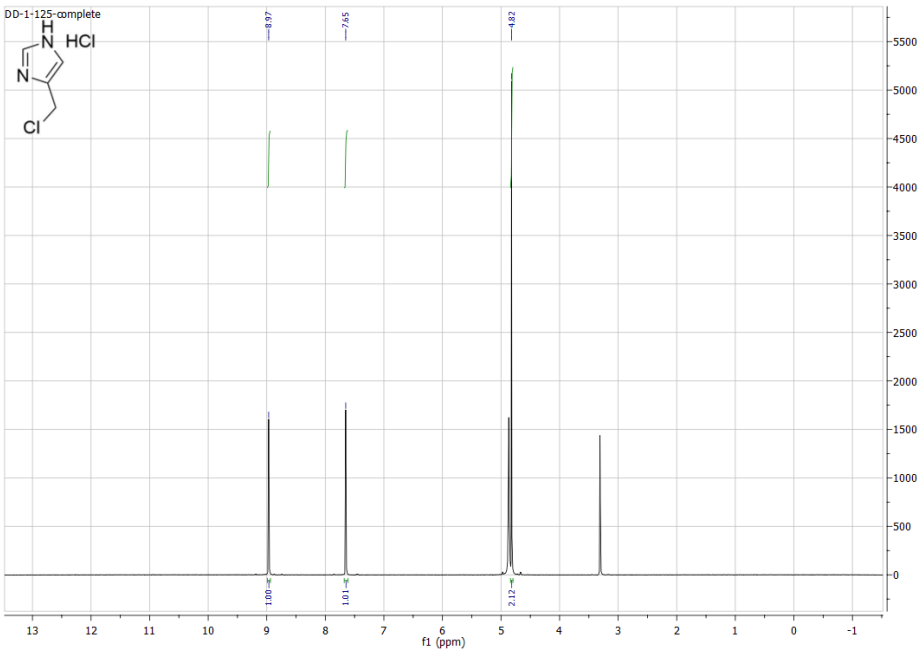

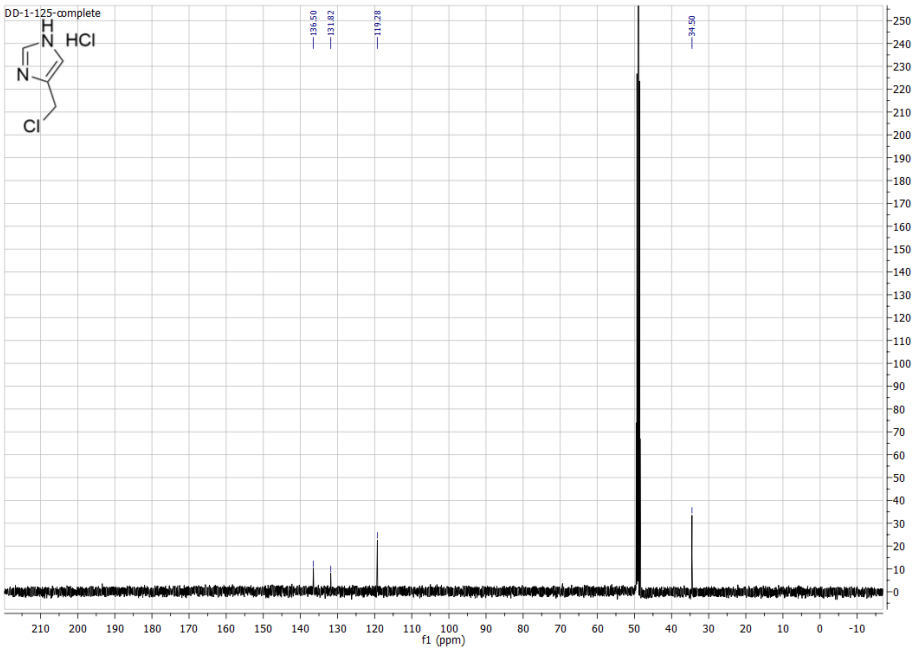

Figure S.46. ^{1}H and ^{13}C NMR of 4-(azidomethyl)-1*H*-imidazole

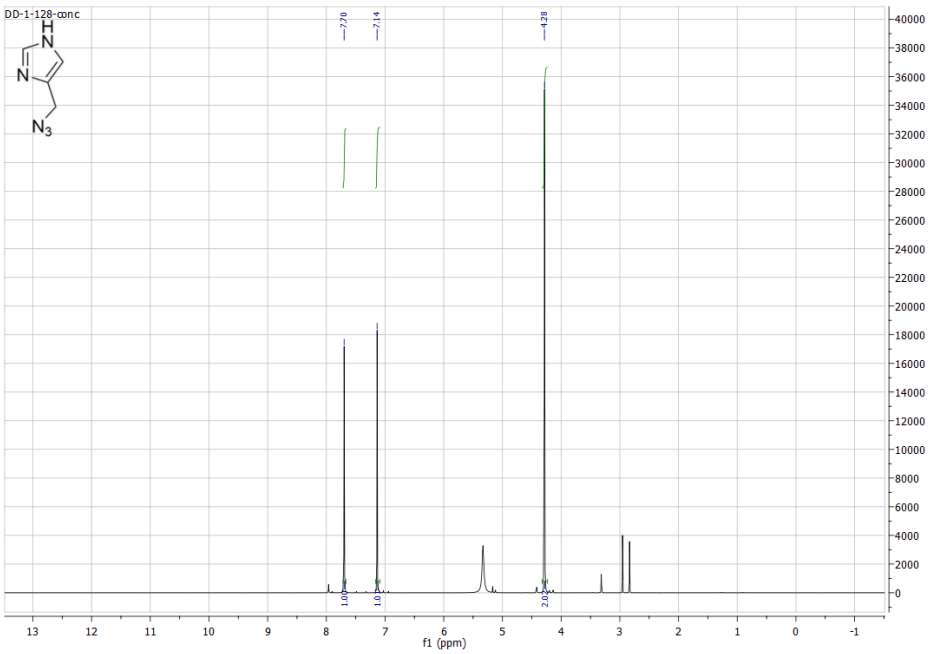

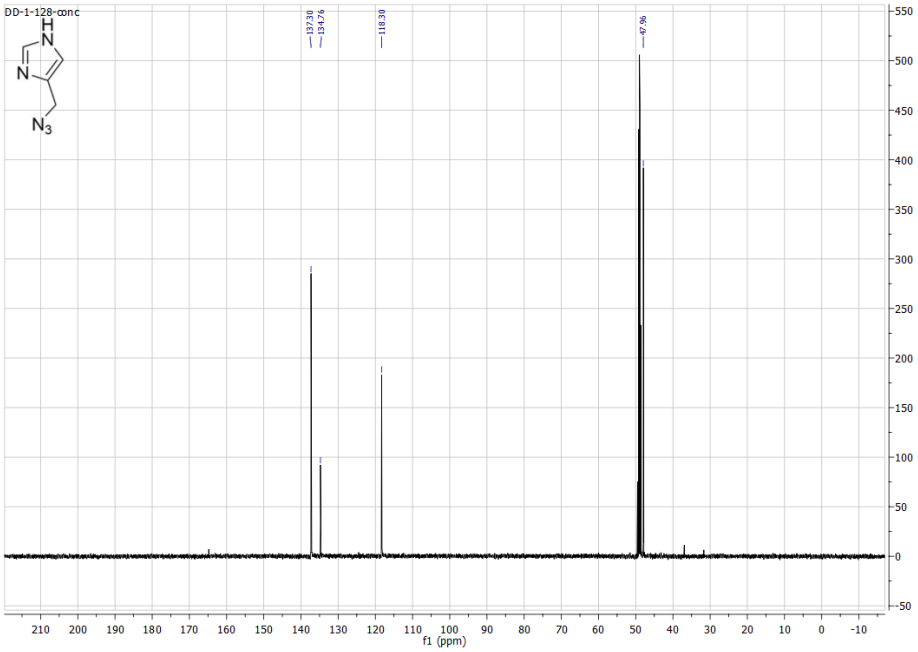

Figure S.47. ^{1}H and ^{13}C NMR of bis(2-(methylthio)ethyl)amine.

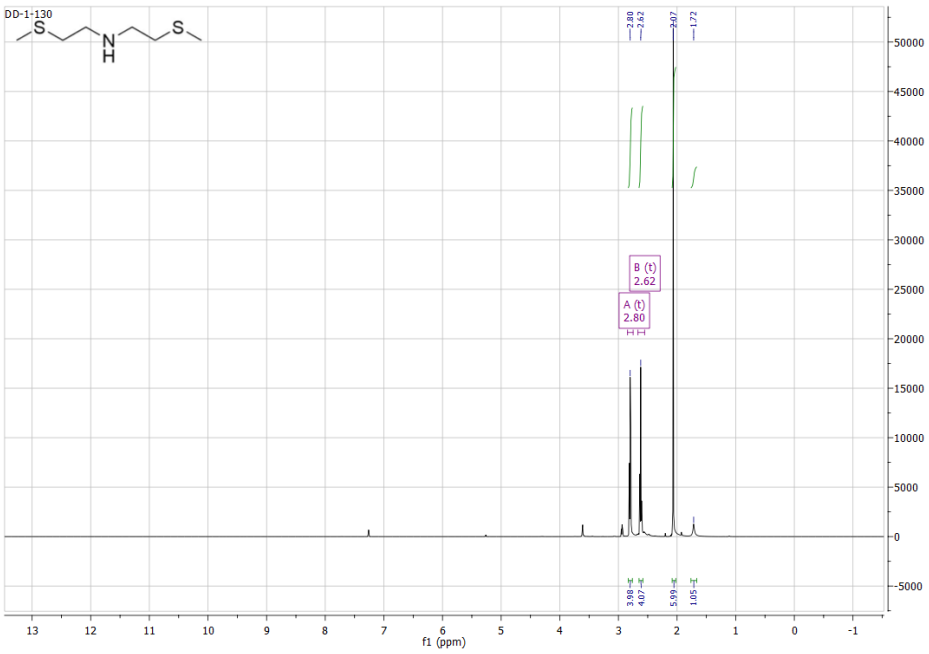

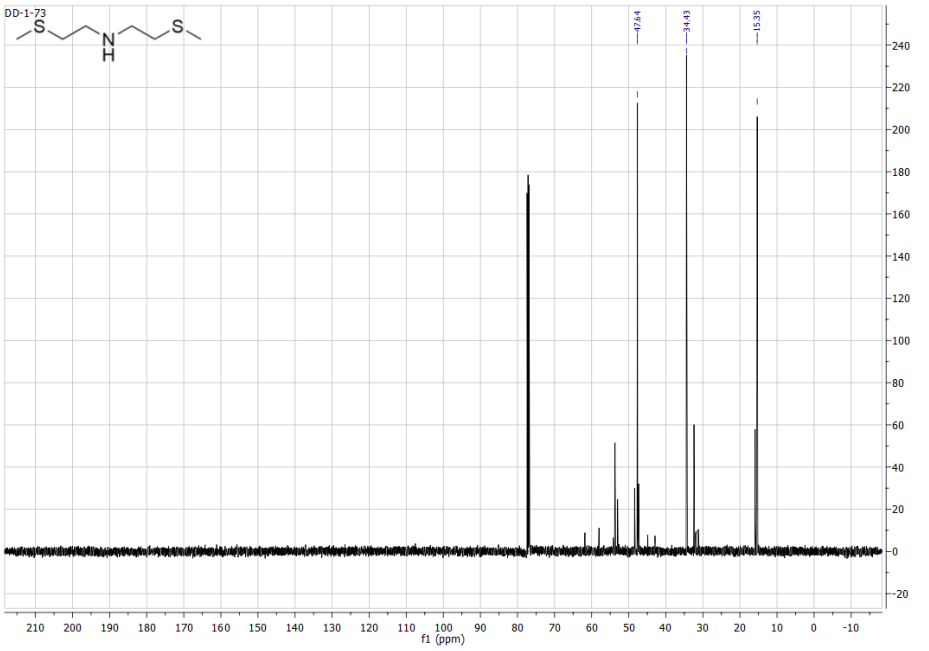

Figure S.48. ^{1}H and ^{13}C NMR of *N*,*N*-bis(2-(methylthio)ethyl)prop-2-yn-1-amine.

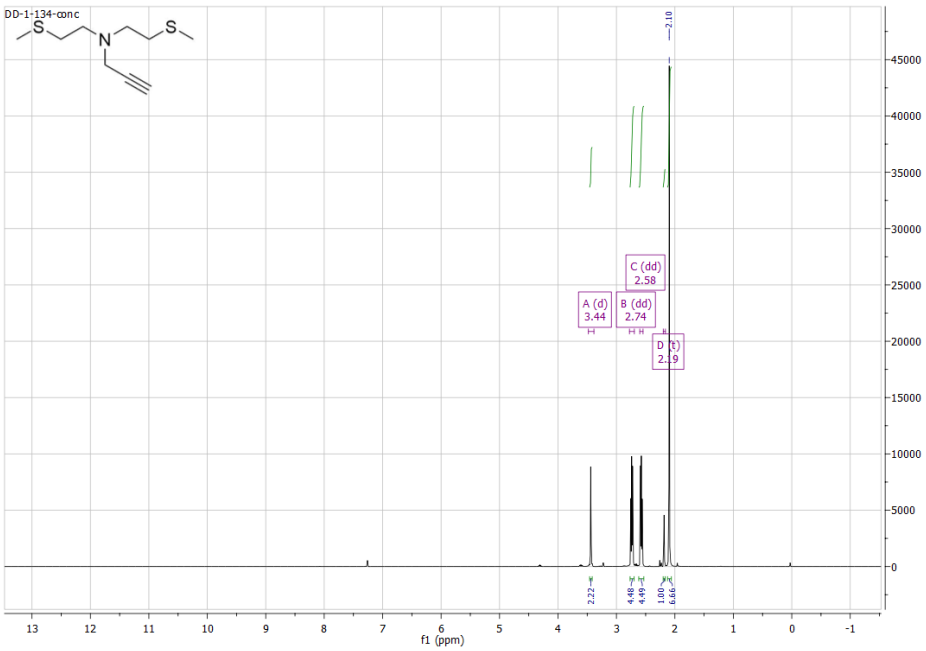

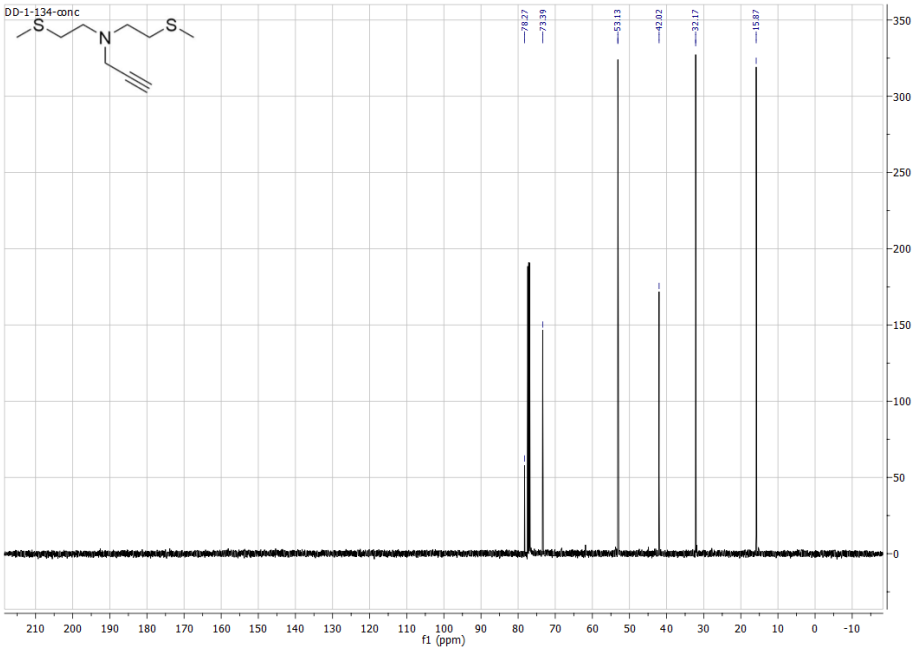

Figure S.49. ^{1}H and ^{13}C NMR of bis(2-(methylthio)ethyl)amine with by-product formation synthesized using ~ 15% NaSMe in aqueous solution.

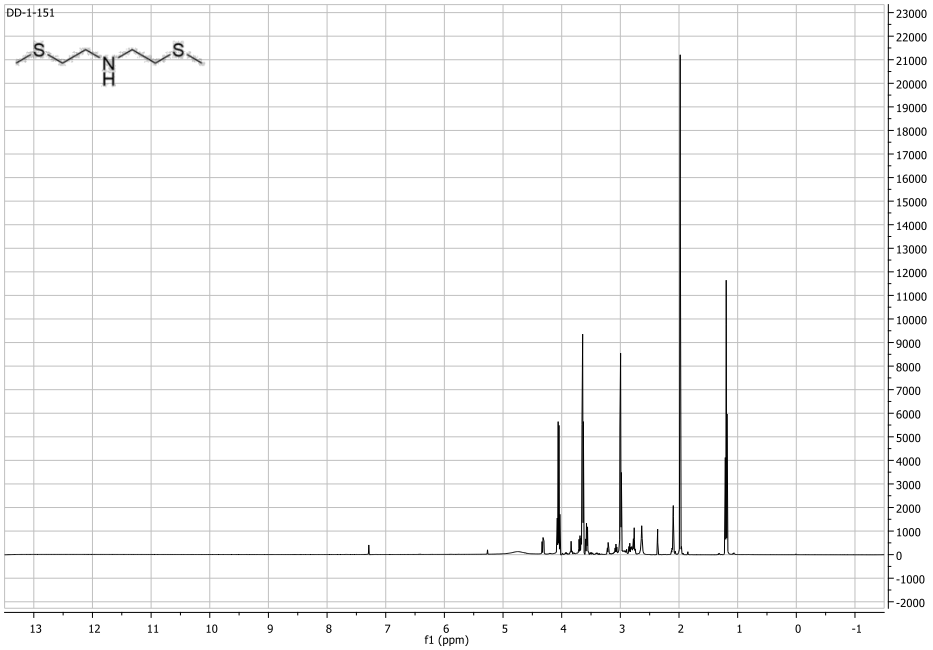

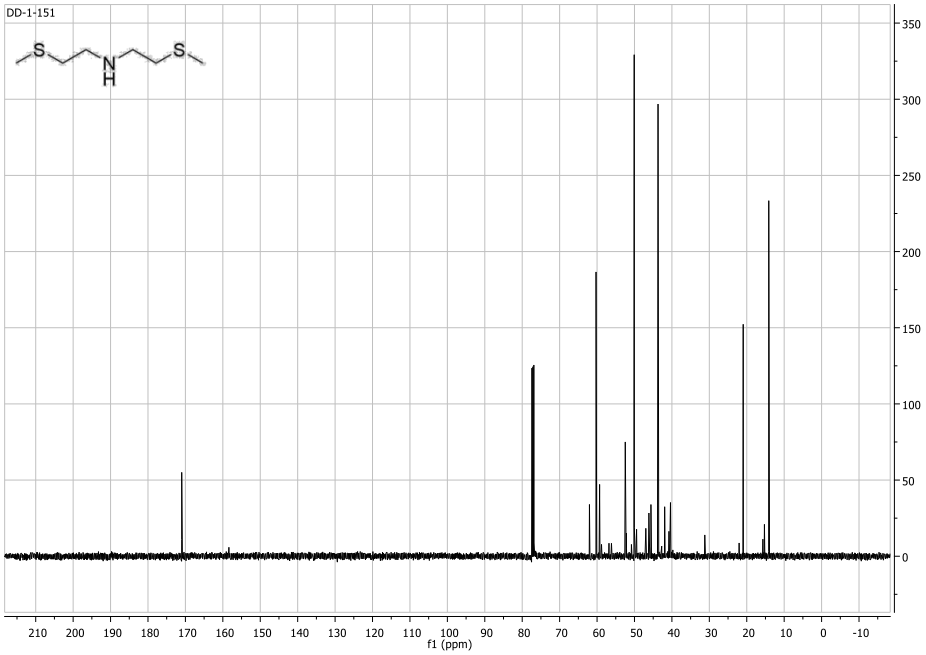

Figure S.50. Mass spectrometry data for synthesis of bis(2-(methylthio)ethyl)amine showing by-product formation (target mass: 165.22).

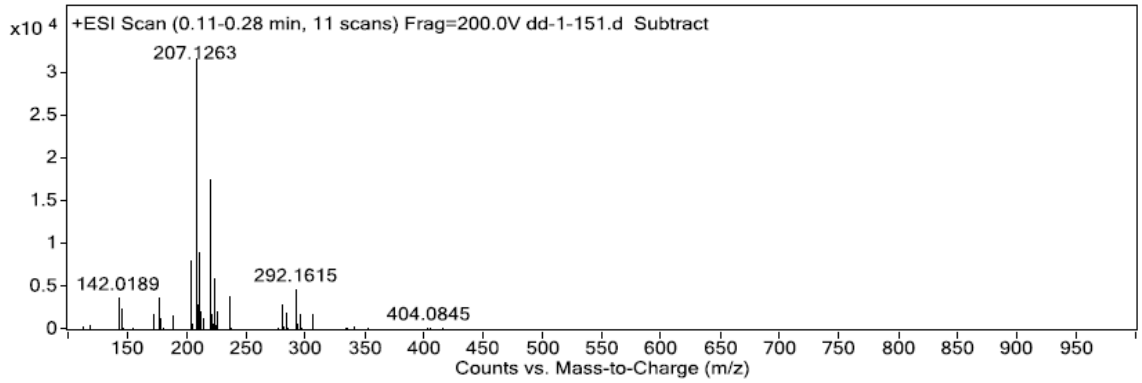

Figure S.51. ^{1}H and ^{13}C NMR of bis(2-(methylthio)ethyl)amine with by-product formation synthesized as literature protocol.

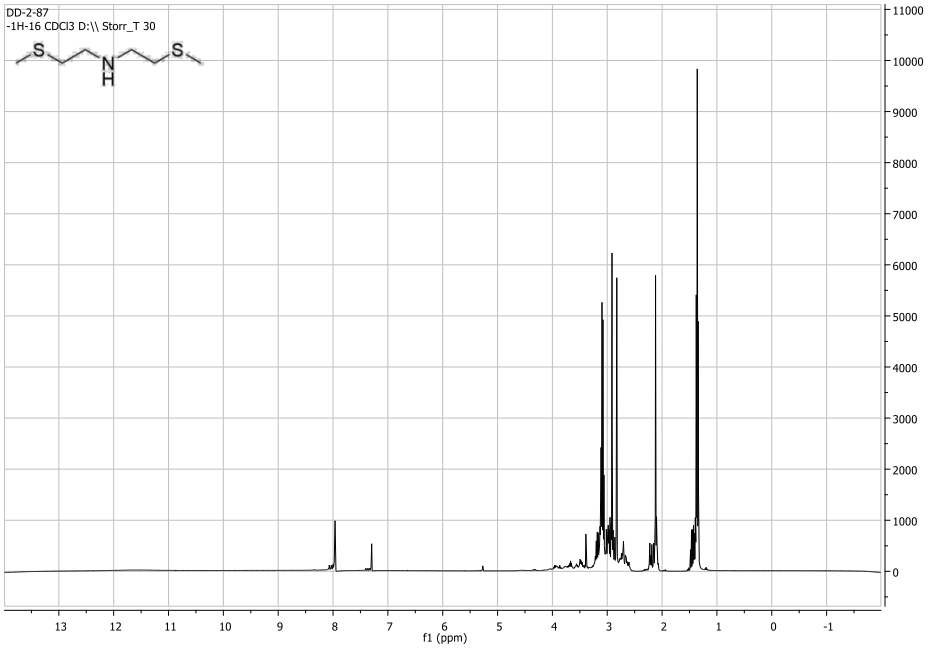

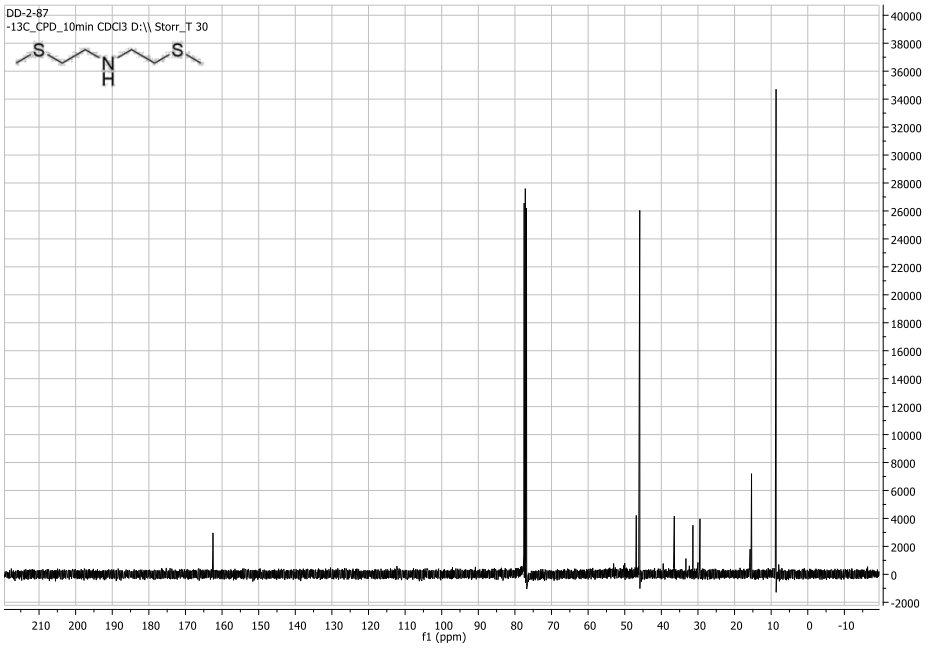

Figure S.52. MS spectra for reaction mixture of Compound 19.

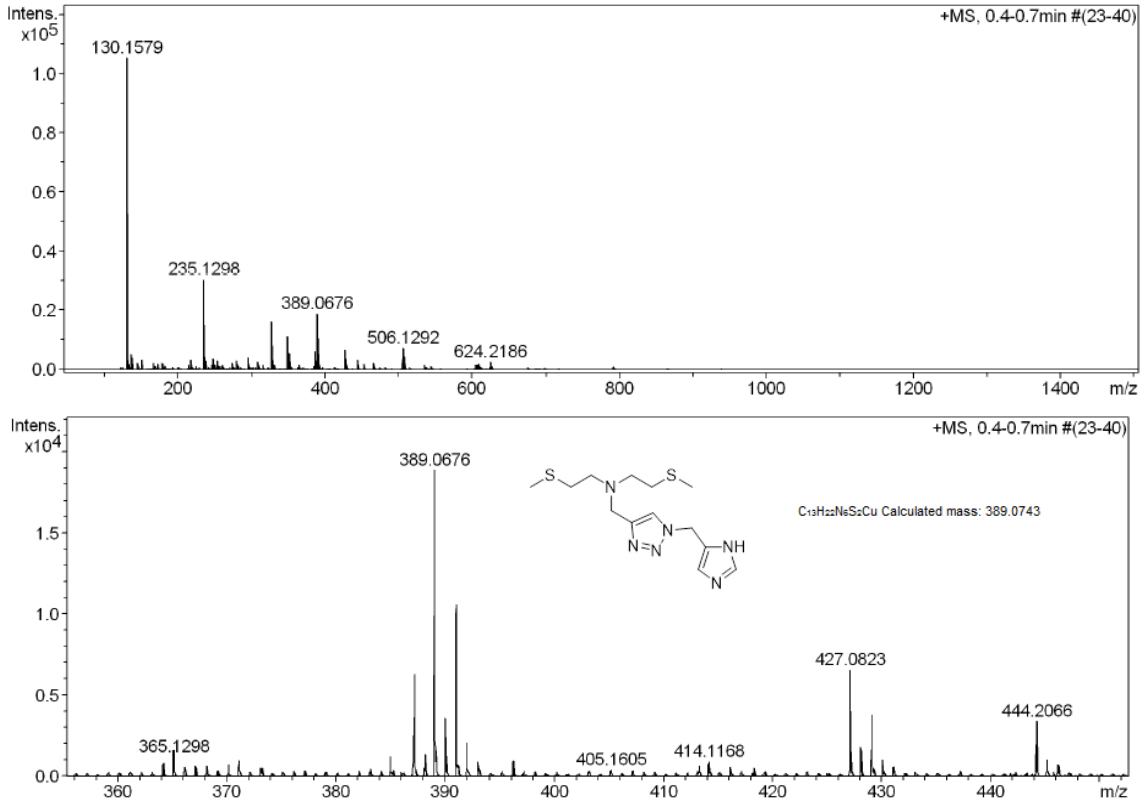

Table S.1. Data for calculating copper concentration within cells for incubation in copper-free media, 100 μM Cu:1 mM His (24 hours), and incubation of chelators at 100 μM: buffer, D-penicillamine, Compound 5, Compound 8, Compound 10, and co-incubation of Compounds 5 and 8 (50 μM each).

Condition	ICP-AES (ng/mL)	Dilution Factor (50x) (ng/mL)	Cu Conc. (nmol Cu/mL)	%RSD	Prot. Conc. (mg/mL)	%RSD	Cu Conc. (nmol Cu/mg protein)	Cu Conc. (nmol Cu/mg protein)
No Cu	29.274	1463.70	23.03	1.6	2.43	10.4	9.48	18.1 ± 17.5
	82.854	4142.70	65.19	1.5	2.45	2.2	26.8	
	8.75	Below Detection Limit						
100 μM Cu 1 mM His	140.666	7033.30	110.7	0.49	3.08	3.5	35.9	43.1 ± 9.8
	162.372	8118.60	127.8	0.57	2.81	6.7	45.5	
	186.992	9349.60	147.1	1.57	3.08	1.5	47.8	
Buffer	162.024	8101.20	127.5	0.16	2.60	4.2	49.0	33.1 ± 26.6
	161.323	8066.15	126.9	2.06	4.07	1.3	31.2	
	151.792	7589.60	119.4	0.87	6.25	1.9	19.1	
D-Pen	112.930	5646.50	88.85	1.63	3.05	6.5	29.1	38.2 ± 15.7
	127.648	6382.40	100.4	1.94	2.89	1.5	34.8	
	181.811	9290.55	146.2	1.14	2.88	3.5	50.8	
Azide (5)	87.819	4390.95	69.09	0.24	2.85	1.5	24.2	26.9 ± 3.5
	107.709	5353.95	84.25	2.93	2.95	4.2	28.6	
	90.485	4524.25	71.19	1.84	2.55	0.8	27.9	
Alkyne (8)	136.823	6841.15	107.6	0.84	3.41	0.4	31.6	32.7 ± 6.0
	138.123	6906.15	108.7	2.23	2.89	3.1	37.6	
	129.609	6480.45	102.0	1.41	3.51	3.1	29.0	
Triazole (10)	169.223	8461.15	133.1	2.30	3.38	11.8	39.4	37.1 ± 2.9
	131.203	6560.40	103.2	1.62	2.92	4.3	35.3	
	160.265	8013.25	126.1	1.20	3.46	3.8	36.4	
Alk+Az (5+8)	122.521	6126.05	96.4	0.91	3.46	73	27.9	30.4 ± 4.4
	139.220	6961.00	109.5	1.33	3.76	2.7	29.2	
	114.494	5724.70	90.08	0.64	2.65	2.8	34.0	